1984

On the dynamic properties of extensive variable control structures

Louis Caston
Lehigh University

ON THE DYNAMIC PROPERTIES OF EXTENSIVE VARIABLE CONTROL STRUCTURES

by

Louis Caston

A thesis

Presented to the Graduate Committee

of Lehigh University

in Candidacy for the degree of

Master of Science

in

Chemical Engineering

Lehigh University

1984

This thesis is accepted and approved in partial fullfillment of the requirements for the degree of Master of Science.

8/8/84
(date)

Christos Georgakis
Professor Christos Georgakis

John C. Chen
Professor John Chen

Appreciation is due to the E. I. DuPont de Nemours and Air Products companies for their financial support throughout the course of this research via their respective fellowships, to Professor Christos Georgakis for introducing me to the concept of extensive variables and their use in process dynamics and control, to Professors Hugo Caram and Cesar Silebi for the numerous enlightening personal discussions that occurred during my stay at Lehigh, to Professor Bill Luyben and Dr. Bjorn Tyreus for their guidance at the start of this research, and to Professor Phillip Blythe for taking time out of his busy schedule to direct me in a complex variables reading course.

Thanks are due to Hans for his patience and help in the completion of this thesis, and to Chris for introducing me to Mike Royko and for all of the enriching discussions and lessons in life.

I would like to thank Chris, Bob K., Jesse, The Ranch, Sarah, Bob B., Monica, Rick, Gina, Alyson, Tracy, Amy, Hakim, Tom, Margie, Tricia, Bill, Pam, Shelley, Dennis, Ata, and Hans for all of the many, many good times. These times really gave life an added meaning to me.

Table of Contents

List of Figures

List of Tables

ABSTRACT

The purpose of this thesis was to investigate the dynamic properties, especially interaction properties, of control structures synthesized using the Extensive Variable Controller Synthesis (EVaCS) technique. The investigation was done using five different multivariable analysis methods. These methods consisted of angle calculations between various vectors that characterize the dynamic properties of a control structure, a modal analysis, the dynamic relative gain array analysis, the inverse Nyquist array analysis, and the characteristic loci analysis. Two different processes were examined in the research.

The first process that was examined consisted of two stirred-tank heaters in series connected by a recycle stream. This process gave a simple approximation to a reactor system. Two different designs were employed. The first design case had a low recycle rate, while the second design case had a high recycle rate. In both designs, the tank volumes were equal. In each of the design cases, the two multivariable control structures synthesized by the EVaCS technique were compared to the conventional structure that might typically be used in controlling this process. This conventional structure controlled the indiviual tank temperatures using the respective energy inputs to the tanks. In all of the

aforementioned analysis techniques and in both design cases, the EVaCS structures proved themselves superior to the conventional structure. Not only that, it was seen that the structures gave good approximations to the process' modal control structure. Also, it was found that the indiviual loops in the structures could be tuned independent of one another.

The second process examined by this thesis was a two stage distillation column. Here also, two different designs were used. The first design case was a low purity separation, while the second design case was a high purity separation. In both designs, the rectifying and stripping sections of the column had equal holdups. For each design case, comparisons were made between the two EVaCS structures and three conventional structures typically employed in distillation control. These conventional structures were the energy balance scheme and two material balance schemes. The first material balance scheme used the distillate flow to control the distillate's composition, while the other material balance scheme used the bottoms flow to control the bottoms' composition. In each of the anlysis techniques and in both designs, the EVaCS structures proved themselves superior to the conventional structures. The EVaCS structures gave a good approximation to the modal control structure for the column in the low purity separation, while in the

high purity separation the structures were the same as the modal control structure. Also, it was seen that the loops in these structures could be tuned independent of one another. This was confirmed by a dynamic simulation of the column in the high purity separation.

Chapter 1

Preliminaries

1.1 Background

Feedback control has its origins in antiquity, some of the earliest applications being Ktesibios' water clock and Philon's oil lamp from the 3rd century B.C. [1]. Through time, as technology advanced, the development of the control field advanced accordingly as necessity dictated. James Watt's steam engine (1788) gave us the first governor for steam engines, and WW II gave us radar-controlled anti-aircraft guns. Naturally, the theoretical advances in the field came with the advances in applications. From the late 1800's to the 1930's, only scalar time response methods were available for use in analysis. With the need for improved amplifier designs came the scalar frequency response methods of Bode and Nyquist in the 1930's. In 1956, the space program gave us vector oriented time response methods, which are collectively known today as state-space methods. These, in turn, gave rise to today's state-of-the-art vector oriented frequency response methods, which began to come about in the late 1960's [2].

It wasn't until the 1940's when process control began to come into existence with its introduction into chemical engineering curricula. Both practitioners and teachers of the field were

mainly concerned with scalar frequency response methods up until the late 1960's. Due to their lack of interest in modern methods, a gap began to appear between applications in process control and theory in the control field. The growth of this gap was accelerated with the advent of the state-space methods, and up until recently it had continued to grow unabated. This was partly due to a lack of suitable measurement instruments for use in process control systems, but the biggest reason was that the chemical process industry (CPI) had no economic incentives to invest in better controller designs [3].

Over the last decade, with ever increasing energy costs and tighter government safety and enviromental regulations, industrial processes have become highly integrated with respect to energy and material flows, and are operating under tightly constrained high-performance process specifications. This had led to more difficult control problems which require better control systems [4]. Even though there exists a tremendous amount of theory in the literature addressing control system design, most of it is not useful from a process control practitioners point of view due to both a general lack of understanding by the practitioner and a lack of relevant information in the theory concerning process control systems design.

Recently, Georgakis [5] authored a paper which introduced a new intuitive approach to process control system design in which extensive thermodynamic properties of the process are used for the synthesis of Extensive Variable Controller Structures (EVaCS). This method requires the practitioner to have steady-state information and some basic knowledge of the dynamics of the process. It gives the control engineer a choice of control structures, the best choice being dictated by the particular design of the process to be controlled. The most favorable attribute of the EVaCS technique is that the structures it gives have zero steady-state interaction and minimal dynamic interaction. The implications of this are that the control loops can be tuned on line without the use of a detailed dynamical model. Furthermore, this tuning can be done for one loop independent of the others in the structure.

1.2 Introduction

A multivariable control system controls a process that has two or more outputs and two or more inputs. These processes are termed multiple-input, multiple-output (MIMO), as opposed to single-input, single-output (SISO). Due to their complicated structure, MIMO systems pose a difficulty in notation. There are two different representations that are commonly used, the state-space and the block diagram.

The state-space representation employs a vector-matrix differential state equation to model the dynamic behavior of the system of interest. This model is a time-domain representation and has the form,

$$\dot{x}(t) = Ax(t) + Bu(t)$$

$$y(t) = Cx(t)$$

where x is a nx1 vector representing the state of the system at any time t, y is a qx1 vector representing the system controlled variables, u is a rx1 vector representing the inputs to the process, A is a nxn plant matrix, B is a nxr input matrix, and C is a qxn output matrix. This representation, though powerful, has not been fully exploited in process control applications due to the necessity of having to describe the process as a system of first-order, constant coefficient, ordinary differential equations. This could prove to be quite a task if the process happens to be an industrial-scale distillation column, for example. Also, this representation cannot handle dead times in the system.

Figure 1 shows a generalized block diagram of a multivariable control system. This representation is in the Laplace domain. In the figure, y is the q-dimensional vector of the system controlled variables, y^s is the set-point vector of the controlled variables, e is the vector of errors in the system, m is the vector of

manipulated variables, u is the vector of system inputs, s represents the system outputs, K is our nxn controller matrix, M defines the relationships between our manipulated variables and our system inputs, G is the matrix of transfer functions describing the process, L is the matrix representing the relationships between our system outputs and controlled variables, and F is a matrix representing any measurement dynamics. The advantages of this representation are that we can refer to transfer functions between different inputs and outputs, with different compensators, and with various loops open or closed [6].

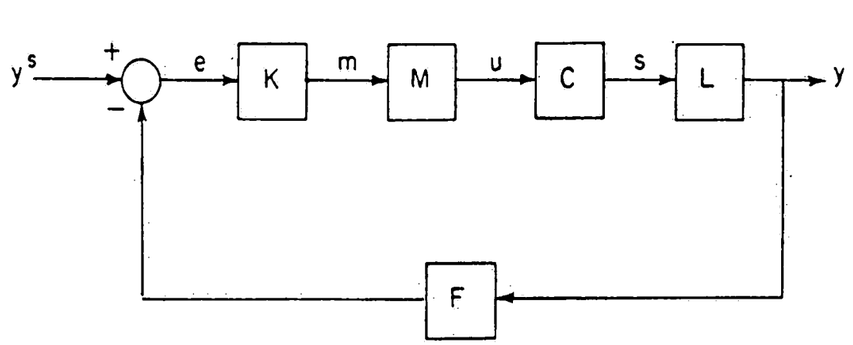

Fig. 1 Generalized Block Diagram of a Multivariable Control System

In the design of a multivariable control system, the control engineer is faced with the task of designing controls to regulate

several variables that are outputs from the same process by adjusting a set of inputs which indiviually affect more than one of the outputs [7]. The task of designing such a system can be separated into two phases. The first, and most important, is the synthesis of the control system's structure, while the second phase consists of tuning the controllers employed in the structure.

In establishing the structure of the control system, there are five questions that need to be answered [8], as shown below.

1. What are the control objectives?
   The designer must decide which of the system variables, be they inputs or outputs, should be controlled at their desired levels.

2. What outputs should be measured?
   The outputs that are measured should give enough information about the process such that the state of the system is determinant. Note that today's technology is not sufficient to allow for the measurement of all possible system outputs.

3. What inputs should be measured?
   If an advanced structure such as feedforward, adaptive or inferential control is to be implemented, the control engineer must decide which of the system's inputs are most apt to supply the necessary information for the given structure. Note that not all system inputs are measureable, either.

4. What inputs should be manipulated?
   This selection entails determining which inputs have sufficiently strong, direct and fast effects on the system outputs.

5. What will be the configuration of the control loops?
   This question deals with establishing linear combinations, generally speaking, of system outputs to be used as controlled variables and linear combinations of system inputs

to serve as manipulated variables. Having established these, the control engineer must then pair them in some appropriate fashion. For a given controlled variable, the paired manipulated variable should have the strongest possible effect on the given controlled variable relative to the other manipulated variables.

Having established the control system's structure, the designer may now proceed to the tuning phase. In most applications in the CPI, three term controllers known as proportional-integral-derivative controllers are used. These controllers act on the error present in a given loop (i.e. the difference in the controlled variable's desired value, as dictated by its set-point, and its actual value) and adjust the appropriate manipulated variable accordingly so as to eliminate the error. The tuning procedure entails weighting the various terms and establishing the controller's sensitivity to the error.

A well designed control system should be non-interacting, stable with high integrity, robust, and have good time-domain performance. In most cases of practical interest, it will not be possible to fully realize all of these attributes. At this point, it would be appropriate to see from what multivariable control concepts these attributes derive from. We employed the concepts of interaction, stability, integrity, robustness, and time domain performance.

A block diagram of a simplified 2x2 interacting control system is shown in figure 2. In the figure, m_j represents input j, y_i represents output i, y_i^s represents the set-point for output i, e_k represents the error in loop k, g_{ij} is the transfer function relating output i to input j, and b_k represents the controller for loop k. Now, assuming that $g_{12} \neq 0 \neq g_{21}$, then this figure shows that we cannot adjust m_1 without affecting both y_1 and y_2. We can say the same about adjusting m_2, also. This phenomenon is termed interaction and it can be very detrimental to the performance of the control system if not addressed properly. The concept of stability deals with that characteristic of the control system which determines whether or not our outputs will remain bounded for a given bounded input in either the open-loop or closed-loop system. If we want to assess the stability of the system with some loops closed and others open, we are dealing with the integrity of the system. A system with high integrity is stable for all combinations of open/closed loops. The concept of robustness deals with how the properties of our control system change as the process characteristics change due to variations in the steady-state operating point, etc. The greater this change can be before the control engineer must adjust the tuning of the controllers, the more robust the system. Finally, good time domain performance entails responding quickly to set-point changes and rapidly

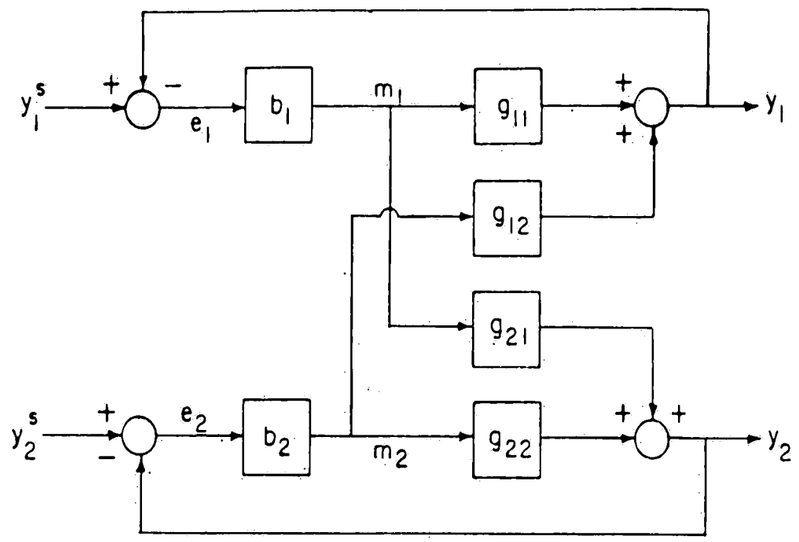

Fig. 2 Block Diagram of a 2x2 Interacting Control System

dampening any disturbances that enter the system.

1.3 Modal Control and Extensive Variable Control Structures

In 1962, H. H. Rosenbrock [3] published a paper that attempted to expose the reasons for the existence of the control theory/process control applications gap as it existed then. In the paper, he established the foundation for what is known today as modal control. This foundation has since been built upon by several authors [9,10]. The essence of the technique is that good control, good being defined as non-interacting with satisfactory closed-loop responses, can be achieved by the proper selection of the control system's controlled variables. The theory of the

technique is based upon the state-space representation, and this has been its major drawback in process control applications, as described previously. Most applications of the technique have been in the control of mechanical systems (airplanes, helicopters, etc.)

A simplified summary of the mathematics of modal control will be shown below. The interested reader can find an extensive treatment of the subject in [10]. We begin with the state-space description of our system.

$$\dot{\mathbf{x}}(t) = A\mathbf{x}(t) + B\mathbf{u}(t) \tag{1.1}$$

$$\mathbf{y}(t) = C\mathbf{x}(t) \tag{1.2}$$

where the symbols have been defined previously. For simplicity, we assume that all of our states are accessible such that $\mathbf{y} = \mathbf{x}$ and that A and B are nxn. Modal control entails selecting some q linear combinations of measurements to serve as our vector of controlled variables. The linear combinations dictated by this technique correspond to the eigenrows (conjugate eigenvectors) v_i of the plant matrix A. This choice of output coordination vectors will give a control system that affects only those modes associated with the v_i and as a result allows the control engineer to choose the closed-loop time constant he desires through the proper selection of that loop's controller gain. Let's make the following transformation,

$$z = Vx \tag{1.3}$$

where z is our controlled vector and V is a nxn matrix whose rows are the eigenrows of the plant matrix. Substituting equation (1.3) into equation (1.1), we have,

$$\dot{z}(t) = \Omega z(t) + Pu(t) \tag{1.4}$$

where Ω is a diagonal matrix of the plant matrix's eigenvalues and P is known as the mode-controllability matrix, which is equal to the product VB. Equation (1.4) shows that the internal dynamics of the process have been decoupled. The implication of this is that essentially non-interacting control is right around the corner.

Now, this is a helpful transformation, but in applications one usually does not have the v_i as an accurate state-space description of a process is difficult to come by. Even if this description was available, it is doubtful that the output coordination vectors would be established using the v_i alone since we cannot model a chemical process perfectly, especially using a state-space description, and the v_i can be sensitive to any errors present in the model. The concepts employed in the EVaCS method allow for the selection of output vectors (termed candidate physical modes) which have intuitive physical appeal and which approximate the v_i (termed mathematical modes). What do we mean by intuitive physical appeal? The candidate physical modes can be interpreted as representing

some extensive thermodynamic quantity that is characteristic of the system. Some example extensive quantities are total energy content, total material content, and total reaction rate. The method also allows for the selection of input coordination vectors to be used in defining the relationships between the control structure's manipulated variables and the inputs to the process. The appropriate pairing of the resultant controlled and manipulated variables is obvious when examined in light of the physical interpretation of the chosen physical modes.

In general, the physical modes are found from steady-state balances around the process to be controlled. Some basic knowledge of the dynamics of the process is also required. Actual examples will best serve the purpose of helping the interested reader to see how these physical modes are obtained as understanding the concepts of the EVaCS technique is the key to successful applications.

1.4 Thesis Objectives

The purpose of this thesis is to demonstrate that the extensive variable concepts used in the EVaCS method allow for the design of multivariable control structures which have minimal interaction characteristics. This is done by examining two different simplified processes typically encountered in the CPI, one being two stirred-tank heaters in series connected with recycle

and the other being a two-stage distillation column. The interaction characteristics of the conventional control systems for these processes are compared to those for the structures obtained using the EVaCS technique. The comparisons are made using a variety of techniques which try to quantify the interaction in a given multivariable control system. These interaction assessment techniques were drawn from both the state-space methods and the vector oriented frequency response methods.

Chapter 2

Methods of Analysis

As stated earlier, the EVaCS method is a conceptual design technique. Using the concept of extensive variables, one can synthesize a number of control structures for a given process, all of which have zero steady-state interaction. This has been shown to be true for a variety of simplified processes by Georgakis [5]. This thesis takes two of the processes examined by Georgakis and assesses the interaction present in the control structures on a dynamic basis.

How does one go about trying to quantify the interaction in a control system? This has been an active area of research for the last decade. Most of the tools that are popular today came from work done by Rijnsdorp [11] and Bristol [12] in 1965 and 1966, respectively. Other more mathematically involved techniques have since been introduced by Tung and Edgar [13], Rosenbrock [14], MacFarlane [15], and Gagnepain and Seborg [16].

This thesis looks at five different ways of assessing the interaction in the control structures of interest to it. The first method of evaluating the structures consists of calculating the angles between the vectors representing the mathematical modes and

those representing the output coordination vectors. These angles are then interpreted in such a way that shows how close the given control structure is to the modal control structure for the process of interest and how well it decouples the process' internal dynamics. The second method used is a modal analysis as suggested by Tung and Edgar [13]. This technique runs along the same lines as the first in that it quantitatively determines how the various outputs are aligned to the modes of the system. The third analysis technique used is McAvoy's dynamic relative gain array [17]. This technique is just the dynamic extension of Bristol's steady-state interaction analysis [12]. The fourth method used is the inverse Nyquist array as proposed by Rosenbrock [14], and the final technique used is MacFarlane's characteristic loci [15]. The next few sections will be devoted to an in-depth discussion of each method.

2.1 Angle Calculations

By using the state-space representation, one may determine the necessary controlled and manipulated variables and the required pairing in order to have a non-interacting control structure. Let's assume that an accurate state-space representation with no modeling errors is available for the process of interest.

$$\dot{x}(t) = Ax(t) + Bu(t) \tag{2.1}$$

For the sake of simplicity, we assume that all of our states are measurable, and that A and B are nxn. Now, the plant matrix and the input matrix are matrices of constant real coefficients for a given steady-state operating point, and they characterize the dynamic properties of the process. In this equation, we see two sources for interaction. The first source is the plant matrix, A. This interaction is internal to the process. The second source is the input matrix, B. This interaction arises when we close the loops of our control system and is due to the fact that a given input usually affects more than one output. The modal control structure transformation, as shown in equation (1.3) in the previous section, eliminates the internal system's interaction. This is the most important of the two types of interaction, as was shown by Ellis and White [9]. By making the modal transformation, one gets the system shown below.

$$\dot{z}(t) = \Omega z(t) + Pu(t)$$

where z is our vector of system controlled variables, u is our vector of system inputs, Ω is a diagonal matrix of the plant matrix's eigenvalues, and P is known as the mode-controllability matrix. Now, if we go one step further and make the following transformation,

$$m(t) = Pu(t) \tag{2.2}$$

we get the system shown below.

$$\dot{z}(t) = \Omega z(t) + m(t) \tag{2.3}$$

Equation (2.2) defines our manipulated vector for us. Each manipulated variable is a linear combination of system inputs as dictated by the rows of the mode-controllability matrix. Equation (2.3) tells us how we would want to pair our controlled and manipulated variables, i.e. z_i to m_i. Note that m_j would have no effect on z_i ($i \neq j$). As Ω is a diagonal matrix, this equation shows that we have totally removed all interaction within the system. Now, let's close our loops using proportional-only controllers.

$$m(t) = K(z^s - z) \tag{2.4}$$

Here K is a diagonal matrix of positive controller gains, and z^s is the vector of set-points. Substituting equation (2.4) into equation (2.3) and rearranging, we get,

$$\dot{z}(t) = (\Omega - K)z(t) + Kz^s \tag{2.5}$$

Equation (2.5) shows that we can have closed-loop eigenvalues whose values are at our discretion through the proper selection of our controller gains, and that our closed-loop system is strictly non-interacting since Ω and K are diagonal. Now, it must be noted that the difficult processes to control have singular P matrices, thus

one can only hope to eliminate the internal interaction in these systems [3].

Using this analysis, we can establish a framework that allows us to see how well a given control structure approximates the modal control structure for the process. Again, we begin with the state-space representation as shown in equation (2.1). Let's make the following transformations,

$$z = Ex = QVx \tag{2.6}$$

$$WQ^{-1}Rm = Bu \tag{2.7}$$

Equation (2.6) gives us our controlled vector, while equation (2.7) gives us our manipulated vector. The complexity of equation (2.7) is necessary in order to make the forthcoming analysis general enough to handle the difficult processes where the P matrix is singular. The P matrix, which is the product of VB, is singular when the input matrix B is singular, as can be shown using a simple application of the Binet-Cauchy theorem [18]. This theorem states that the determinant of a matrix C which is the product of AB is simply the product of the determinants of A and B. As V will be non-singular if our model is well posed, P will be singular when B is singular. The matrix V used in equation (2.6) has been previously defined. The matrix W in equation (2.7) is a matrix

whose columns are the eigenvectors of the plant matrix. Matrices Q and R are indicative of the control system's design, and therefore are at the designer's discretion. The best case analysis done previously had Q = R = I, I begin the identity matrix. Substituting equations (2.6) and (2.7) into our original state-space equation, we get the following system.

$$\dot{z}(t) = QQQ^{-1}z(t) + Rm(t) \qquad (2.8)$$

The rows of of E in equation (2.6) are the designer's output coordination vectors. By comparing equation (2.6) to the modal transformation shown in equation (1.3), we see that in order for the system to approximate the process' modal control structure, our output vectors must approximate the eigenrows of the plant matrix, A. We can assess how well these output vectors approximate the eigenrows by calculating the angles between them. The closer these angles are to zero, the better the given structure approximates the modal control structure.

Now, as we stated earlier, the most important step in our control system design is the elimination of the internal interaction present in the system. We can see how well we have done this by interpreting Q.

$$Q = EW \qquad (2.9)$$

Again, the rows of E are the designer's output vectors. Expanding this product, we have,

$$Q = \begin{bmatrix} h_1^T w_1 . \ . \ . \ . \ h_1^T w_n \\ . \ . \ . \ . \ . \ . \ . \ . \ . \\ h_n^T w_1 . \ . \ . \ . \ h_n^T w_n \end{bmatrix} \tag{2.10}$$

where h_i represents output vector i and w_j represents eigenvector j. As we have already shown that the best case is for Q = I, we want the h_i perpindicular to the w_j, $i \neq j$, so as to have zeroes for the non-diagonal elements. As the magnitude of an eigenvector is arbitrarily defined, equation (2.10) also shows that the magnitude of the output vector is irrelevant as we have two degrees of freedom here in order to make the diagonal elements of Q equal to one. Only the weighting of the indiviual elements of the output vector matter as this determines the direction of the vector.

Thus, our first method in analyzing the interaction in the system consists of calculating the angles between the h_i and v_k, w_j. The closer the h_i are to their corresponding v_i, the better the structure will approximate the process' modal control structure. As the h_i become orthogonal to the various w_j, $i \neq j$, the internal dynamics will be increasingly decoupled. No attempt is made here to analyze the interaction that arises when the loops are closed as this is of secondary importance.

The angle between two vectors is found using the definition of the dot product. Let's look at two vectors, say a and b, both of which are assumed to be of dimension n. It is defined that the angle η_{ab} between a and b is found as follows.

$$\eta_{ab} = \cos^{-1} \frac{a^T b}{|a||b|} \tag{2.11}$$

where

$$a^T b = \sum_{i=1}^{n} a_i b_i \tag{2.12}$$

and $| \; |$ represents the Euclidean norm of the particular vector.

2.2 Modal Analysis

In 1981, Tung and Edgar published a theoretical approach to interaction analysis that was based upon a state-space representation [13]. Their analysis allows the control engineer to calculate the various controller contributions to a given system output for a step change in that output's set-point. If the control system design is a good one, then the principal controller's contribution will be dominant over the sum of the interacting controllers' contributions.

The method begins with the state-space model of the process of interest. For simplicity, we assume that all of our states are measurable and that our plant matrix and input matrix are square and of the same order.

$$\dot{x}(t) = Ax(t) + Bu(t)$$

Let's consider a set-point change from 0 to some x^0. At our new steady-state, assuming that our process description is not changed due to non-linearities, we have the following.

$$0 = Ax^0 + Bu^0 \tag{2.13}$$

Assuming that our system is open-loop stable, and that we can invert our input matrix, we can solve for the perturbation in our system inputs.

$$\begin{aligned} u^0 &= B^{-1}(-A)x^0 \\ &= [(-A)^{-1}B]^{-1}x^0 \end{aligned} \tag{2.14}$$

Equation (2.14) allows us to effect a set-point change by making the appropriate perturbations in our system inputs.

Now, let's assume that we are at steady-state and we input a set-point change into our system as a step function. We can Laplace transform our state equation easily and after the appropriate matrix manipulations we will obtain the following equation.

$$x(s) = (Is - A)^{-1}Bu^0/s \tag{2.15}$$

Substituting equation (2.14) into equation (2.15), we have,

$$x(s) = (Is-A)^{-1}B[(-A)^{-1}B]^{-1}x^0/s \tag{2.16}$$

Following Tung and Edgar [13], we can rewrite this to obtain,

$$x(s) = \beta(s)[\beta(0)]^{-1}x^{0}/s \tag{2.17}$$

By carrying out the matrix multiplication, one will end up with a matrix of transfer functions $\sigma_{ij}(s)$ that give the relationships between the outputs and the set-points of the controllers. It is interesting to note that for $s = 0$ (i.e. steady-state), this resultant matrix is Bristol's [12] relative gain array.

Having these transfer functions, we can invert all those associated with a given output to obtain the contributions of the various controllers to the time response of the respective output. Assuming we want to see the response of output i to a change in its set-point, we have,

$$\frac{x_i(s)}{x_i^{0}} = \sum_{k=1}^{n} \beta_{ik}(s)\beta_{ki}^{(-1)}(0)/s \tag{2.18}$$

where the summation is carried over the n controllers in the structure. The kth term in the summation is the contribution given by controller k. The best case would be for all terms other than the ith term in the summation to be zero. Transforming this equation into the time domain, we have,

$$\frac{x_i(t)}{x_i^{0}} = \sum_{k=1}^{n} (a_0^{i,k} + a_1^{i,k}e^{\lambda_1 t} + \ldots + a_n^{i,k}e^{\lambda_n t}) \tag{2.19}$$

where the λ_j are the eigenvalues of the plant matrix. We can

rearrange this equation to clearly see the contributions given by the various controllers.

$$\frac{x_i(t)}{x_i^o} = (a_o^{i,1} + \sum_{j=1}^{n+1} a_j^{i,1} e^{\lambda_j t}) \qquad (2.20)$$
$$\cdots\cdots\cdots + (a_o^{i,n} + \sum_{j=1}^{n+1} a_j^{i,n} e^{\lambda_j t})$$

Again, the kth term in the above summation (each term consisting of a summation itself) is the contribution given by controller k. Note that the sum of the $a_o^{i,k}$ is equal to one as they represent the various λ_{ik} in Bristol's steady-state array. This equation gives a quantitative description of the interaction present within the system for this situation, i.e. a change in set-point.

In those cases where we have linear combinations of states/system inputs in our control system, as in the analysis done in the previous section (equations (2.6)-(2.8)), we can still use this analysis. Rewriting our state equation by substituting equations (2.6)-(2.7) into equation (2.1), we have,

$$\dot{z}(t) = EAE^{-1}z(t) + Rm(t) \qquad (2.21)$$

We can simply define $A^* = EAE^{-1}$ and $B^* = R$ and repeat the analysis given in equations (2.13)-(2.20) with the new matrices. As A and A^* are similar matrices, the eigenvalues shown in equations (2.19)-(2.20) will remain the same. Thus, the effect of these substitutions is to alter the $a_j^{i,k}$ in the equations.

2.3 Relative Gain Array Analysis

In 1966, E. H. Bristol [12] published an intuitive method known as the relative gain array that is based on a steady-state analysis. This method gave insight into the interaction within a multivariable control system. As was said in the previous section, Tung and Edgar [13] proved the method rigorously in 1981. After its publication, the method went unnoticed for several years before industry and academia alike began to make use of it. Since then, several authors have begun to expand and develop the method, most notably T. J. McAvoy [17,19,20]. McAvoy's most significant contribution has been the dynamic extension of Bristol's steady-state approach.

The method proposed by Bristol assumes that the process is a multivariable, time-invariant one described by a square gain matrix between the manipulated and controlled variables of the control system. This interaction measure attempts to answer the question of how the measured transfer function between a given manipulated variable and the corresponding controlled variable is affected by the perfect control of all other controlled variables. Let's have the following description of the process of interest,

$$c = \beta m \tag{2.22}$$

Here c is our vector of controlled variables, m is our vector of

manipulated variables, and the β_{ij} are the process steady-state gains between c_i and m_j at the steady-state operating point. The measure chosen by Bristol is the ratio of the open- loop gain to the closed- loop gain when all other control loops are closed and operating perfectly. Mathematically, this is defined as,

$$\lambda_{ij} = \frac{\partial c_i/\partial m_j\big|_{m_k=0,k\neq j}}{\partial c_i/\partial m_j\big|_{c_k=0,k\neq i}} \tag{2.23}$$

The numerator in equation (2.23) is simply β_{ij}. To get the denominator, one need simply invert β to get the relationship for m in terms of c and carry out the prescribed differentiation to show that it is $[\beta_{ji}{}^{(-1)}]^{-1}$, that is, the reciprocal of element j,i of the inverse of β. The matrix of the λ_{ij} is known as the relative gain array.

If $|\lambda_{ij}| > 1$, then the open-loop sensitivity of c_i to m_j is greater than the corresponding closed-loop sensitivity. The implication is that the m_k tend to cancel the effect of m_j on c_i in the closed-loop enviroment. This is undesirable and is termed negative interaction. If $|\lambda_{ij}| < 1$, then the closed-loop sensitivity of c_i to m_j is greater than the corresponding open-loop sensitivity. This implies that the m_k tend to enhance the effect of m_j on c_i in the closed-loop enviroment, and thus, it is termed positive interaction. Even though this is desirable, it is so only

up to a certain point. Too much of an enhanced sensitivity can lead to stability problems. If $\lambda_{ij} < 0$, then the effect of m_j on c_i is reversed in the closed-loop enviroment relative to the open-loop enviroment. If $\lambda_{ii} < 0$, then the control system will exhibit inverse or unstable response.

The relative gain array itself has several interesting properties as described by Bristol [12] in his paper. One of the most useful properties is that the elements of any row or column must sum to one. Thus, when dealing with 2x2 systems, one need only calculate the 1,1 element of the array to know the entire array.

T. J. McAvoy [17] expanded Bristol's steady-state approach to include dynamics with his paper in 1977. Essentially, all he did was to substitute transfer functions where Bristol had steady-state gains. He was able to show that the 1,1 element of the now dynamic relative gain array for a 2x2 interacting system could be found as,

$$\lambda(s) = \frac{1}{1 - \frac{G_{12}(s)G_{21}(s)}{G_{11}(s)G_{22}(s)}} \tag{2.24}$$

For the sake of simplicity, the 1,1 subscripts have been dropped. Here, $G_{ij}(s)$ represents the transfer function between output i and input j (as seen previously in figure 2). The Bristol number, i.e.

the steady-state λ for a 2x2 system, is simply found by performing the calculation shown in equation (2.24) for $s = 0$.

It was four more years before McAvoy [19] published a paper giving insight into the significance of λ. He based his work on a foundation layed by Rijnsdorp in 1965 in which Rijnsdorp derived the following equation for a 2x2 interacting control system.

$$\frac{-e_1}{\xi^*} = \frac{1 + Q_2}{1 + Q_1 + Q_2 + Q_1Q_2/\lambda} \qquad Q_i = C_iG_{ii} \qquad (2.25)$$

Here e_1 is the error in loop 1, ξ^* is a disturbance function, C_i is the controller transfer function for loop i (with an integral term), and G_{ii} is the principal transfer function for loop i (as opposed to an interacting transfer function G_{ij}, $i \neq j$). The importance of this equation is that the denominator gives us our stability (and therefore design) equation for our multivariable system. Rewriting equation (2.25), we have,

$$\frac{-e_1}{\xi^*} = \frac{1}{1 + Q_1\dfrac{(1/Q_2 + 1/\lambda)}{(1/Q_2 + 1\ )}} \qquad (2.26)$$

McAvoy analyzed two cases, both of which were amenable to an analytic elucidation. The first case had Q_1 and Q_2 having widely separated loop speeds, while the second case was for $Q_1 = Q_2$. The frequency at which Q_i crosses the negative real axis in the complex

plane of its polar plot is an implicit indication of how quickly the loop will respond to a step input. McAvoy used this natural frequency as an indication of the loop's speed. If the controllers have integral modes and the speed of Q_2 is much greater than Q_1, then we have the situation given in figure 3.

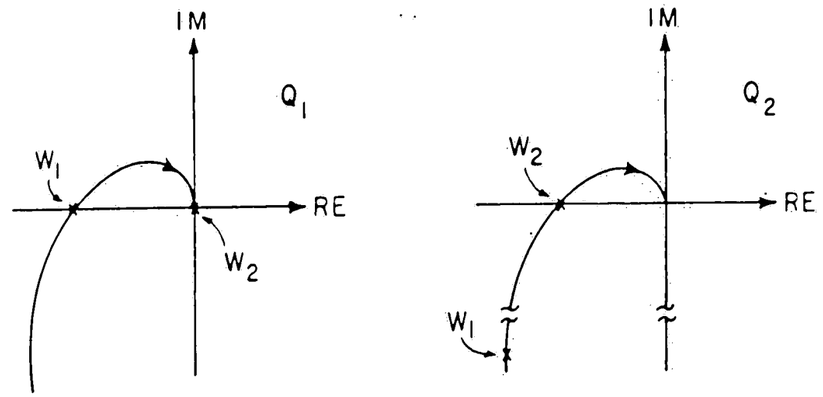

Fig. 3 Nyquist plots for Q_1 and Q_2 with Integral Modes

Here, ω_1 is the natural frequency of loop 1 and ω_2 is the natural frequency of loop 2.

The importance of equation (2.26) now becomes apparent. In assessing the interaction in the control system, we want to see how a given transfer function is affected near its natural frequency. When loop 1 is near its natural frequency, we have $|Q_2| \gg 1$. This

allows us to rewrite equation (2.26) as,

$$\frac{-\varepsilon_1}{\xi^*} = \frac{1}{1 + Q_1/\lambda} \tag{2.27}$$

Thus, in designing the controller for loop 1 we have to modify our transfer function by dividing by λ. In determining the effect of the interaction on loop 2, we can change the subscripts in equation (2.25) to get,

$$\frac{-\varepsilon_2}{\xi^*} = \frac{1}{1 + Q_2\frac{(1 + Q_1/\lambda)}{(1 + Q_1)}} \tag{2.28}$$

Near the critical frequency for loop 2, we have $|Q_1| \sim 0$. Thus, equation (2.28) can be simplified to,

$$\frac{-\varepsilon_2}{\xi^*} = \frac{1}{1 + Q_2} \tag{2.29}$$

This shows that loop 2 is not affected by the interaction.

When $Q_1 = Q_2$, we can factor the denominator in equation (2.25) to get,

$$\frac{-\varepsilon_1}{\xi^*} = \frac{1}{(1 + Q_1/r_1)(1 + Q_1/r_2)} \tag{2.30}$$

where $r_i = \lambda \pm [\lambda^2 - \lambda]^{1/2} = r_1(+), r_2(-)$. Each of the factors in equation (2.30) resembles the traditional SISO design equation. If $|\lambda| < 1$, then the term with r_1 will determine the stability limit. If $|\lambda| > 1$, then the term with r_2 will determine the stability limit. Thus, these two cases give us limiting conditions to consider in our designs as far as assessing the effect of the

interaction is concerned.

Knowing our loop speeds and having λ, we can assess the effect of the interaction on our system's performance. In general, the previous analysis allows us to calculate a modified principal transfer function G_{ii}^{*} from G_{ii} as,

$$G_{ii}^{*} = \frac{G_{ii}}{\Delta(\lambda)} \tag{2.31}$$

where we have three different values for $\Delta(\lambda)$ depending upon the particular case/loop.

1. Loop speeds widely separated

   a. slow loop - $\Delta(\lambda) = \lambda$

   b. fast loop - $\Delta(\lambda) = 1$

2. Loops identical

   a. both loops - $\Delta(\lambda) = \lambda \pm [\lambda^2 - \lambda]^{1/2}$

      where + sign is used if $|\lambda| < 1$
      and - sign is used if $|\lambda| > 1$

Writing equation (2.31) in polar form, we have,

$$G_{ii}^{*} = \frac{|G_{ii}|}{|\Delta|} e^{i(\delta-\alpha)} \tag{2.32}$$

Here δ is the argument of G_{ii} and α is the argument of Δ. Equation (2.32) is in the form that we need in order to assess the effect of the interaction on our system's performance. We can see that the

interaction will affect both our gain, and our natural frequency through the effect on the argument of G_{ii}.

If $|\Delta| > 1$, then our effective gain in the interacting enviroment will be reduced. This implies that we should expect to see more sluggish behavior for that particular loop when the other loop in the system is closed. Whenever the $|\Delta| < 1$, our effective gain is increased implying that we should expect to see a more oscillatory response. When $\alpha > 0$, the modified principal transfer function will reach its natural frequency faster than the principal transfer function. Thus, as our natural frequency in the interacting enviroment is smaller than in the SISO enviroment, our speed of response will decrease. For $\alpha < 0$, G_{ii}^{*} will take longer to cross the negative real axis relative to G_{ii}. The modified natural frequency will therefore be higher than the natural frequency of the loop in its SISO enviroment, which implies that our speed of response will be increased. From this, we can say that our ideal case would be for $|\Delta| \sim 1$ for all frequencies. This being the case, then necessarily $\alpha \sim 0$.

Now, it needs to be pointed out that when calculating $\Delta(\lambda)$, one must define a Riemann surface for λ as Δ is a multivalued function [21]. In the course of this research, two different cases

were encountered. Both are shown in figure 4 with their corresponding Riemann surfaces.

Fig. 4 Riemann Surfaces for $\Delta(\lambda)$

Both surfaces had branch points at (1,0), and the origin was deleted. From a practical standpoint, deleting the origin presented no problem because if λ was ever 0, then you had no control system, anyway. In the diagrams, α represents the argument of λ, while ω represents the frequency for which the calculation was made. As can be seen in the figure, the only difference between the surfaces is their respective branch cut. The surface

for case I has its branch cut lying along the positive real axis beginning at one and extending to positive infinity. The surface for case II has its branch cut lying along the real axis beginning at one, also, but it extends to negative infinity, instead.

2.4 Inverse Nyquist Array Analysis

In the late 1960's, the available vector oriented frequency response design techniques for multivariable control systems suffered from a number of deficiencies. The most severe of these were the difficulties encountered in trying to incorporate engineering constraints and the tendency of the methods to produce complicated controller structures where simpler schemes would suffice. In 1969, Rosenbrock [14] published a new design technique known as the inverse Nyquist array. This method has been developed by a number of authors and is currently one of the more popular techniques of its kind for use in designing industrial multivariable process control systems. A number of successful applications have been reported in industry (e.g. Tyreus [22]).

In describing the method, reference is made to figure 1 during the course of this discussion. For the sake of simplicity, we will relabel G to be our effective plant matrix (which is simply the product MGL from the figure). With this change in mind, we have from figure 1,

$$y = G_m = GK_e \tag{2.33}$$

Denoting the product GK as Q ,which is called the open-loop transfer function, we have (assuming F = I),

$$y = Q(y^s - y) \tag{2.34}$$

Rearranging this slightly, we obtain our closed-loop transfer function H.

$$H = (I + Q)^{-1}Q \tag{2.35}$$

and

$$H^{-1} = I + Q^{-1} \tag{2.36}$$

To avoid confusion later in the discussion, we denote H^{-1} as $\tilde{H}$ and Q^{-1} as $\tilde{Q}$. Now, if we have some loops closed and others open, this can be represented mathematically by having a one on the diagonal of F for those loops that are closed and a zero, otherwise. If this was to be incorporated into equation (2.36), matrix I would be replaced by F. For the purposes of this discussion, we assume that all loops are closed, therefore F = I.

What we want from the technique is the inverse Nyquist path for the principal closed-loop transfer functions, h_{ii}. By definition, we have,

$$h_{ii}(i\omega) = \tilde{H}_{ii}(i\omega)/|\tilde{H}(i\omega)| \tag{2.37}$$

Here $\tilde{H}_{ii}$ is the cofactor of element i,i of the inverse of H. Equation (2.37) gives us the Nyquist path for h_{ii}. We obtain the inverse Nyquist path by inverting h_{ii},

$$h_{ii}^{-1} = |\tilde{H}|/\tilde{H}_{ii} \tag{2.38}$$

We can expand equation (2.38) to obtain,

$$h_{ii}^{-1} = \tilde{h}_{ii} + \sum_{j=1}^{n} \tilde{h}_{ij}\tilde{H}_{ij}/\tilde{H}_{ii} \tag{2.39}$$

Here $\tilde{h}_{ij}$ represents element i,j of $\tilde{H}$ and $\tilde{H}_{ij}$ represents its corresponding cofactor. The summation term in equation (2.39) gives the modification that would have to be made to $\tilde{h}_{ii}$ in order to have it represent the actual h_{ii}^{-1}, which is what we want. This modification is due to the interaction that is present within the system. If our system was diagonal, i.e. there was no interaction, then the summation term would be zero. Assuming that the summation's contribution is small, then we can approximate h_{ii}^{-1} by $\tilde{h}_{ii}$.

Now, from equation (2.36), we see that we can obtain the $\tilde{h}_{ii}$ from $\tilde{q}_{ii}$ simply by moving the origin from (0,0) to (-1,0). The power of this technique is that, assuming the summation term is small, we can plot inverse Nyquist diagrams of the $\tilde{q}_{ii}$ and treat the corresponding designs of the controllers as if they were SISO. We can tell if our assumption about the summation is correct by

employing a theorem derived by Rosenbrock which gives the designer an easy check. For each frequency ω, define

$$d_i = \sum_{\substack{j=1 \\ j \neq i}}^{n} |\tilde{q}_{ji}(i\omega)| \tag{2.40}$$

At that point lying on $\tilde{q}_{ii}(i\omega)$ for the given ω, center a circle of radius d_i. This circle is known as the Gershgorin disc. The union of all such circles that are generated as we change the frequency defines a region within which the true path of the actual transfer function in the interacting enviroment must lie. The greater the interaction, the greater this region, and vice versa. As long as no disc encircles the origin, then our previous assumption is valid. Otherwise, we cannot use the method until we have designed decouplers which are adequate in decreasing the interaction.

It should be noted that the summation in equation (2.40) is over the rows of $\tilde{Q}$. Thus, the corresponding Gershgorin discs are termed row Gershgorin discs. The summation could have been carried over the columns of $\tilde{Q}$, also. As might be expected, these discs are called column Gershgorin discs. The union of these discs is termed the row(column) Gershgorin bands. If the row(column) Gershgorin bands do not contain the origin, then $\tilde{Q}$ is termed row(column) dominant. Either row dominance or column dominance implies diagonal dominance, but the opposite is not always true. Strictly speaking, $\tilde{Q}$ is considered diagonally dominant as long as there

exists no frequency for which $\tilde{Q}$ is not row or column dominant. In order for the method to be applicable to the process of interest, $\tilde{Q}$ must be diagonally dominant.

The Gershgorin discs gives the designer insight into the magnitude of the interaction present within the system. They also allow us to define regions of certain stability and uncertain stability within our gain space. By assuming that the true path of the transfer function lies along one of the boundaries set by the Gershgorin bands, we can delineate a line segment for the ultimate gain of the loop of interest. The intersection of these line segments for the various loops gives us our certainty and uncertainty stability regions in our gain space.

2.5 Characteristic Loci Analysis

In 1970, MacFarlane [23] layed a foundation for the application of linear operator theory to multivariable control system analysis. This foundation was used in developing his characteristic locus design method, which came about three years later [15]. In establishing this technique, MacFarlane attempted to exploit the properties of linear vector spaces to arrive at a vector generalization of the Bode-Nyquist classical design technique. Even though the technique is an important addition to control theory, it has yet to be fully developed as far as a design

procedure is concerned. Experience on part of the user is necessary, as seen by Schwanke [24], et al. in their attempt to use the technique to design a control system for a pilot scale distillation column .

This thesis was not concerned with using the technique for design, though. Instead, the theory was used primarily for an additional method of assessing interaction. Also, it was used as a rigorous way of determining the actual stability limit in the gain space for the control structures of interest. This last point is one of the niceties of the theory developed by MacFarlane.

The technique makes extensive use of the dyadic representation of a matrix. As was shown previously in equation (2.35), our closed-loop transfer function can be expressed in terms of our open-loop transfer function as,

$$H = (I + Q)^{-1}Q$$

or, after some manipulations, we obtain,

$$H(i\omega) = \sum_{i=1}^{n} \frac{\lambda_i(i\omega)}{1 + \lambda_i(i\omega)} w_i v_i^T \qquad (2.41)$$

where n is the order of H, λ_i is the ith eigenvalue of H, w_i is the corresponding eigenvector, and v_i is the corresponding eigenrow.

This expression gives us some insight into interaction, itself. Now, suppose that at some low frequency ω_1, we have $|\lambda(i\omega_1)| \gg 1$ for i = 1,2,....,n. Then, we can see that equation (2.41) can be rewritten as

$$H = \sum_{i=1}^{n} w_i v_i^T = I \tag{2.42}$$

This shows that at low frequencies, with this assumption intact, our system is non-interacting. We can make our eigenvalues large by having high gains. The gains are limited due to stability requirements which invariably require that the $|\lambda(i\omega_h)| \ll 1$ for some higher frequency ω_h. At this point, we have

$$H = \sum_{i=1}^{n} \lambda_i w_i v_i^T = Q \tag{2.43}$$

Equation (2.43) shows that high frequency interaction is not affected by the action of feedback controllers. The only way to avoid high frequency interaction is to have Q become diagonal at high frequencies. Referring back to equation (2.42), for most systems of practical interest, we will have some $|\lambda_i| \gg 1$, but there will be others that will not be sufficiently large to arrive at equation (2.42). Thus, in general, we will expect low frequency interaction.

Now, as we have stated before, we want our y_i^s to affect y_i alone. One possible way of doing this is to align the eigenvectors

of H with the various unit basis vectors, e_j. Here, e_j is the jth column of the nxn identity matrix. Let's do the following, let

$$y^s = y^s e_j \tag{2.44}$$

If it were the case that $w_j = e_j$, then by substituting equation (2.44) into equation (2.41) and recalling the biorthogonality principle, we would have,

$$H(i\omega) = y^s \frac{\lambda_j(i\omega)}{1 + \lambda_j(i\omega)} \tag{2.45}$$

Equation (2.45) shows that the reference input from equation (2.44) would affect only output j, i.e. no interaction would be in the system.

This analysis gives a convenient measure of interaction, that being the angles between the eigenvectors $w_j(i\omega)$ of H and the unit basis vectors $e_j(i\omega)$ as a function of frequency ω. This angle is defined as,

$$\eta(i\omega) = \cos^{-1} \frac{w_j^T(i\omega) e_j(i\omega)}{w_j(i\omega)} \tag{2.46}$$

where w_j is the eigenvector which produces the minimum angle η_j with e_j at frequency ω. If η_j is small at high frequencies, then interaction effects arising from the jth input will be small. Note that only when all of the η_j are 0, i.e. all of the w_j are in exact alignment with the e_j, does this imply that Q is diagonal.

We also used MacFarlane's [15] theory to rigorously calculate the stability limit in the gain space for the control structures of interest to it. For an open-loop system which is asymptotically stable, the theory states that no single eigenvalue of Q can encircle the (-1,0) point in the complex plane. This encirclement theorem is very helpful in calculating our gain space. If we set,

$$Q(s) = Q'(s) = kK'(s)G(s) \qquad K' = \mathrm{diag}(k_i) \tag{2.47}$$

we can say that the eigenvalues of Q'(s) will be the same as those of Q(s) multiplied by k. We can solve for the eigenvalues of Q' and determine the scaling constant k which brings us to our point of instability. If the diagonal elements of K' are such that they correspond to the components of a normalized vector in our gain space, then this scaling constant is the projection of the normalized vector into the gain space to that point which defines the stability limit in the space. By sweeping this normalized gain vector throughout the space, and performing the required calculations for each of the vectors, we can map our gain space.

Page 40, paragraph one, should read
Now, suppose that at some low frequency ω_0, we have $|\lambda_{gi}(j\omega_0)| >> 1$ for $i = 1, 2, \ldots, n$" where j is $\sqrt{-1}$.

Page 42, equation (7.47), should read
$Q(s) = RQ'(s) = RK'(s)G(s)$ $K' = \text{diag}(k_i)$

Page 43, paragraph 2, the recycle flows is given by rq, not $(1+r)q$.

Chapter 3

A Process of Tanks in Series with Recycle

3.1 Definition

The first process that was examined consists of two stirred-tank heaters in series connected by a recycle stream, and is shown in Figure 5. This system was selected because it is a simple approximation to a reactor system. In this case, the recycle stream would be used to increase the overall conversion.

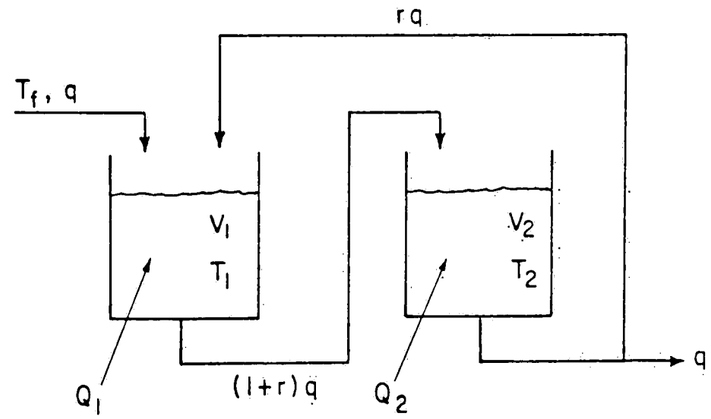

Fig. 5 Stirred-Tank Heaters Process with Recycle

In Figure 5, q represents the throughput flow, (1+r)q the recycle flow, V_i is the volume of tank i, T_i is the temperature of tank i, and Q_i represents the energy input to tank i.

In modeling the process, we assume that the flows through the system are perfectly controlled such that q remains constant. Let's try and control the tank temperatures. If we write an energy balance over each tank, assuming that the tank is well-mixed, we have the following model.

$$\frac{V_1}{q}\frac{dT_1}{dt} = T_f - (1+r)T_1 + rT_2 + \frac{Q_1}{\rho C_p q} \tag{3.1}$$

$$\frac{V_2}{q}\frac{dT_2}{dt} = (1+r)T_1 - (1+r)T_2 + \frac{Q_2}{\rho C_p q}$$

where ρ is the liquid density and C_p is the liquid heat capacity, both of which are assumed to be constant. Dimensionalizing our equations, we have,

$$\alpha \dot{T}_1 = T_f - (1+r)T_1 + rT_2 + Q_1^* \tag{3.2}$$

$$(1-\alpha)\dot{T}_2 = (1+r)T_1 - (1+r)T_2 + Q_2^*$$

where α is the fraction of the total system volume occupied by tank one $[V_1/(V_1+V_2)]$, and time is now dimensionless with respect to the total system time constant $[q/(V_1+V_2)]$. Q_i^* is the effective heat input to tank i $[Q_i/\rho C_p q]$.

Equation (3.2) represents the expanded form of our state-space model. Writing the equations in the form of equation (1.1), we have the tank temperatures as our state vector, the effective heat inputs as our input vector, and the following plant matrix and input matrix,

$$A = \begin{bmatrix} -\frac{(1+r)}{\alpha} & \frac{r}{\alpha} \\ \frac{1+r}{1-\alpha} & -\frac{(1+r)}{1-\alpha} \end{bmatrix} \tag{3.3}$$

$$B = \begin{bmatrix} \frac{1}{\alpha} & 0 \\ 0 & \frac{1}{1-\alpha} \end{bmatrix}$$

As all of our states are accessible, i.e. we can measure both of our tank temperatures, we need not worry about defining an output matrix. It should be stated that models for use in process control system analyses are best written in terms of perturbations from the steady-state [25]. As this model is linear to begin with, we need not go through any process linearization. Having our state-space model we can easily obtain our plant transfer function matrix as,

$$G(s) = (Is - A)^{-1}B \tag{3.4}$$

A plot of this system's eigenvalues as a function of α is shown in Figure 6a for the case where $r = 0.5$, a low recycle rate. The corresponding plot for a high recycle rate, $r = 2.0$, is shown in Figure 6b. The speeds of the two modes of this system are dictated by their corresponding eigenvalues. As can be seen in these plots, the eigenvalues are the least separated when $\alpha = 0.5$, i.e. both tanks have the same volume. With this in mind, the following two different design cases were used during the course of the analyses to come.

Case I $\alpha = 0.5$ $r = 0.5$

Case II $\alpha = 0.5$ $r = 2.0$

As seen by the value of α, both tanks are of equal size. The two cases differ in their recycle rate, one case having a low recycle and the other having a high recycle.

In establishing our controlled variables, we are looking for a linear combination of states, described mathematically as follows.

$$s_i = h_i^T x \tag{3.5}$$

where s_i is our resulting controlled variable and h_i is our output coordination vector. The conventional control structure assessed in this thesis controls the indiviual tank temperatures. This is an intensive variable control structure and will be referred to as the IVaCS structure for the remainder of this chapter. For the IVaCS structure, we have the following output vectors,

$$h_1^T = (1,0) \tag{3.6}$$
$$h_2^T = (0,1)$$

The EVaCS method gives the designer a choice of output vectors, termed candidate physical modes. In order to establish our candidate physical modes for these structures, we employ the following extensive energy concepts.

1. energy balance of tank 1

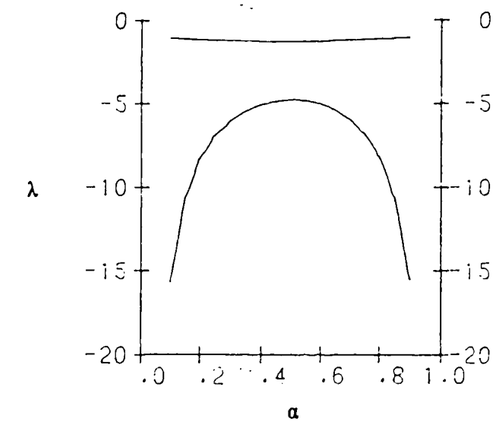

(a)

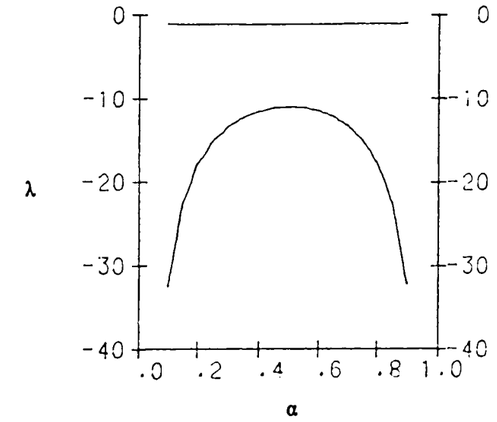

(b)

Fig. 6 Eigenvalues of Tank's Process as a Function of α

2. energy balance of tank 2

3. energy content of total system (tank1 + tank 2)

If we wanted to control the energy balance of tank 1, we could use the linear combination of states present in the energy balance, as shown below,

$$s_3 = -(1+r)T_1 + rT_2 \tag{3.7}$$

$$h_3^T = [-(1+r), r]$$

Notice that all we did was use the steady-state part of the balance. Likewise, to control the energy balance of tank 2, we simply use the combination,

$$s_4 = (1+r)T_1 - (1+r)T_2 \sim T_1 - T_2 \tag{3.8}$$

$$h_4^T = (1,-1)$$

Notice that scaling is not important. The important point in this is the weighting of the states. Now, the total energy content of the system will be influenced by the relative size of the tanks. Since scaling is not important, we can use the following linear combination to control the total content,

$$s_5 = \alpha T_1 + (1-\alpha)T_2 \tag{3.9}$$

$$h_5^T = (\alpha, 1-\alpha)$$

Table 1 summarizes the various output coordination vectors.

In establishing our manipulated variables, we are looking for

a linear combination, generally speaking, of system inputs.

$$u_i = p_i^T m \tag{3.10}$$

where u_i is our manipulated variable and p_i is the input coordination vector describing that particular combination of process inputs. The conventional structure controls the various tank temperatures with their respective heat inputs. Thus, we have,

$$p_1^T = (1,0) \tag{3.11}$$
$$p_2^T = (0,1)$$

In searching for our input vectors to control the energy balances of the tanks, we would expect to find a linear combination of system inputs in our energy balances. These are the combinations that we want to use in our structure. Thus, we have for controlling the energy balance for tank 1,

$$p^T = (1,0) = p_1^T \tag{3.12}$$

Likewise, for tank 2,

$$p^T = (0,1) = p_2^T \tag{3.13}$$

Using the interpretation of the total content, we have the following input vector for use in defining its controlled variable,

$$p_3^T = (1,1) \tag{3.14}$$

Table 1 Summary of Output Coordination Vectors for Stirred-Tanks in Series

$h_1^T = (1,0)$	Intensive variable output vector for controlling tank 1 temperature
$h_2^T = (0,1)$	Intensive variable output vector for controlling tank 2 temperature
$h_3^T = [-(1+r),r]$	Extensive variable output vector for controlling tank 1 energy balance
$h_4^T = (1,-1)$	Extensive variable output vector for controlling tank 2 energy balance
$h_5^T = (\alpha,1-\alpha)$	Extensive variable output vector for controlling total energy content of both tanks

Table 2 Summary of Input Coordination Vectors for Stirred-Tanks in Series

$p_1^T = (1,0)$	Input vector for controlling tank 1 temperature and tank 1 energy balance
$p_2^T = (0,1)$	Input vector for controlling tank 2 temperature and tank 2 energy balance
$p_3^T = (1,1)$	Input vector for controlling total energy content of both tanks

Table 2 summarizes the input coordination vectors.

3.2 Results and Discussion

Figure 7a,c show the angles as a function of α between the output coordination vectors for the IVaCS structure, h_1 and h_2, with the slow eigenrow of the system for the two recycle rates considered, while figure 7b,d show the angles with the fast eigenrow of the system. The only time either of these two output vectors approximate the slow mathematical mode is when one tank is much smaller than the other. Neither output vector ever really gives a good approximation to the fast mode of the system. Thus, the IVaCS structure does not approximate the modal control structure, especially in our two design cases.

It is a known fact that if the loops in a multivariable control structure are of different speeds, then the interaction within the structure will be less than if the loops were of the same speeds. In establishing an EVaCS structure, we have at our disposal any two of the three possible candidate physical modes given to us by the previous extensive energy analysis. In selecting the two output vectors to be used in the structure, we want to choose one to approximate the slow mode of the system and the other to approximate the fast mode of the system. This is so because the speeds of the modes of the system are dictated by the

eigenvalues of the plant matrix, which are usually distinct and separated for chemical process systems. As seen previously in Figure 6, this process has the property of distinct and separated eigenvalues.

Figure 8a,c show the angles as a function of α in the low and high recycle designs between our total energy content physical mode, h_5, and the eigenrow corresponding to the slow mathematical mode of the system. The corresponding angles with the energy balance physical modes, h_3 and h_4, are shown in Figure 8b,d for the respective design cases. These plots show that the total energy content physical mode gives a good approximation to the slow mathematical mode, and this approximation improves as the recycle rate increases. Figure 9a,c show the angles between h_5 and the fast mathematical mode of the system, while the corresponding angles with h_3 and h_4 are shown in Figure 9b,d. These plots show that the energy balance physical modes give reasonable approximations to the fast mode of the system, and these approximations improve considerably with an increasing recycle rate.

Along with the IVaCS structure, the angle calculations suggest two additional EVaCS structures for controlling this process in the

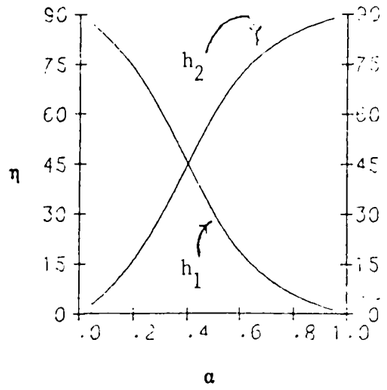

(a)

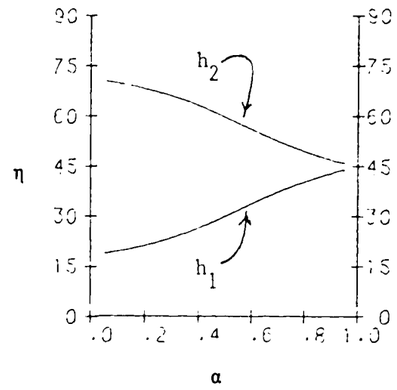

(b)

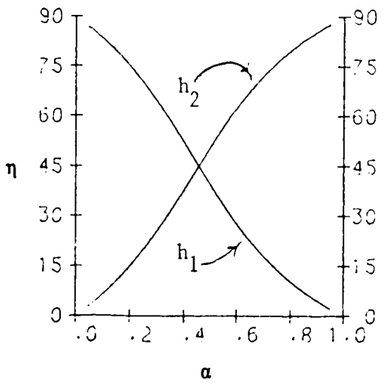

(c)

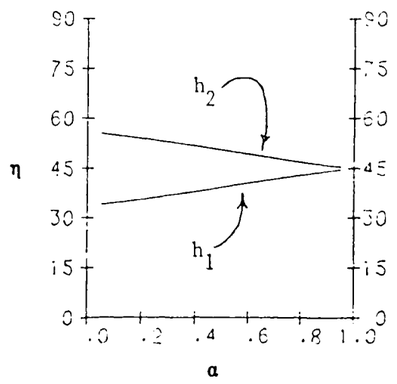

(d)

Fig. 7 Angle Calculations in Degrees for Tank's Slow,Fast Modes' Eigenrow with IVaCS Output Vectors, h_1 and h_2
a–with slow mode, low recycle b–with fast mode, low recycle
c–with slow mode, high recycle d–with fast mode, high recycle

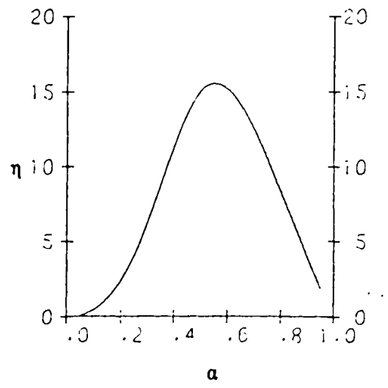

(a)

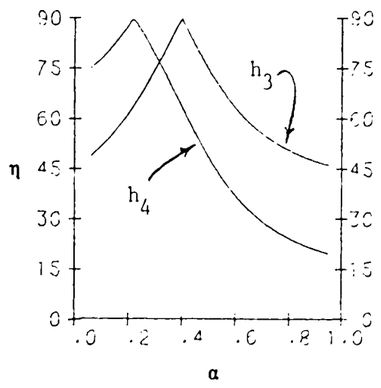

(b)

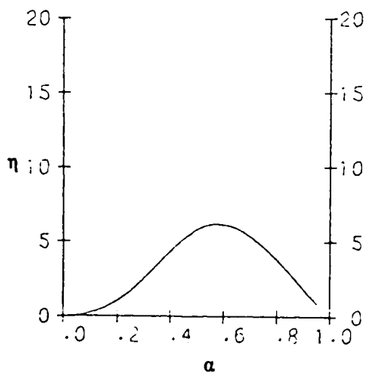

(c)

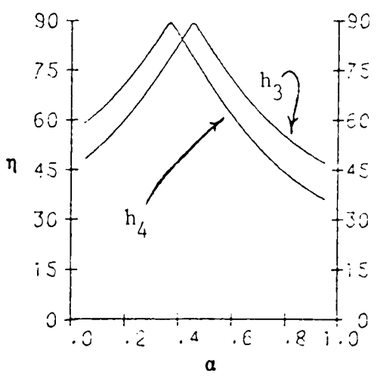

(d)

Fig. 8 Angle Calculations in Degrees for Tank's Slow Mode's Eigenrow with EVaCS Output Vectors, h_3,h_4 and h_5
a–with h_5, low recycle b–with h_3,h_4, low recycle
c–with h_5, high recycle d–with h_3,h_4, high recyle

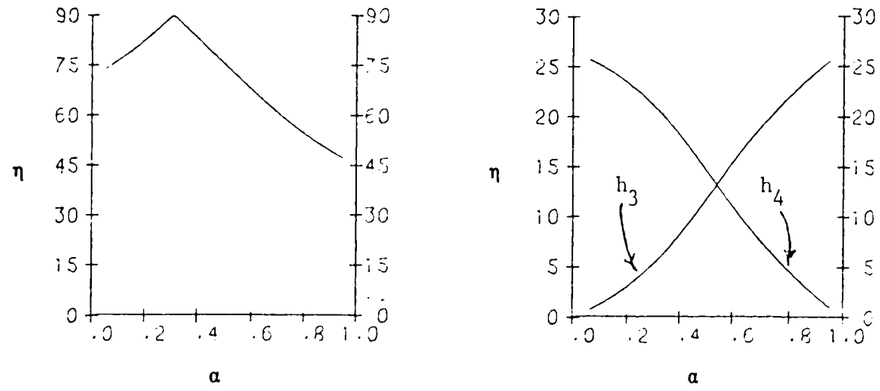

(a)

(b)

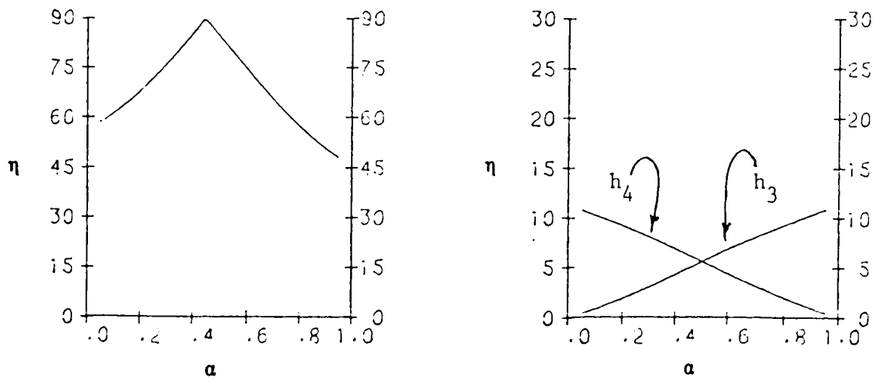

(c)

(d)

Fig. 9 Angle Calculations in Degrees for Tank's Fast Mode's Eigenrow with EVaCS Output Vectors, h_3,h_4 and h_5
a–with h_5, low recycle b–with h_3,h_4, low recycle
c–with h_5, high recycle d–with h_3,h_4, high recycle

design cases that we are assessing. All three structures are summarized below.

	Output Coordination Vectors	Input Coordination Vectors
IVaCS	h_1	p_1
	h_2	p_2
EVaCS I	h_3	p_1
	h_5	p_3
EVaCS II	h_4	p_2
	h_5	p_3

As stated earlier, in assessing how well our given control structure approximates the modal control structure for the process we want to see how well our output vectors approximate their respective plant matrix's eigenrows. The angles between these vectors should be as close to zero as possible. Also, in order to decouple the internal dynamics, we want the output vectors to be as nearly orthogonal as possible to all other eigenvectors besides the eigenvector corresponding to the eigenrow of interest. As seen already, the IVaCS structure does not approximate the modal structure as its output vectors are substantially different from the system's eigenrows. This being the case, we would not expect this intensive variable control structure to decouple the process' internal dynamics. Our EVaCS structures seem to do a reasonable job in approximating the modal control structure, but we cannot be

certain of the degree of decoupling in the process' internal dynamics. We can see this, as shown earlier, by calculating the angles between the total content physical mode, h_5, and the eigenvector corresponding to the fast mode, and by calculating the angles between the indiviual tank content physical modes, h_3 and h_4, and the slow mode's eigenvector. The best case would be for all of these angles to be ninety degrees. The total content/fast eigenvector angles are shown in figure 10a,c while the indiviual tank contents/slow eigenvector angles are shown in figure 10b,d. For our particular design of $\alpha = 0.5$, these figures show that some interaction will be present as the process dynamics have not been completely decoupled. Whether or not the interaction will be significant remains to be seen.

Table 3 summarizes the plant transfer function matrices of the various control structures for the low recycle design case while table 4 summarizes the plant transfer function matrices of the high recycle design case. Appendix I contains a summary for both design cases of the plant matrices and input matrices for use in their respective state-space models.

The modal analysis of Tung and Edgar [13], as described previously, was done using the plant transfer functions in tables

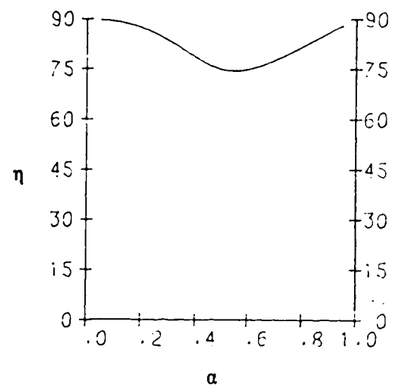

(a)

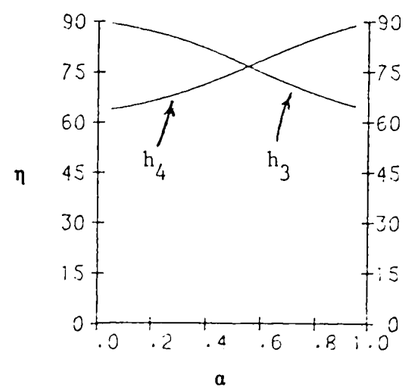

(b)

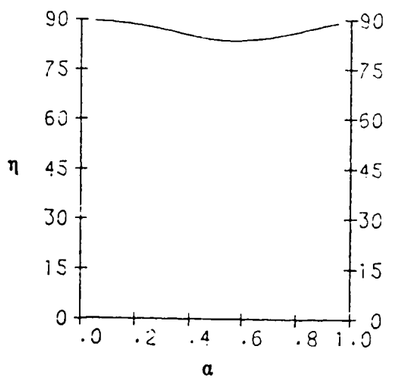

(c)

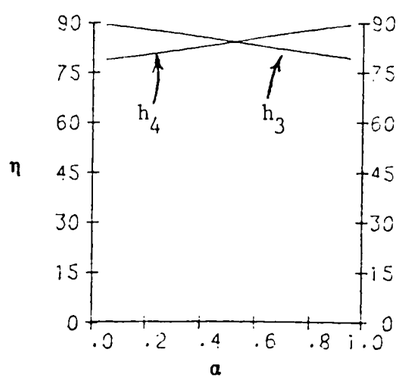

(d)

Fig. 10 Angle Calculations for Slow, Fast Modes' Eigenvectors with EVaCS Physical Modes in Tank's Low and High Recycle Designs
a-fast mode with h_5, low b-slow mode with h_3,h_4, low
c-fast mode with h_5, high d-fast mode with h_3,h_4, high

Table 3 Plant Transfer Function Matrices for
Stirred-Tank Heaters in Series
Low Recycle Design Case

$$\alpha = 0.5 \qquad r = 0.5$$

$$\lambda_1 = -1.26795 \qquad \lambda_2 = -4.73205$$

$$d(s) = (s - \lambda_1)(s - \lambda_2)$$

IVACS

$$G(s) = \frac{1}{d(s)} \begin{bmatrix} 2(s+3) & 2 \\ 6 & 2(s+3) \end{bmatrix}$$

EVACS I

$$G(s) = \frac{1}{d(s)} \begin{bmatrix} s+4 & 2 \\ -s & 4(s+1.5) \end{bmatrix}$$

EVACS II

$$G(s) = \frac{1}{d(s)} \begin{bmatrix} s+6 & -2 \\ 2s & -4(s+1) \end{bmatrix}$$

Table 4 Plant Transfer Function Matrices for
Stirred-Tank Heaters in Series
High Recycle Design Case

$$\alpha = 0.5 \qquad r = 2.0$$

$$\lambda_1 = -1.10102 \qquad \lambda_2 = -10.89898$$
$$d(s) = (s - \lambda_1)(s - \lambda_2)$$

IVACS
$$G(s) = \frac{1}{d(s)} \begin{bmatrix} 2(s+6) & 8 \\ 12 & 2(s+6) \end{bmatrix}$$

EVACS I
$$G(s) = \frac{1}{d(s)} \begin{bmatrix} s+10 & 2 \\ -4s & 10(s+1.2) \end{bmatrix}$$

EVACS II
$$G(s) = \frac{1}{d(s)} \begin{bmatrix} s+12 & -2 \\ 2s & -4(s+1) \end{bmatrix}$$

3 and 4. Briefly, the analysis consisted of looking at the time domain response of x_i/x_i^s. This response could be broken down into contributions from the various controllers in the structure. For our 2x2 system, we had,

$$\frac{x_i}{x_i^s} = \Delta_{i1} + \Delta_{i2} \tag{3.15}$$

Here Δ_{ij} is the contribution given by controller j to the response of output i. The calculation procedure that was required to obtain the Δ_{ij} involved the following,

1. calculate the change in the manipulated variables required to effect a change in the set-point of a given controller. This was shown earlier, equation (2.14), to be,

$$u^0 = G(0)^{-1}x^0$$

where x^0 is the new set-point vector.

2. calculate the step change response in the Laplace domain as,

$$x(s) = G(s)G(0)^{-1}x^0/s$$

3. invert the various elements responsible for the time response to get the Δ_{ij}.

Note that this method is independent of the controllers' tuning. Thus, it gives us information about the interaction that is inherent to the control system's structure.

The time response for the IVaCS low recycle system was calculated as,

$$\frac{x_1}{x_1^S} = \frac{x_2}{x_2^S} = \Delta_1 + \Delta_2$$

where

$$\Delta_1(\eta) = 1.5 - 1.183e^{-1.3\eta} - 0.317e^{-4.7\eta} \qquad (3.16)$$

$$\Delta_2(\eta) = -0.5 + 0.683e^{-1.3\eta} - 0.183e^{-4.7\eta}$$

$\eta = t/\tau$ τ = total system time constant

The Δ_1 response is the principal controller's contribution while the Δ_2 response is the interacting controller's contribution. These dimensionless responses are plotted in figure 11a, and they indicate that the interaction is significant and unfavorable as the controllers are fighting one another.

The time responses for the IVaCS high recycle system are shown below and are plotted in figure 11b.

$$\Delta_1(\eta) = 3.0 - 2.725e^{-1.1\eta} - 0.275e^{-10.9\eta} \qquad (3.17)$$

$$\Delta_2(\eta) = -2.0 + 2.225e^{-1.1\eta} - 0.225e^{-10.9\eta}$$

It can be seen that the loop interaction has increased significantly.

The time responses for the EVaCS I low recycle system were calculated in the format shown in equation (3.15). These are shown below and plotted in figures 12a and 12b.

loop 1 (slow) (3.18)

$$\Delta_{11}(\eta) = 1.0 - 0.993e^{-1.3\eta} - 0.067e^{-4.7\eta}$$

$$\Delta_{12}(\eta) = 0.0$$

loop 2 (fast)

$$\Delta_{21}(\eta) = 0.145e^{-1.3\eta} - 0.145e^{-4.7\eta}$$

$$\Delta_{22}(\eta) = 1.0 - 0.211e^{-1.3\eta} - 0.789e^{-4.7\eta}$$

There are some significant points that manifest themselves in this analysis. The first is that the fast loop does not interact with the slow loop at all since $\Delta_{12} = 0$. The second point is that there is no steady-state interaction of the slow loop with the fast loop as Δ_{21} goes to 0 as η goes to ∞, and the dynamic interaction that is present is minimal. The third point is that the total response of the slow loop is strictly associated with the slow mode of the system, and the total response of the fast loop is strictly associated with the fast mode of the system. These points are what we set out for in the design.

The time responses for the EVaCS I high recycle system are shown below and plotted in figures 12c and 12d.

loop 1 (slow) (3.19)

$$\Delta_{11}(\eta) = 1.0 - 0.990e^{-1.1\eta} - 0.010e^{-10.9\eta}$$

$$\Delta_{12}(\eta) = 0.0$$

loop 2 (fast)

$$\Delta_{21}(\eta) = 0.082e^{-1.1\eta} - 0.082e^{-10.9\eta}$$

$$\Delta_{22}(\eta) = 1.0 - 0.092e^{-1.1\eta} - 0.908e^{-10.9\eta}$$

These results show conclusively that the two loops have minimal interaction, and that the loop 1 response is strictly due to the slow mode of the system and the loop 2 response is strictly due to the fast mode of the system. What we have here is a control structure that is very close to the modal control structure, as suggested by our previous angle calculations. Also, we see that the lack of decoupling in the internal dynamics of the process that the angle calculations showed is not significant.

The time responses for the EVaCS II low recycle system were also calculated in the format shown in equation (3.15). The Δ_{ij} are shown below and are plotted in figures 13a and 13b.

loop 1 (slow)

$$\Delta_{11}(\eta) = 1.0 - 1.077e^{-1.3\eta} + 0.077e^{-4.8\eta}$$

$$\Delta_{12}(\eta) = 0.0$$

loop 2 (fast)

$$\Delta_{21}(\eta) = - 0.289e^{-1.3\eta} + 0.289e^{-4.8\eta}$$

$$\Delta_{22}(\eta) = 1.0 + 0.366e^{-1.3\eta} - 1.366e^{-4.8\eta}$$

Even though the interaction is slightly greater than the interaction shown in the EVaCS I low recycle system, those conclusions reached there are equally applicable here.

The time responses for the EVaCS II high recycle system are shown below and are plotted in figures 13c and 13d.

loop 1 (slow)

$$\Delta_{11}(\eta) = 1.0 - 1.010e^{-1.1\eta} + 0.010e^{-10.9\eta} \tag{3.20}$$

$$\Delta_{12}(\eta) = 0.0$$

loop 2 (fast)

$$\Delta_{21}(\eta) = - 0.102e^{-1.1\eta} + 0.102e^{-10.9\eta}$$

$$\Delta_{22}(\eta) = 1.0 + 0.112e^{-1.1\eta} - 1.112e^{-10.9\eta}$$

Again, these results show conclusively that the two loops have minimal interaction and the total loop responses are strictly due to their respective modes.

What we have done in this analysis is to show that the use of extensive energy concepts allow for the easy synthesis of <u>two</u> control structures. Both structures have zero steady-state interaction and minimal dynamic interaction. Also, both do a good job of approximating the modal control structure for the process.

The next method used to evaluate the various control systems was McAvoy's [17] dynamic relative gain array. This analysis was used to give a best case ,widely separated loop speeds, and a worst case, that being when the loops are identical, assessment of the interaction present in the given control structure. Note that the analysis is not independent of the controllers' tuning as the weighting of the integral (and possibly derivative) term of the controller affects a loop's speed.

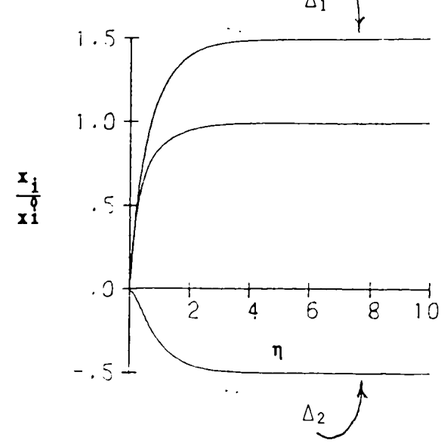

(a)

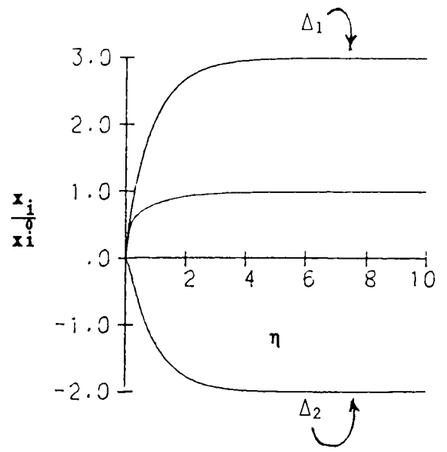

(b)

Fig. 11 Dimensionless Set-Point Responses for IVaCS
in Tank's Low and High Recycle Designs
a-response for both loops, low recycle
b-response for both loops, high recycle

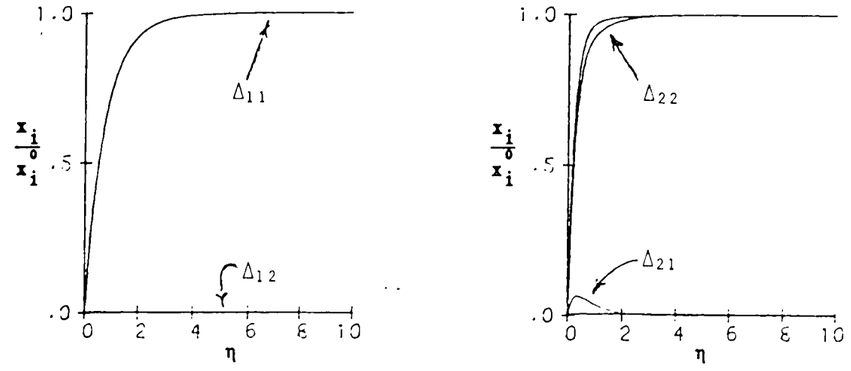

(a)

(b)

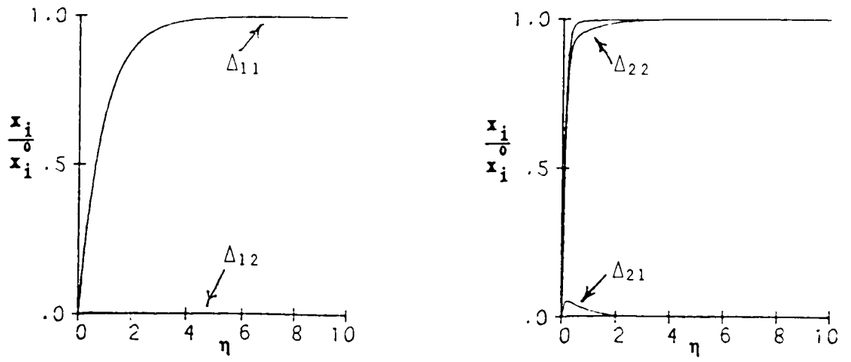

(c)

(d)

Fig. 11 Dimensionless Set-Point Responses for EVaCS I in Tank's Low and High Recycle Designs
a-slow loop, low recycle b-fast loop, low recycle
c-slow loop, high recycle d-fast loop, high recycle

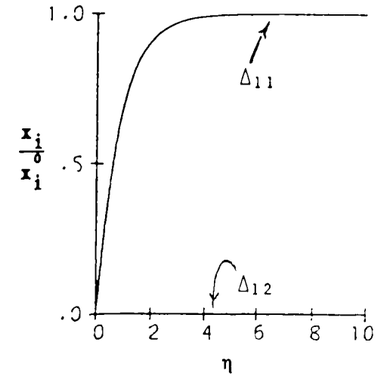

(a)

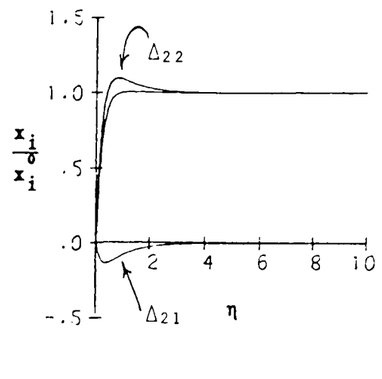

(b)

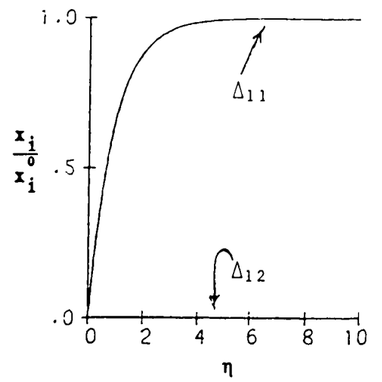

(c)

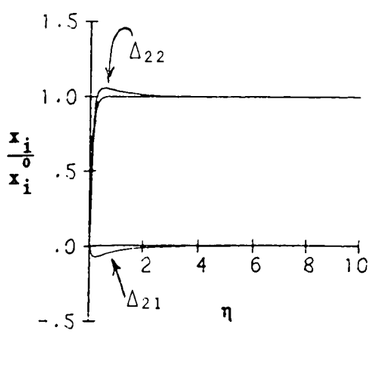

(d)

Fig. 12 Dimensionless Set-Point Responses for EVaCS II in Tank's Low and High Recycle Designs
a-slow loop, low recycle b-fast loop, low recycle
c-slow loop, high recycle d-fast loop, high recycle

The analysis of the IVaCS system began by calculating $\lambda(s)$ for both design cases. These are shown in figures 14a and 14b. Immediately, we notice the magnitude of λ. This indicates that the amount of interaction present within the system is quite significant for both design cases, especially in the high recycle case, whenever one loop is much faster than the other. As the principal transfer functions of the system are identical, as seen in tables 3 and 4, this situation would arise if one loop had a large amount of integral action and the other a small amount. The slower loop, i.e. the one with the large amount of integral action, would have a sluggish response due to its decreased gain. Its phase angle would be decreased, as measured clockwise from the positive real axis, which would increase its natural frequency. These two effects are counteractive as far as the slow loop's response is concerned. The decreased gain indicates a decreased sensitivity of the controlled variable to its manipulated variable while the increased natural frequency indicates a faster speed of response. Both of these effects tend to stabalize the slow loop. As discussed in Chapter 2, the fast loop would not be affected by the interaction.

Figures 14c and 14d show the plot of $\Delta(\lambda)$ for the case where $|\lambda| > 1$ and both loops are identical. As our principal transfer

functions are identical, this situation would correspond to both loops having identical reset times. The Δ plots show that a significant amount of unfavorable interaction would be present within the system for this situation. The loop responses would be highly oscillatory due to the increased gains, and the speed of response would be decreased due to the decreased critical frequency, which is caused by the increased phase angle. Both of these effects tend to decrease loop stability.

The analysis of the EVaCS I system also begin by calculating λ(s) for both design cases. These are shown in figures 15a and 15b, for the respective design cases. The interaction for this situation, i.e. widely separated loop speeds, is minimal to begin with and actually decreases as the recycle rate increases. This is due to the structure becoming a better approximation to the modal control structure for the process, as was discussed previously. These plots of λ show that the interaction in this situation is essentially negligible, thus allowing the two controllers to be tuned independent of one another.

Figures 15c and 15d show the plot of Δ(λ) for the case where $|\lambda| < 1$ and both loops are identical. This situation would correspond to the fast loop having some smaller reset time than the

slow loop. The loop responses would be highly oscillatory due to the increased gains, but the speed of response would remain unchanged due to the negligible phase contribution from the interaction. In tuning the loops as such, it can be seen that they were tuned contrary to the desired goal as the slow loop was made fast and the fast loop was made slow.

The analysis of the EVaCS II structure proceeded in the same fashion as the analyses done for the IVaCS and EVaCS I structures. The plots of $\lambda(s)$ are shown in figures 16a and 16b for the respective design cases. These show that the interaction is essentially negligible when one loop is much faster than the other, and that the interaction decreases with increasing recycle rate (as in EVaCS I).

Figures 16c and 16d show the plots of $\Delta(\lambda)$ for the case where $|\lambda| > 1$ and both loops are identical. Again, this would correspond to the fast loop having some degree more of integral action than the slow loop. The loop responses would be slightly more oscillatory due to the interaction, while the speed of response could be slightly slower or slightly faster depending upon the natural frequency of the loop in its SISO enviroment. This seems to suggest that an optimum reset time could exist for the loops.

This analysis confirms that the EVaCS structures have zero steady-state interaction as $\lambda(0) = 1$ for all cases. This was found to be true originally by Georgakis [5]. The loops in the structures have been shown to exhibit minimal dynamic interaction, also. Insight has been gained into the recommended tuning procedure for the various loops, i.e. keep the loop speeds as wide as possible.

The fourth way of assessing the interaction in the structures was Rosenbrock's [14] inverse Nyquist array. The details of the analysis were discussed in Chapter 2, but will be briefly reviewed. The analysis entails plotting the diagonal elements of $(GK)^{-1}$ as a function of frequency. Insight into the magnitude of the interaction within the system is gained by looking at the system's Gershgorin discs. For this analysis, the controller matrix K was chosen to be $K = \mathrm{diag}(k_i)$, where k_i was taken to be 1 or -1 so as to make the product $g_{ii}k_i > 0$.

INA plots of the diagonal elements of the IVaCS system are shown in figures 17a-b,c-d for the low and high recycle design cases. Column Gershgorin discs are used. These plots show that the system is not column dominant, neither was it row dominant, thus implying that the interaction is significant. It is

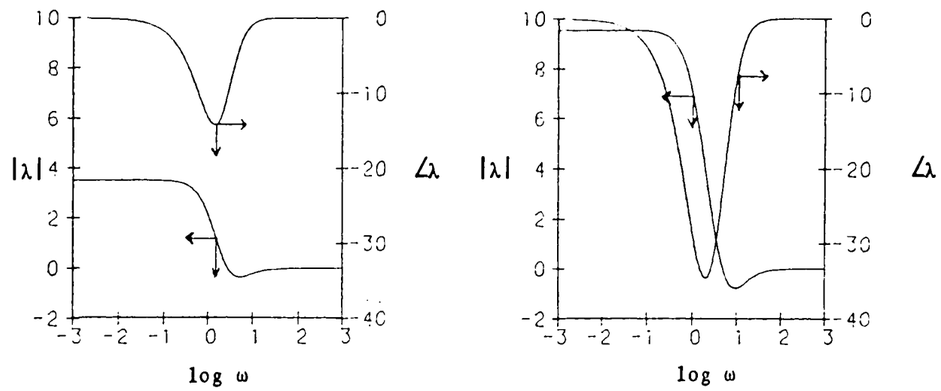

(a)

(b)

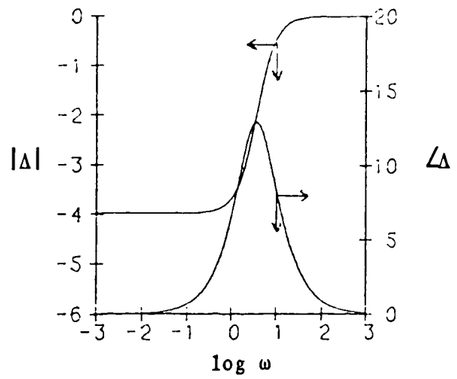

(c)

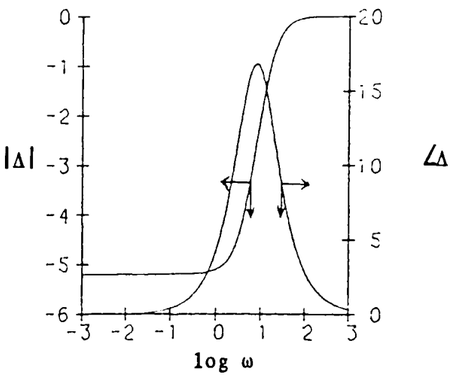

(d)

Fig. 14 Dynamic Relative Gain Array Analyses Plots for IVaCS in Tank's Low and High Recycle Designs
a–Bode plot of λ, low recycle b–Bode plot of λ, high recycle
c–Bode plot of Δ, low recycle d–Bode plot of Δ, high recycle

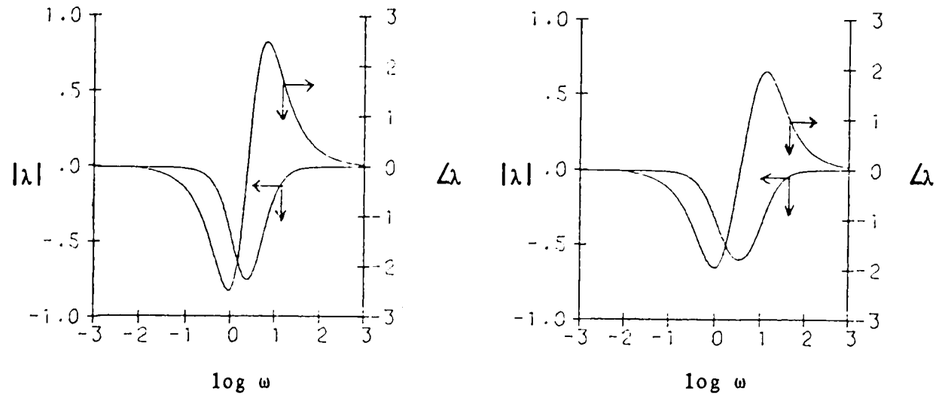

(a)

(b)

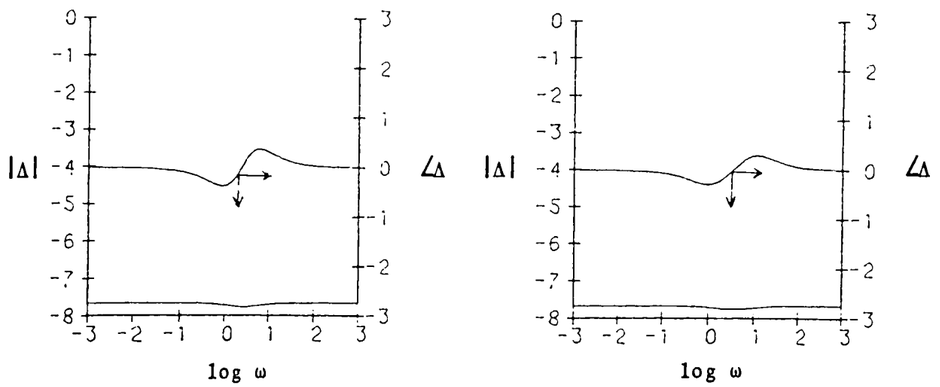

(c)

(d)

Fig. 15 Dynamic Relative Gain Array Analyses Plots for EVaCS I in Tank's Low and High Recycle Designs
a-Bode plot of λ, low recycle b-Bode plot of λ, high recycle
c-Bode plot of Δ, low recycle d-Bode plot of Δ, high recycle

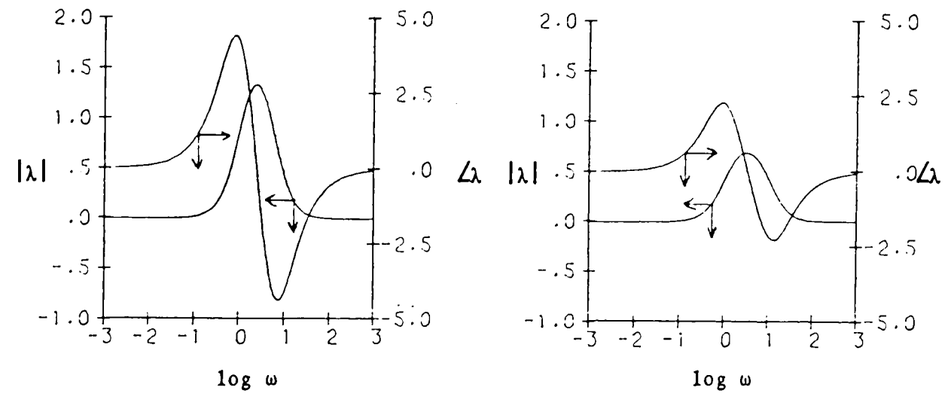

(a)

(b)

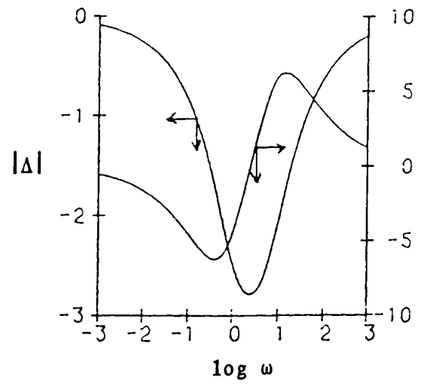

(c)

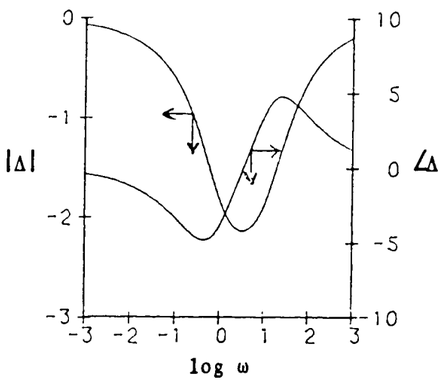

(d)

Fig. 16 Dynamic Relative Gain Array Analyses Plot for EVaCS II in Tank's Low and High Recycle Designs
a-Bode plot of λ, low recycle b-Bode plot of λ, high recycle
c-Bode plot of Δ, low recycle d-Bode plot of Δ, high recycle

interesting to note that $(GK(0))^{-1}_{ii}$ is the reciprocal of what is considered the effective process gain for loop i. As the recycle rate increases, this gain decreases for both loops, thus implying that the sensitivity of the controlled variables to their respective manipulated variables decreases. This is, without a doubt, an undesirable phenomenon.

INA plots with column Gershgorin discs of the diagonal elements of the EVaCS I system are shown in figures 18a-b,c-d. These plots show that the system is very column dominant, thus implying that the interaction is not too great. The sensitivity of the slow loop (loop 1) remains unchanged with the recycle rate, while the sensitivity of the fast loop (loop 2) actually <u>increases</u> with the recycle rate.

The INA plots with column Gershgorin discs for the EVaCS II structure are shown in figure 19a-b,c-d. These plots show that the interaction is not too great here, either. The sensitivity of the slow loop (loop 1) remains unchanged with the recycle rate, while the sensitivity of the fast loop (loop 2) decreases with increasing recycle.

The final analysis method used here was MacFarlane's [15]

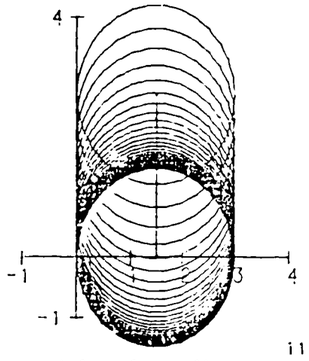

with column discs

(a)

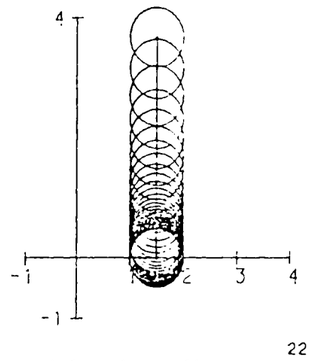

with column discs

(b)

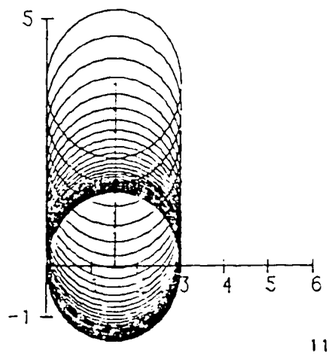

with column discs

(c)

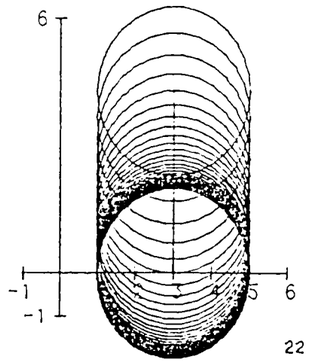

with column discs

(d)

Fig. 17 Inverse Nyquist Array Plots for Diagonal Elements in IVaCS Structure in Tank's Low and High Recycle Designs
a-tank one's loop, low recycle b-tank two's loop, low recycle
c-tank one's loop, high recycle d-tank two's loop, high recycle

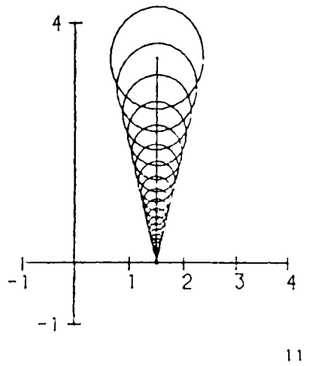

with column discs

(a)

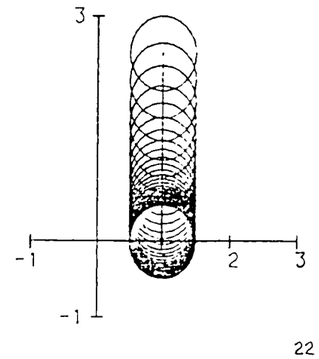

with column discs

(b)

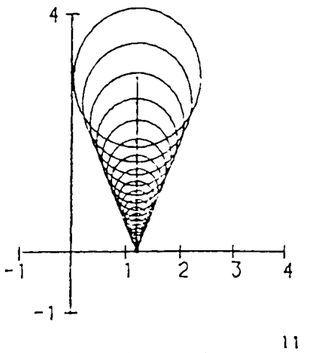

with column discs

(c)

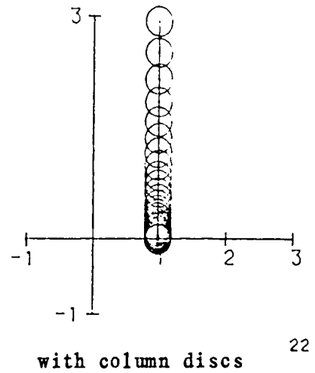

with column discs

(d)

Fig. 18 Inverse Nyquist Array Plot for Diagonal Elements in EVaCS I Structure in Tank's Low and High Recycle Designs
a-slow loop, low recycle b-fast loop, low recycle
c-slow loop, high recycle d-fast loop, high recycle

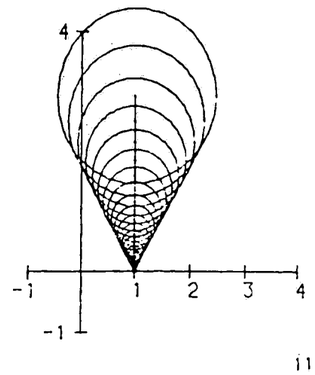

with column discs

(a)

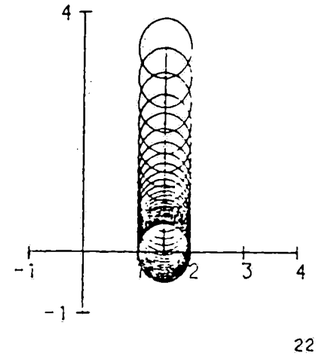

with column discs

(b)

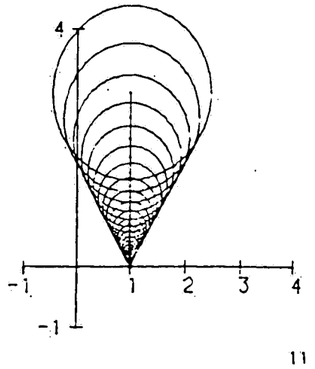

with column discs

(c)

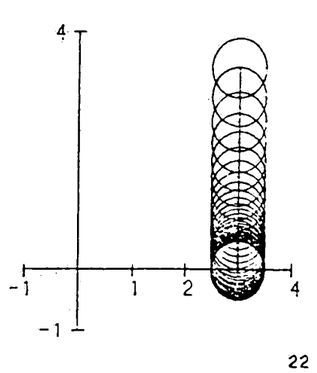

with column discs

(d)

Fig. 19 Inverse Nyquist Array Plot for Diagonal Elements in EVaCS II Structure in Tank's Low and High Recycle Designs
a-slow loop, low recycle b-fast loop, low recycle
c-slow loop, high recycle d-fast loop, high recycle

interaction criteria. The details of this analysis have been discussed previously in Chapter 2. Briefly, the analysis entails looking at the angles between the eigenvectors of Q(s) and the conventional basis vectors, i.e. those vectors corresponding to the columns of the appropriate identity matrix. Non-interacting systems will have eigenvectors that are perfectly aligned with these basis vectors. In this analysis, we took our controller matrix K to be diag(k_i) where k_i was chosen to be 1 or -1 such that the product $k_i g_{ii} > 0$.

The plots of these angles for the IVaCS system are shown in figures 20a-b for the respective design cases. They both show that the interaction within the system is significant and constant independent of frequency. Plots of the interaction angles for the EVaCS I structure are shown in figures 21a-b for the respective design cases. These plots show that the interaction at low frequencies is one-way (technically speaking, this is not termed interaction), and at high frequencies it reverses itself while still remaining one-way. Only in the vicinity of a limited range of frequencies do we have what would be termed interaction, and this is small when compared to the IVaCS. The interaction angles for the EVaCS II system are shown in figures 22a-b for the respective design cases. The discussion given for the EVaCS I

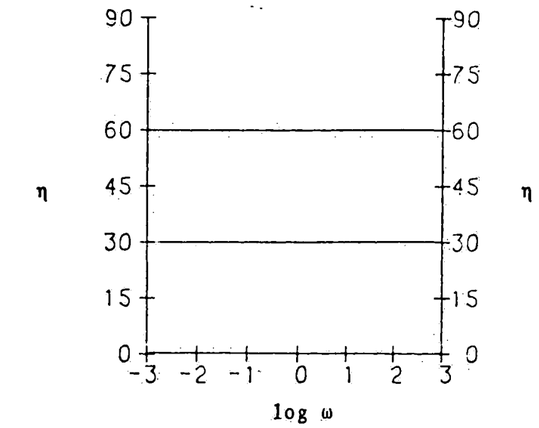

(a)

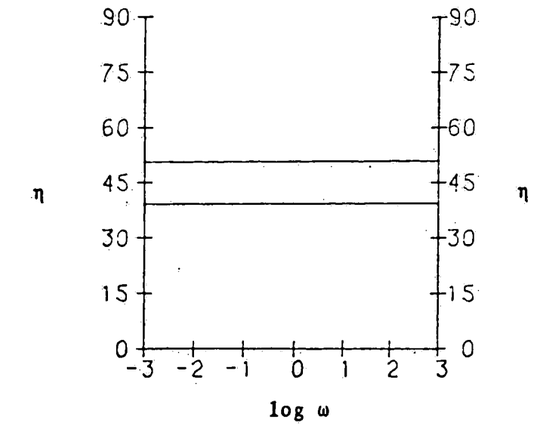

(b)

Fig. 20 Characteristic Loci Interaction Angles in Degrees for IVaCS in Column's Low and High Recycle Designs
a-low recycle b-high recycle

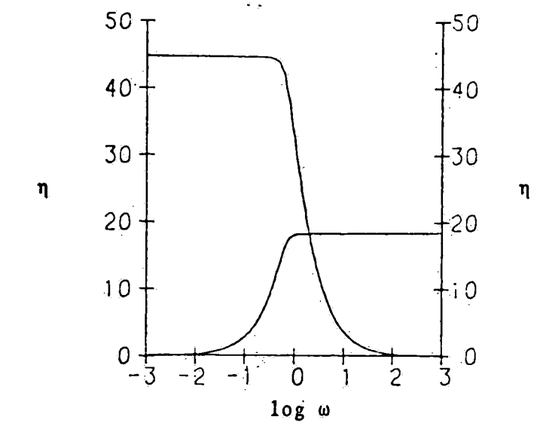

(a)

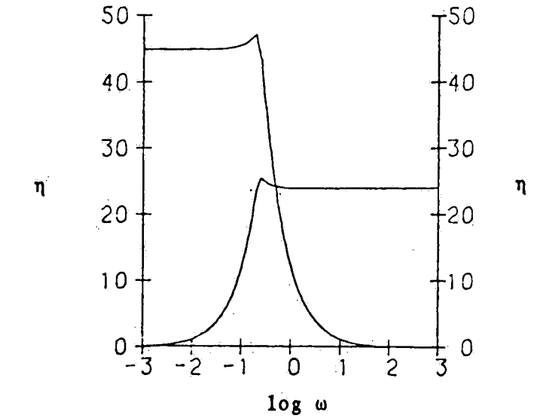

(b)

Fig. 21 Characteristic Loci Interaction Angles in Degrees for EVaCS I in Column's Low and High Recycle Designs
a-low recycle b-high recycle

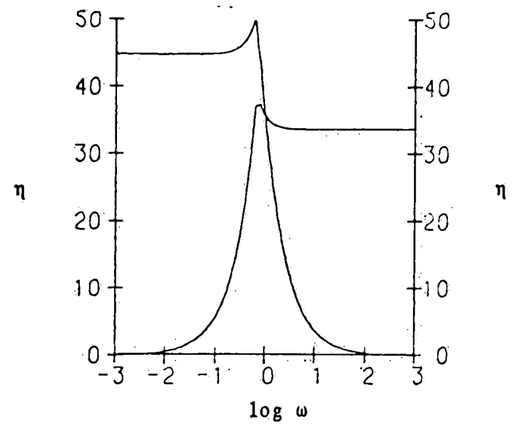

(a)

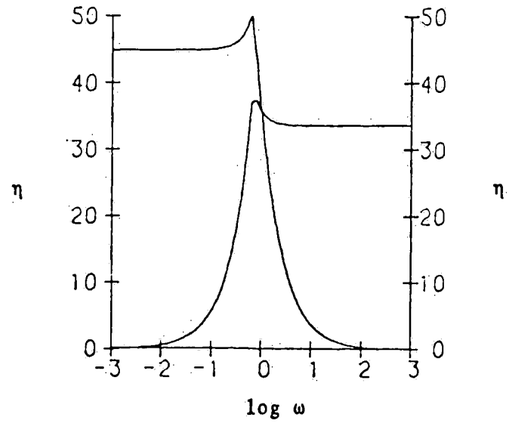

(b)

Fig. 22 Characteristic Loci Interaction Angles in Degrees for EVaCS II in Column's Low and High Recycle Designs
a-low recycle b-high recycle

structure applies here equally well.

As they stand now, the control structures are not of sufficiently high order to be unstable. Thus, as a point of interest, it was decided to add coil and thermocouple dynamics to the process so as to allow for the calculation of gain spaces. Each plant transfer function matrix shown in tables 3 and 4 was post-multiplied by a coil dynamics matrix and pre-multiplied by a thermocouple dynamics matrix, both of which are shown in table 5. The time constant chosen for the coil dynamics was essentially the same as that for the fast mode of the process in the low recycle design. The time constant for the thermocouple dynamics was chosen to be 10% of the time constant for the fast mode in the low recycle design. The gain spaces were calculated for all structures in both the low and high recycle design cases as outlined by MacFarlane [15], and approximations to the gain spaces were calculated as outlined by Rosenbrock [6]. It should be noted that since we are multiplying the process matrices by diagonal matrices, the dynamic relative gain array analysis does not change.

The actual gain space plots for the IVaCS system are shown in figures 23a-b for the respective design cases. As can be seen in figures 24a-b,c-d, this system is not column dominant ,nor was it

Table 5 Coil and Thermocouple Dynamics Matrices
for Stirred-Tanks in Series

Coil $$G_C(s) = \begin{bmatrix} \frac{1}{0.25s+1} & 0 \\ 0 & \frac{1}{0.25s+1} \end{bmatrix}$$

Thermocouple $$G_T(s) = \begin{bmatrix} \frac{1}{0.02s+1} & 0 \\ 0 & \frac{1}{0.02s+1} \end{bmatrix}$$

row dominant, thus no approximation to the gain space could be found from the INA. The shape of the stability limit in these gain spaces confirm what our previous analyses have shown, i.e. the interaction is significant within this structure, especially for the high recycle situation.

The gain spaces for the EVaCS I system are shown in figures 25a-b for the respective design cases. Also, the certain stability (the inner rectangle) and uncertain stability (the outer rectangle) limits which define the approximation to the gain spaces are shown. These limits were calculated from the INA plots shown in figures 26a-b,c-d for the respective design cases. The certain stability limit was calculated by assuming that the given loop transfer function lay on the inner limit, i.e. closest to the origin, defined by the Gershgorin bands. The loop is guarenteed to be stable for all loop proportional gains that are less than the ultimate gain calculated from this inner limit. The uncertain stability limit was calculated by assuming that the loop transfer function lay on the outer limit defined by the the Gershgorin bands. One cannot be sure if the loop will be stable or not if a proportional gain is chosen that lies between the certain and uncertain stability limits. The loop will definitely be unstable if a gain is chosen that is greater than the uncertain limit. The

INA plots shown in figure 26, and used to calculate the limits, were made using column discs. The plots of the gain spaces show that the interaction is negligible, as can be inferred from their shape. The actual gain space is essentially that part of the gain space delineated by the SISO ultimate gains.

The gain spaces for the EVaCS II system are shown in figures 27a-b, while the INA plots with column discs used for the gain space approximations are shown in figures 28a-b,c-d. Again, these plots show that the interaction for this system is negligible.

These analyses have shown that extensive energy concepts have allowed for the synthesis of two controller structures for this system that have zero steady-state interaction and minimal dynamic interaction. These control structures were synthesized easily, and have an intuitive physical appeal. As to which EVaCS structure is better than the other, for our particular design they probably would function equally well. This is founded in the results of the angle calculations and the various other analyses presented. Definitely, either EVaCS structure is superior to the IVaCS structure.

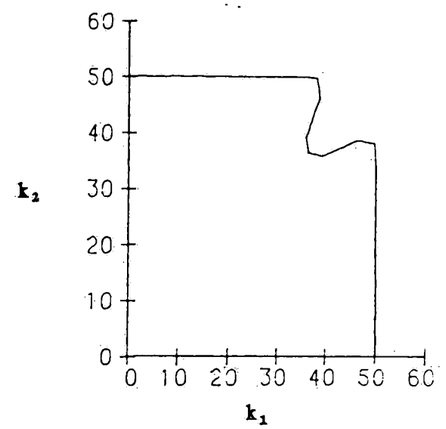

(a)

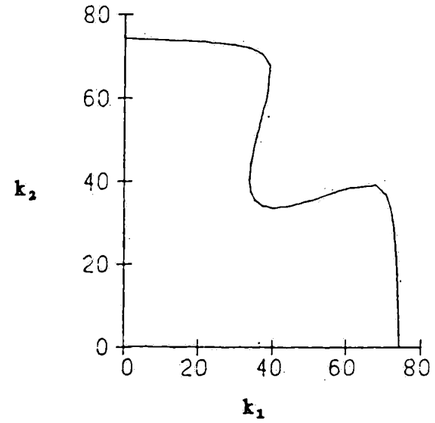

(b)

Fig. 23 Gain Space Plots for IVaCS
in Tank's Low and High Recycle Designs
a-low recycle b-high recycle
k_1 is top loop's proportional gain
k_2 is bottom loop's proportional gain

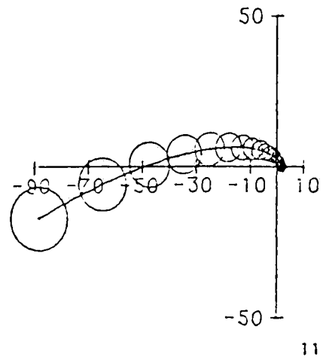

with column discs

(a)

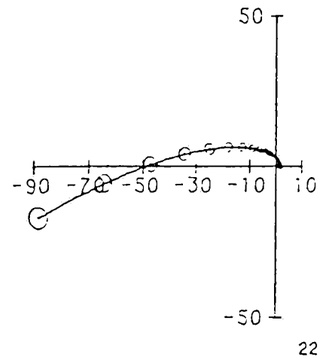

with column discs

(b)

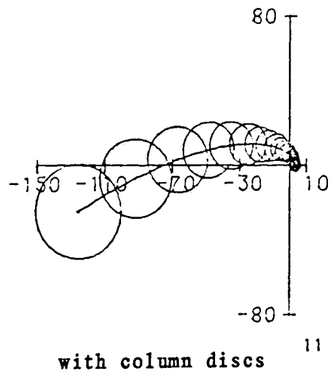

with column discs

(c)

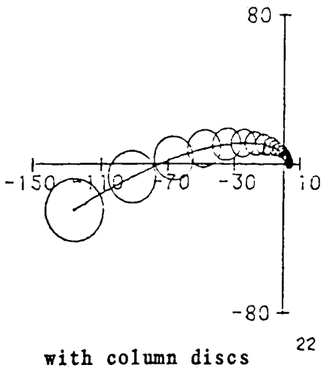

with column discs

(d)

Fig. 24 Inverse Nyquist Array Plots for IVaCS Gain Space Approximations in Tank's Low and High Recycle Designs
a-top loop, low recycle b-bottom loop, low recycle
c-top loop, high recycle d-bottom loop, high recycle

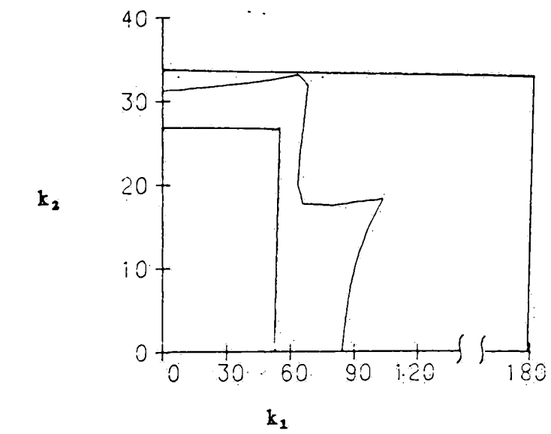

(a)

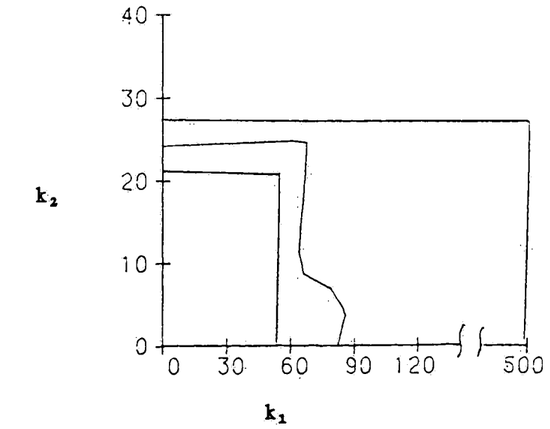

(b)

Fig. 25 Gain Space Plots for EVaCS I
in Tank's Low and High Recycle Designs
a-low recycle b-high recycle
k_1 is top loop's proportional gain
k_2 is bottom loop's proportional gain

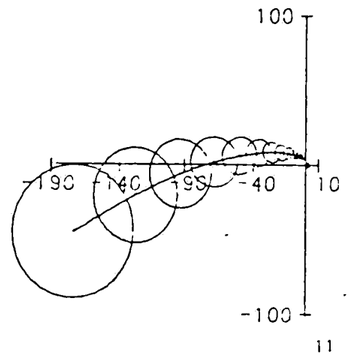

with column discs

(a)

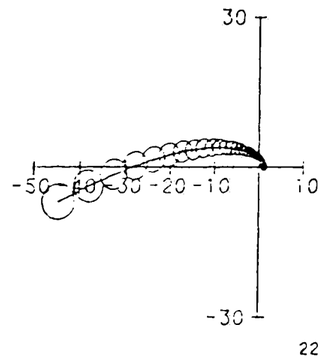

with column discs

(b)

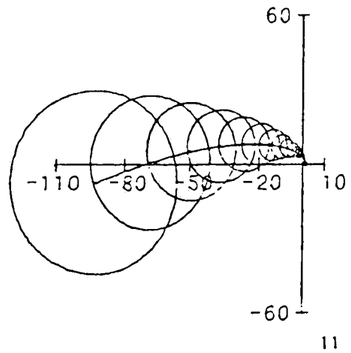

with column discs

(c)

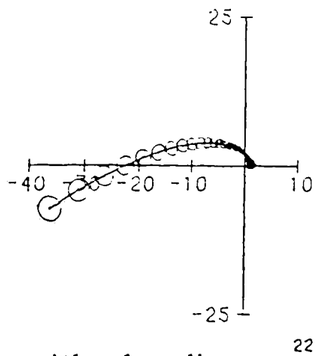

with column discs

(d)

Fig. 26 Inverse Nyquist Array Plots for EVaCS I Gain Space Approximations in Tank's Low and High Recycle Designs
a-top loop, low recycle b-bottom loop, low recycle
c-top loop, high recycle d-bottom loop, high recycle

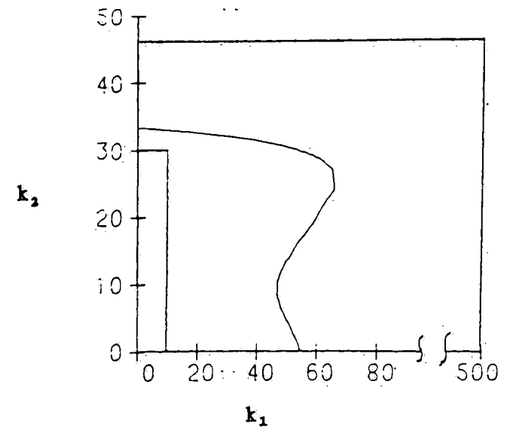

(a)

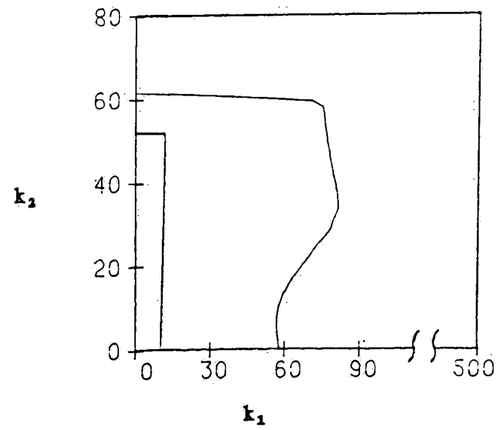

(b)

Fig. 27 Gain Space Plots for EVaCS II in Tank's Low and High Recycle Designs
a-low recycle b-high recycle
k_1 is top loop's proportional gain
k_2 is bottom loop's proportional gain

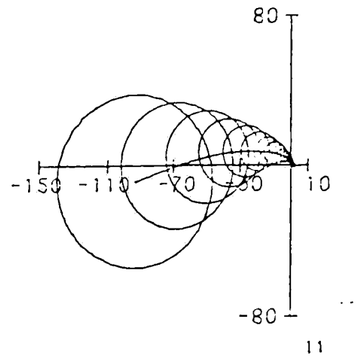

with column discs

(a)

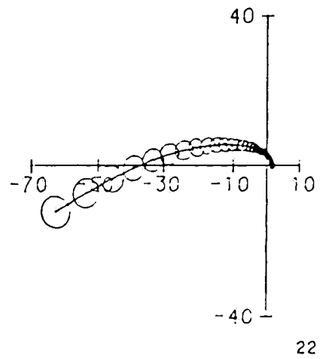

with column discs

(b)

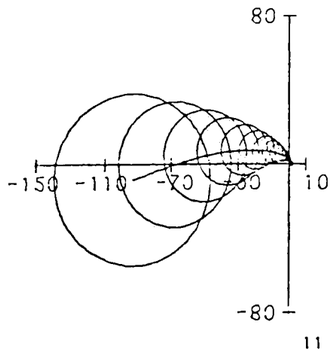

with column discs

(c)

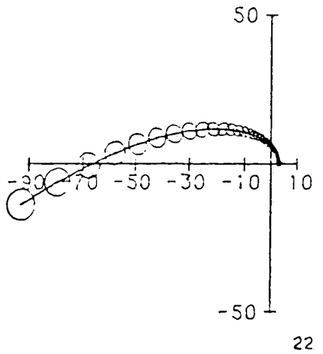

with column discs

(d)

Fig. 28 Inverse Nyquist Array Plots for EVaCS II Gain Space Approximations in Tank's Low and High Recycle Designs
a-top loop, low recycle b-bottom loop, low recycle
c-top loop, high recycle d-bottom loop, high recycle

Chapter 4

A Two Stage Distillation Process

4.1 Definition

The second process examined by this thesis was a two-stage binary distillation column. This system approximates an industrial distillation column in that the rectifying and stripping sections have been lumped into single, very effecient stages. A diagram of the system is shown in Figure 29.

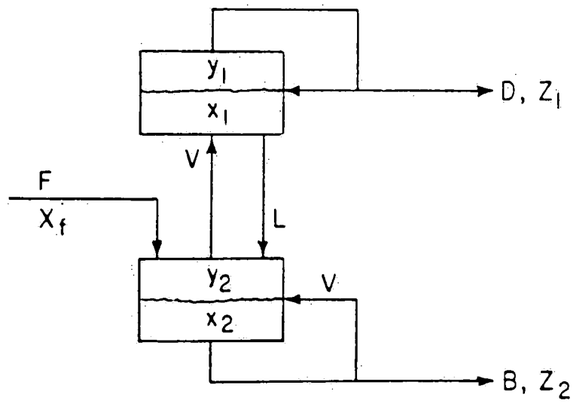

Fig. 29 Two Stage Distillation Process

In figure 29, F is the feed flow to the column, D is the distillate flow, B is the bottoms flow, L is the column's reflux stream, V is the vapor boil-up, z_1 is the distillate's terminal

composition, y_1 is the first stage vapor composition, x_1 is the first stage liquid composition, y_2 is the second stage vapor composition, x_2 is the second stage liquid composition, and z_2 is the bottoms' terminal composition.

In modeling the process, we assume that the feed is at its bubble point, that the column flows are equimolal, and that the trays are 100% efficient. By assuming negligible accumulator holdup and condenser dynamics, such that $y_1 = z_1$, our first-stage material balance over the light component is,

$$M_R \frac{dx_1}{dt} = L(z_1-x_1) - V(z_1-y_2) \tag{4.1}$$

By assuming negligible bottoms holdup and reboiler dynamics, such that $x_2 = z_2$, our second-stage material balance over the light component is,

$$M_S \frac{dx_2}{dt} = L(x_1-z_2) + F(x_f-z_2) - V(y_2-z_2) \tag{4.2}$$

We assume thermodynamic equilibrium relationships of the form,

$$y = H(x) \qquad x = H^{-1}(y) \tag{4.3}$$

Here, H is the relationship that gives the vapor's equilibrium composition in terms of the liquid composition, and H^{-1} is the relationship that gives the liquid's equilibrium composition in terms of the vapor composition. By dividing equations (4.1)-(4.2) through with our steady-state feed rate F, and

multiplying/dividing the capacitance terms by $M_R + M_S$, we obtain the following system of equations describing our process after substituting the relationships from equation (4.3),

$$\gamma\dot{x}_1 = m_1(z_1-H^{-1}(z_1)) - m_2(z_1-H(z_2)) \tag{4.4}$$

$$(1-\gamma)\dot{x}_2 = m_1(H^{-1}(z_1)-z_2) + (x_f-z_2) - m_2(H(z_2)-z_2)$$

Here m_1 is the reflux to feed ratio, m_2 is the vapor boil-up to feed ratio, and the feed rate F is assumed to be constant. Also, γ is the fraction of total column holdup in the rectifying section $[M_R/(M_R+M_S)]$, and time is dimensionless with respect to the column time constant $[F/(M_R+M_S)]$. Linearizing the equations, and expressing the derivatives in terms of z_1 and z_2, we have,

$$\gamma f_{11}\delta\dot{z}_1 \sim -[\frac{D}{F} + m_1 f_{11}]\delta z_1 + m_2 f_{22}\delta z_2 \tag{4.5}$$
$$+ (z_1-f_1)\delta m_1 - (z_1-f_2)\delta m_2$$

$$(1-\gamma)\delta\dot{z}_2 \sim m_1 f_{11}\delta z_1 - [\frac{B}{F} + m_2 f_{22}]\delta z_2 \tag{4.6}$$
$$+(f_1-z_2)\delta m_1 - (f_2-z_2)\delta m_2$$

where $D/F = m_2 - m_1$, $B/F = 1 - D/F$, f_{11} is the derivative of the inverse relationship shown in equation (4.3) with respect to z_1 evaluated at the steady-state z_1, f_{22} is the derivative of the assumed relationship H shown in equation (4.3) with respect to z_2 evaluated at the steady-state z_2, f_1 is the first stage light component liquid composition and is equal to $H^{-1}(z_1)$, and f_2 is the second stage light component vapor composition which is equal to

$H(z_2)$.

Equations (4.5)-(4.6) represent the expanded form of our state-space model. Writing these equations in the form of equation (1.1), we have the terminal compositions as our state vector, our input vector having m_1 and m_2 as its elements, and the following plant matrix and input matrix,

$$A = \begin{bmatrix} -\left(\frac{D}{F} + m_1 f_{11}\right) & m_2 f_{22} \\ \hline \gamma f_{11} & \gamma f_{11} \\ \\ \frac{m_1 f_{11}}{1-\gamma} & -\left(\frac{B}{F} + m_2 f_{22}\right) \\ & \hline 1-\gamma \end{bmatrix} \qquad (4.7)$$

$$B = \begin{bmatrix} \frac{z_1 - f_1}{\gamma f_{11}} & -\frac{(z_1 - f_2)}{\gamma f_{11}} \\ \\ \frac{f_1 - z_2}{1-\gamma} & -\frac{(f_2 - z_2)}{1-\gamma} \end{bmatrix}$$

We can obtain our plant transfer function matrix as shown in equation (3.4).

Two different designs were used in this research. In both designs, it was assumed that the two components in the system had a constant relative volatility, α. The designs themselves were specified using a symmetry factor ω, and a separation factor s, both of which are shown below.

$$\omega = \frac{1 + z_1}{z_2} \qquad s = \frac{z_1(1-z_2)}{z_2(1-z_1)} \qquad (4.8)$$

The first design case was chosen to be an easy separation, i.e. small flows within the column such that both terminal compositions were of a low purity. The second design case was chosen to be a difficult separation, i.e. large flows within the column. This design gave high purity terminal compositions relative to the previous design. The corresponding steady-state model parameters are shown in table 6. In both designs, the column flows are such that D/F = B/F.

Figure 30a shows a plot of the system eigenvalues as a function of γ in the low purity design case. As can be seen, the eigenvalues are the least separated when $\gamma \sim 0.5$. This corresponds to the rectifying and stripping sections having approximately the same holdups. Figure 30b shows the corresponding plot of the eigenvalues in the high purity design case. As can be seen in the plot, the eigenvalues are widely separated for all values of γ. Again, these eigenvalues are the least separated when $\gamma \sim 0.5$. With this in mind, γ was choosen to be 0.5 in both design cases. The various design specifications used are summarized below.

Case I Easy Separation, Low Purity
$\gamma = 0.5$ $x_f = 0.5$ $\omega = 1.0$ $\alpha = 3.0$ $s = 4.5$

Case II Difficult separation, High Purity
$\gamma = 0.5$ $x_f = 0.5$ $\omega = 1.0$ $\alpha = 10.0$ $s = 99.01$

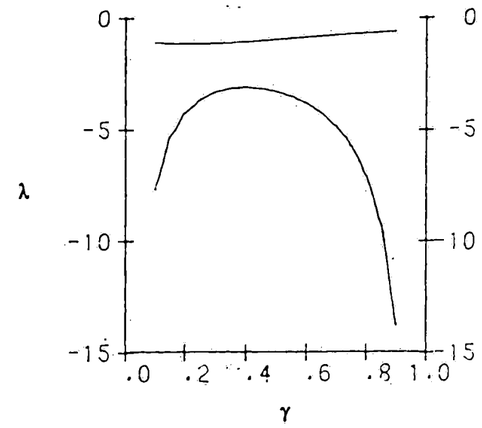

(a)

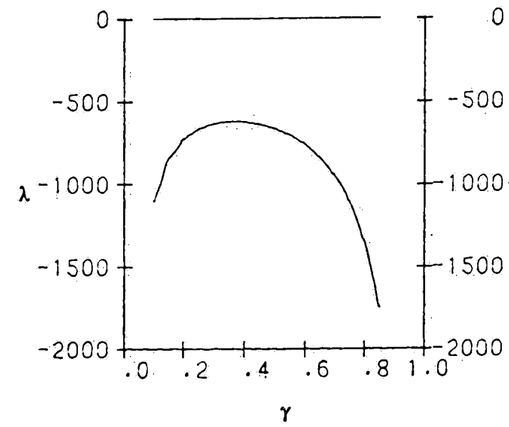

(b)

Fig. 30 Eigenvalues of Distillation Process as a Function of γ

Table 6 Linearized Model Parameters for Distillation Design Cases

	Low Purity Separation	High Purity Separation
z_1	0.68	0.91
z_2	0.32	0.09
m_1	0.27	81.89
m_2	0.77	82.39
$\frac{D}{F}$	0.50	0.50
$\frac{B}{F}$	0.50	0.50
f_1	0.41	0.499
f_2	0.59	0.501
f_{11}	1.11	3.01
f_{22}	1.11	3.01

Low Purity Design Specifications

$\gamma = 0.5 \quad x_f = 0.5 \quad \omega = 1.0 \quad \alpha = 3.0 \quad s = 4.5$

High Purity Design Specifications

$\gamma = 0.5 \quad x_f = 0.5 \quad \omega = 1.0 \quad \alpha = 10.0 \quad s = 99.01$

We will use three of the conventional control schemes typcially used in controlling distillation processes. One is known as an energy balance scheme, and the other two are known as material balance schemes. All three control the terminal compositions. These structures are intensive variable in nature, and their output coordination vectors are shown below.

$$h_1^T = (1,0) \qquad (4.9)$$

$$h_2^T = (0,1)$$

Our respective controlled variables s_i can be found as shown in equation (3.5). In order to establish the candidate physical modes, or output vectors, for use in the EVaCS structures, we employ the following extensive material concepts.

1. material balance of rectifying section
2. material balance of stripping section
3. material content of total column

If we want to control the rectifying balance, we simply measure that combination of states shown in equation (4.5),

$$h_3^T = (\frac{D}{F} + m_1 f_{11}, -m_2 f_{22}) \qquad (4.10)$$

Again, what matters in this selection is the way the two states are weighted in the output vector. To control the stripping balance, we have,

$$h_4^T = (-m_1 f_{11}, \frac{B}{F} + m_2 f_{22}) \qquad (4.11)$$

The total content of the column will be proportional to,

$$\gamma x_1 + (1-\gamma)x_2 \tag{4.12}$$

Perturbing this equation and expressing it in terms of the terminal compositions, we have,

$$\gamma f_{11}\delta z_1 + (1-\gamma)\delta z_2 \tag{4.13}$$

Thus, the physical mode for our total energy content is,

$$h_s^T = (\gamma f_{11}, 1-\gamma) \tag{4.14}$$

Table 7 summarizes the various output coordination vectors for this process.

The next step that we need to take is towards establishing our manipulated variables. The energy balance scheme uses the reflux rate to control the top composition, while the boil-up rate is used to control the bottom composition. Thus, we have,

$$p_1^T = (1,0) \tag{4.15}$$
$$p_2^T = (0,1)$$

Our manipulated variables can be found as shown in equation (3.10) using our system input vector. This structure will be known as the L,V structure. One of the material balance structures, which we will term the D,V structure, controls the top composition by the distillate flow rate, while the bottoms composition is

controlled with the boil-up rate. Thus, we have the following input coordination vectors for this system,

$$p_3^T = (-1,1) \qquad (4.16)$$
$$p^T = (0,1) = p_2^T$$

The other material balance scheme controls the top composition using the reflux flow, while the bottoms flow rate is used to control the bottoms composition. This structure is termed the L,B structure, and its input vectors are defined as,

$$p^T = (1,0) = p_1^T \qquad (4.17)$$
$$p_4^T = (1,-1)$$

The input coordination vector used to control the rectifying balance for the EVaCS structure is found from the steady-state part of equation (4.5). Using the linear combination of system inputs present in the equation, we have,

$$p_5^T = [z_1-f_1,-(z_1-f_2)] \qquad (4.18)$$

Likewise, the input vector used to control the stripping balance is defined as,

$$p_6^T = [f_1-z_2,-(f_2-z_2)] \qquad (4.19)$$

In pairing a manipulated variable with the total column content controlled variable, we have at our disposal any of the four flows in the column, i.e. D, B, L, or V. We arbitrarily choose the

distillate flow rate to control the total content of the column. Thus, we have,

$$p^T = (-1,1) = p_3^T \tag{4.20}$$

Again, as stated previously, the most important part of the synthesis procedure is the proper choice of controlled variables. Table 8 summarizes the input coordination vectors.

4.2 Results and Discussion

Figures 31a-d show the angles as a function of γ between the IVaCS output coordination vectors and the slow math mode and fast math mode, respectively. These calculations show that only one of these output vectors approximates the slow mathematical mode and this only when one section of the column is much smaller than the other. Neither output vector ever approximates the fast mode of the column. Thus, the three IVaCS structures do not approximate the modal control structure for the process in either of the two design cases.

In establishing an EVaCS structure, we have at our disposal any two combinations of the three possible candidate physical modes shown in table 7. Figure 32a,c shows the angles as a function of γ between the total content physical mode, h_s, and the system's slow mathematical mode in the low and high purity cases, respectively.

Table 7 Summary of Output Coordination Vectors for Distillation Column

$h_1^T = (1,0)$	Intensive variable output vector for controlling distillate's composition
$h_2^T = (0,1)$	Intensive variable output vector for controlling bottom's compostion
$h_3^T = [\frac{D}{F} + m_1 f_{11}, -m_2 f_{22}]$	Extensive variable output vector for controlling rectifying section's material balance
$h_4^T = [-m_1 f_{11}, \frac{B}{F} + m_2 f_{22}]$	Extensive variable output vector for controlling stripping section's material balance
$h_5^T = (\gamma, 1-\gamma)$	Extensive variable output vector for controlling total material content

Table 8 Summary of Input Coordination Vectors for Distillation Column

$p_1^T = (1,0)$	Input vector representing the reflux rate
$p_2^T = (0,1)$	Input vector representing the boil-up rate
$p_3^T = (-1,1)$	Input vector representing the distillate rate
$p_4^T = (1,-1)$	Input vector representing the bottoms rate
$p_5^T = [z_1-f_1,-(z_1-f_2)]$	Input vector for controlling rectifying section's material balance
$p_6^T = [f_1-z_2,-(f_2-z_2)]$	Input vector for controlling stripping section's material balance

Figure 32b,d show the angles between the slow mode and the material balance modes, h_3 and h_4, in both design cases. As can be seen, the total content mode gives a good approximation to the slow mathematical mode in the low purity design while it essentially is the slow mode in the high purity design. The material balance modes do not give approximations to the system's slow mode. Figure 33a,c show the angles as a function of γ between the total content physical mode and the system's fast mathematical mode in the respective design cases. As can be seen, the total content does not give an approximation to the fast mode. The angles between the material balance contents and the fast mathematical mode are shown in Figure 33b,d. These physical modes approximate the fast eigenrow reasonably well for the low purity separation, and they essentially are the fast eigenrow in the high purity separation.

Considering these angle calculations, we arrive at two EVaCS structures for this system. Along with the IVaCS structures, they are summarized below.

	Output Coordination Vector	Input Coordination Vector
L,V	h_1	p_1
	h_2	p_2
D,V	h_1	p_3
	h_2	p_2

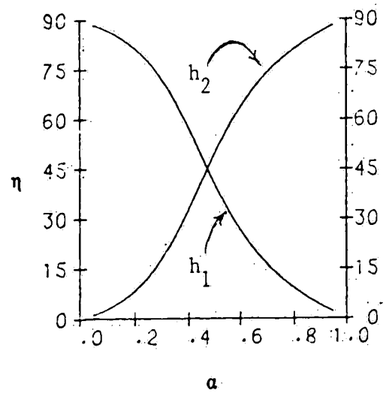

(a)

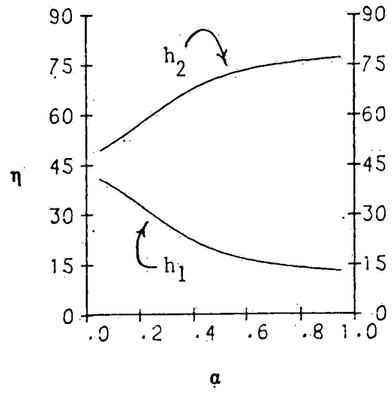

(b)

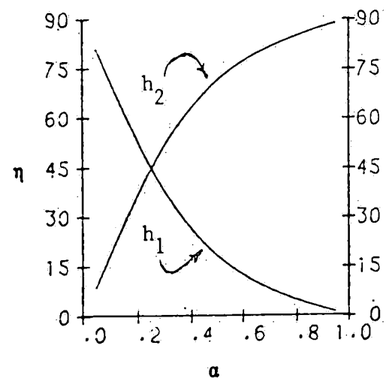

(c)

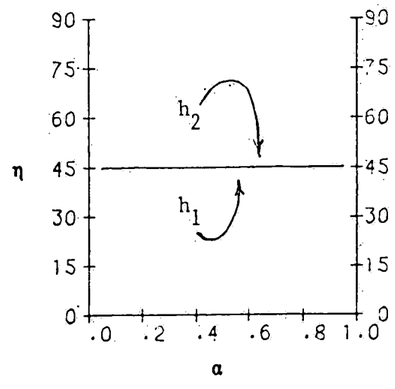

(d)

Fig. 31 Angle Calculations in Degrees for Column's Slow,Fast Modes' Eigenrow with IVaCS Output Vectors, h_1 and h_2
a-with slow mode, low purity b-with fast mode, low purity
c-with slow mode, high purity d-with fast mode, high purity

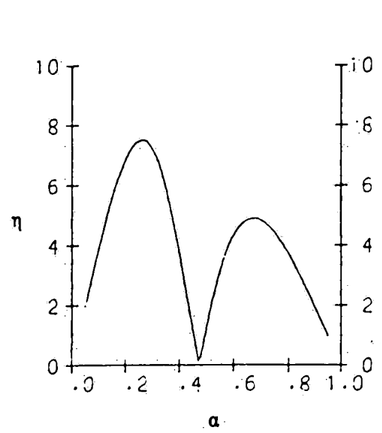

(a)

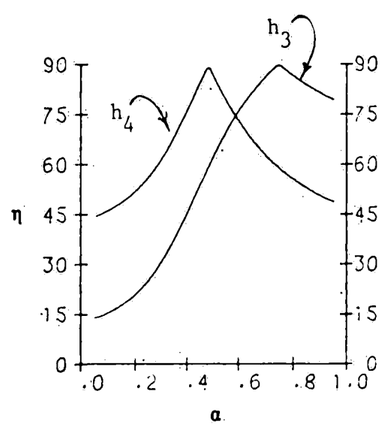

(b)

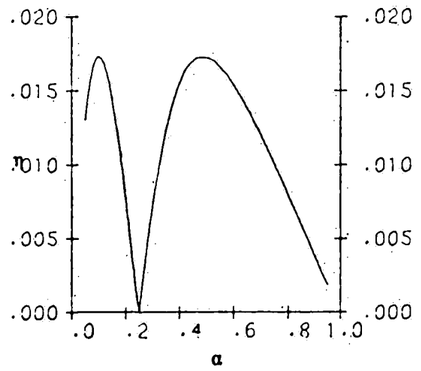

(c)

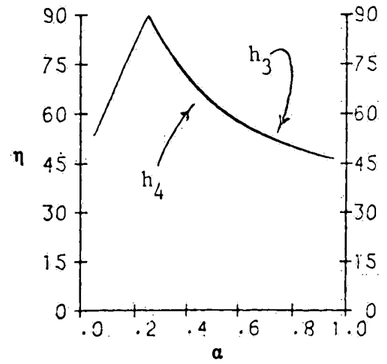

(d)

Fig. 32 Angle Calculations in Degrees for Column's Slow Mode's Eigenrow with EVaCS Output Vectors, h_3,h_4 and h_5
a–with h_5, low purity b–with h_3,h_4, low purity
c–with h_5, high purity d–with h_3,h_4, high purity

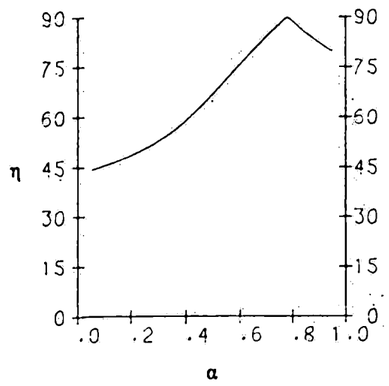

(a)

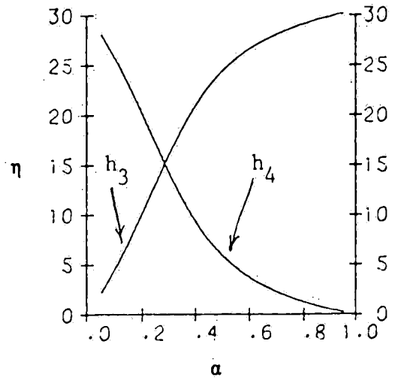

(b)

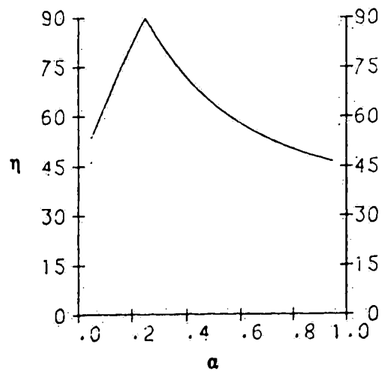

(c)

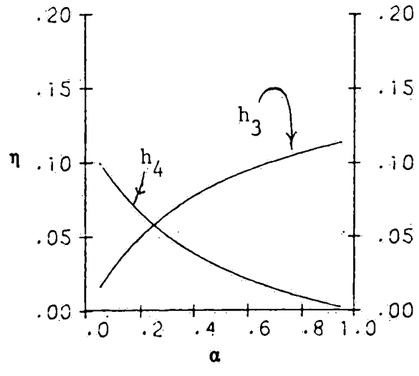

(d)

Fig. 33 Angle Calculations in Degrees for Column's Fast Mode's Eigenrow with EVaCS Output Vectors, h_3,h_4 and h_5
a–with h_5, low purity b–with h_3,h_4, low purity
c–with h_5, high purity d–with h_3,h_4, high purity

L,B	h_1	p_1
	h_2	p_4
EVaCS I	h_3	p_5
	h_5	p_3
EVaCS II	h_4	p_6
	h_5	p_3

We have already shown that the various IVaCS structures, i.e. the energy balance scheme and the two material balance schemes, do not approximate the process' modal control structure. Therefore, we would not expect them to decouple the column's internal dynamics. The EVaCS structures seem to do a respectable job of approximating the column's modal control structure. A plot of the angles as a function of γ between the total content physical mode and the fast eigenvector is shown in Figure 34a,c for the respective design cases, while a plot of the rectifying(stripping)/slow eigenvector angles is shown in Figure 34b,d. As all of the angles are essentially ninety degrees for our particular designs, the EVaCS structures have decoupled the internal dynamics of the process. The rectifying content physical mode for the EVaCS I structure seems to be lacking somewhat in the low purity separation, but the extent of this interaction remains to be seen.

Table 9 summarizes the plant transfer function matrices for

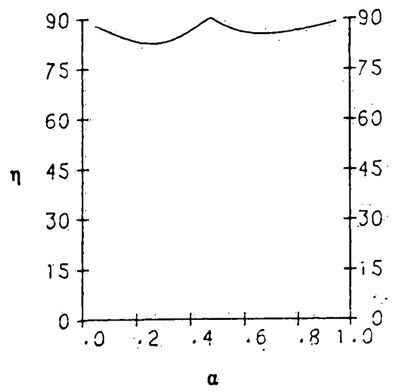

(a)

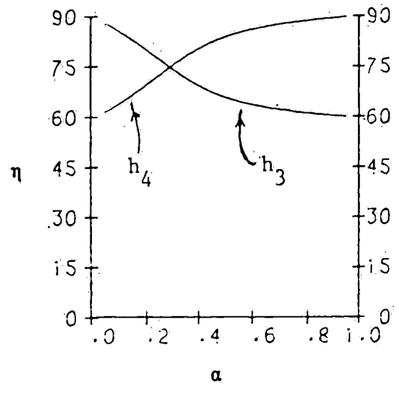

(b)

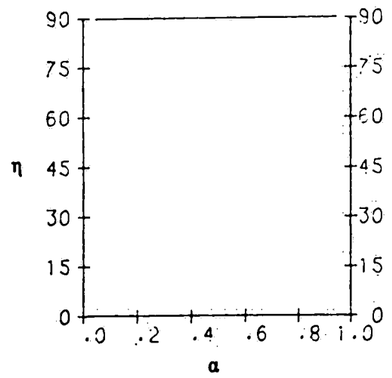

(c)

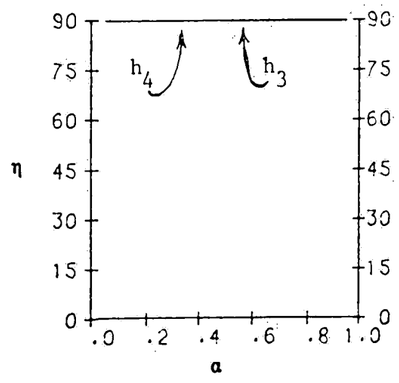

(d)

Fig. 34 Angle Calculations for Slow, Fast Modes' Eigenvectors with EVaCS Physical Modes in Column's Low, High Purity Separations
a-fast mode with h_3,low b-slow mode with h_3,h_4,low
c-fast mode with h_3,high d-slow mode with h_3,h_4,high

the various structures in the low purity separation design case. Table 10 summarizes the same for the high purity separation case. Appendix II contains a summary for both design cases of the various plant matrices and input matrices for use in their respective state-space models. Notice that these EVaCS structures were derived using physical modes based on the light component. The same results would have been found had material balances been made over the heavy component.

The modal analysis of Tung and Edgar [13] has been described previously. The forthcoming analyses of the various structures in the low and high purity separations were done using the transfer function matrices shown in tables 9-10. All time responses were calculated as,

$$\frac{x_i}{x_i^s} = \Delta_{i1} + \Delta_{i2}$$

where Δ_{ij} is the contribution given by controller j to the response of output i.

The time response for the L,V structure's low purity separation design case was calculated as,

loop 1 (top) (4.21)

$$\Delta_{11}(\eta) = 2.086 - 2.107e^{-0.9\eta} + 0.021e^{-3.2\eta}$$

$$\Delta_{12}(\eta) = -1.086 + 1.332e^{-0.9\eta} - 0.246e^{-3.2\eta}$$

Table 9 Plant Transfer Function Matrices for
Distillation Column
Low Purity Design Case

$\gamma = 0.5 \quad x_f = 0.5 \quad \omega = 1.0 \quad \alpha = 3.0 \quad s = 4.5$

$\lambda_1 = -0.92125 \qquad \lambda_2 = -3.24688$

$d(s) = (s - \lambda_1)(s - \lambda_2)$

L,V $\quad G(s) = \frac{1}{d(s)} \begin{bmatrix} 0.476(s+3.333) & -0.168(s+7.560) \\ 0.188(s+2.991) & -0.531(s+1.638) \end{bmatrix}$

D,V $\quad G(s) = \frac{1}{d(s)} \begin{bmatrix} -0.476(s+3.333) & 0.308(s+1) \\ -0.188(s+2.991) & -0.343(s+0.897) \end{bmatrix}$

L,B $\quad G(s) = \frac{1}{d(s)} \begin{bmatrix} 0.308(s+1.0) & 0.168(s+7.560) \\ -0.343(s+0.897) & 0.531(s+1.638) \end{bmatrix}$

EVACS I $\quad G(s) = \frac{1}{d(s)} \begin{bmatrix} -0.359(s+3.168) & 0.103 \\ 0.619s & 3.168(s+0.944) \end{bmatrix}$

EVACS II $\quad G(s) = \frac{1}{d(s)} \begin{bmatrix} -0.359(s+3.271) & -0.103 \\ 0.196s & 3.271(s+0.914) \end{bmatrix}$

Table 10 Plant Transfer Function Matrices for
Distillation Column
High Purity Design Case

$\gamma = 0.5 \quad x_f = 0.5 \quad \omega = 1.0 \quad \alpha = 10.0 \quad s = 99.01$

$\lambda_1 = -0.49753 \qquad \lambda_2 = -661.14518$

$d(s) = (s - \lambda_1)(s - \lambda_2)$

L,V $\quad G(s) = \frac{1}{d(s)} \begin{bmatrix} 0.272(s+991.0) & -0.270(s+997.0) \\ 0.815(s+328.9) & -0.820(s+326.9) \end{bmatrix}$

D,V $\quad G(s) = \frac{1}{d(s)} \begin{bmatrix} -0.272(s+991.0) & 0.002(s+1) \\ -0.815(s+328.9) & -0.005(s+0.332) \end{bmatrix}$

L,B $\quad G(s) = \frac{1}{d(s)} \begin{bmatrix} 0.002(s+1.0) & 0.270(s+997.0) \\ -0.005(s+0.332) & 0.820(s+326.9) \end{bmatrix}$

EVACS I $\quad G(s) = \frac{1}{d(s)} \begin{bmatrix} -0.817(s+660.6) & 0.668 \\ 405.8s & 660.6(s+0.498) \end{bmatrix}$

EVACS II $\quad G(s) = \frac{1}{d(s)} \begin{bmatrix} -0.817(s+661.3) & -0.668 \\ 133.9s & 661.3(s+0.497) \end{bmatrix}$

loop 2 (bottom)

$$\Delta_{21}(\eta) = -1.086 + 1.049e^{-0.9\eta} + 0.037e^{-3.2\eta}$$

$$\Delta_{22}(\eta) = 2.086 - 1.274e^{-0.9\eta} - 0.812e^{-3.2\eta}$$

The response for the high purity separation case was,

(4.22)

loop 1 (top)

$$\Delta_{11}(\eta) = 81412.6 - 81433.0e^{-0.5\eta} + 20.4e^{-661.1\eta}$$

$$\Delta_{12}(\eta) = -81411.6 + 81432.2e^{-0.5\eta} - 20.6e^{-661.1\eta}$$

loop 2 (bottom)

$$\Delta_{21}(\eta) = -81411.6 + 81349.7e^{-0.5\eta} + 61.9e^{-661.1\eta}$$

$$\Delta_{22}(\eta) = 81412.6 - 81349.9e^{-0.5\eta} - 62.7e^{-661.1\eta}$$

These responses are plotted in Figures 35a-b,c-d, respectively. In the low purity separation, the interaction within this structure is significant, and it becomes enormous in the high purity case. In both design cases, the controllers fight each other.

The time response for the D,V structure's low purity separation design case is shown below,

(4.23)

loop 1 (top)

$$\Delta_{11}(\eta) = 0.739 - 0.746e^{-0.9\eta} + 0.007e^{-3.2\eta}$$

$$\Delta_{12}(\eta) = 0.261 - 0.029e^{-0.9\eta} - 0.232e^{-3.2\eta}$$

loop 2 (bottom)

$$\Delta_{21}(\eta) = 0.261 - 0.252e^{-0.9\eta} - 0.009e^{-3.2\eta}$$

$$\Delta_{22}(\eta) = 0.739 + 0.027e^{-0.9\eta} - 0.766e^{-3.2\eta}$$

The time response for the high purity case was,

loop 1 (top)

$$\Delta_{11}(\eta) = 0.502 - 0.502e^{-0.5\eta}$$

$$\Delta_{12}(\eta) = 0.498 - 0.251e^{-0.5\eta} - 0.247e^{-661.1\eta} \qquad (4.24)$$

loop 2 (bottom)

$$\Delta_{21}(\eta) = 0.498 - 0.498e^{-0.5\eta}$$

$$\Delta_{22}(\eta) = 0.502 + 0.250e^{-0.5\eta} - 0.752e^{-661.1\eta}$$

These responses are plotted in Figures 36a-b,c-d, respectively. The interaction in the low purity case is tolerable, but in the high purity case both controllers give essentially the same steady-state contributions to the system outputs. Thus, one would want to decouple this system, if possible.

The low purity separation time response for the L,B structure is plotted in Figures 37a-b, and is shown below,

loop 1 (top)

$$\Delta_{11}(\eta) = 0.404 - 0.044e^{-0.9\eta} - 0.360e^{-3.2\eta}$$

$$\Delta_{12}(\eta) = 0.596 - 0.731e^{-0.9\eta} + 0.135e^{-3.2\eta} \qquad (4.25)$$

loop 2 (bottom)

$$\Delta_{21}(\eta) = 0.596 + 0.022e^{-0.9\eta} - 0.618e^{-3.2\eta}$$

$$\Delta_{22}(\eta) = 0.404 - 0.247e^{-0.9\eta} - 0.157e^{-3.2\eta}$$

The high purity separation time response is shown below, and is plotted in Figures 37c-d.

loop 1 (top)

$$\Delta_{11}(\eta) = 0.498 - 0.251e^{-0.5\eta} - 0.247e^{-661.1\eta} \qquad (4.26)$$

$$\Delta_{12}(\eta) = 0.502 - 0.502e^{-0.5\eta}$$

loop 2 (bottom)

$$\Delta_{21}(\eta) = 0.502 + 0.250e^{-0.5\eta} - 0.752e^{-661.1\eta}$$

$$\Delta_{22}(\eta) = 0.498 - 0.498e^{-0.5\eta}$$

As can be seen, the interacting controller's contribution is greater than the principle controller's contribution in all cases. This is totally unacceptable.

The time response for the EVaCS I low purity separation case is shown below.

loop 1 (slow) (4.27)

$$\Delta_{11}(\eta) = 1.0 - 0.990e^{-0.9\eta} - 0.010e^{-3.2\eta}$$

$$\Delta_{12}(\eta) = 0.0$$

loop 2 (fast)

$$\Delta_{21}(\eta) = 0.024e^{-0.9\eta} - 0.024e^{-3.2\eta}$$

$$\Delta_{22}(\eta) = 1.0 - 0.034e^{-0.9\eta} - 0.966e^{-3.2\eta}$$

The high purity separation time response was,

loop 1 (slow) (4.28)

$$\Delta_{11}(\eta) = 1.0 - 1.0e^{-0.418\eta}$$

$$\Delta_{12}(\eta) = 0.0$$

loop 2 (fast)

$$\Delta_{21}(\eta) = 0.0$$

$$\Delta_{22}(\eta) = 1.0 - 1.0e^{-661.1\eta}$$

These responses are plotted in Figures 38a-b,c-d, respectively. This analysis shows us three significant points. The first is that

there is no steady-state interaction in the structure for either design case. Also, their is essentially no dynamic interaction in the low purity separation, and none at all in the high purity separation. Finally, we see conclusively that the slow loop's response is strictly associated with the slow mode of the system, while the fast loop's response is strictly associated with the fast mode of the system.

The time response for the EVaCS II structure's low purity separation case is shown below and plotted in Figures 39a-b.

(4.29)

loop 1 (slow)
$\Delta_{11}(\eta) = 1.0 - 1.002e^{-0.9\eta} + 0.002e^{-3.2\eta}$

$\Delta_{12}(\eta) = 0.0$

loop 2 (fast)
$\Delta_{21}(\eta) = - 0.007e^{-0.9\eta} + 0.007e^{-3.2\eta}$

$\Delta_{22}(\eta) = 1.0 + 0.010e^{-0.9\eta} - 1.010e^{-3.2\eta}$

The time response for the high purity separation is shown below and plotted in Figures 39c-d.

(4.30)

loop 1 (slow)
$\Delta_{11}(\eta) = 1.0 - 1.0e^{-0.5\eta}$

$\Delta_{12}(\eta) = 0.0$

loop 2 (top)
$\Delta_{21}(\eta) = 0.0$

$\Delta_{22}(\eta) = 1.0 \qquad - 1.0e^{-661.1\eta}$

The remarks made for the EVaCS I system apply here, also. In essence, we have shown that both of the EVaCS structures give us our modal control structure for the process. At this point, the reader should recall how easily these structures were synthesized.

The dynamic relative gain array analysis as done by McAvoy [17] has been described previously. The forthcoming analyses were done by calculating $\lambda(i\omega)$ and the appropriate $\Delta(\lambda)$. The interpretation of $\lambda(i\omega)$ gives us a measure of the interaction in the system when one loop has a natural frequency widely separated from the other loop's natural frequency. The interpretation of $\Delta(\lambda)$ gives a measure of the interaction when both loops are identical.

Bode plots of $\lambda(i\omega)$ from the L,V structure are shown in Figures 40a-b for both design cases, respectively. The size of λ is quite large, indicating that the interaction within the system is quite significant when the loop speeds are widely separated. This situation would arise when the two loops had reset times that were of different orders of magnitude. The response of the slow loop, i.e. the loop with the small reset time, would be very sluggish due to the loop's decreased gain. This is especially true in the high purity separation. Its phase angle, as measured

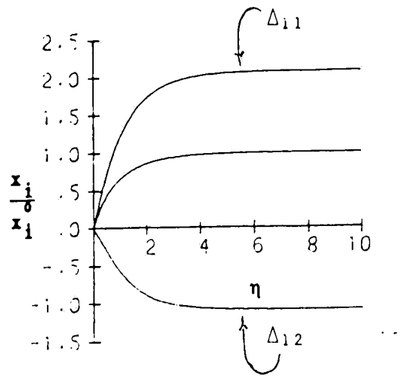

(a)

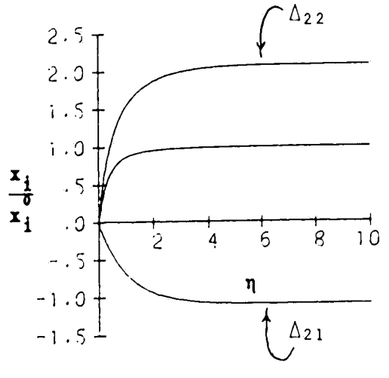

(b)

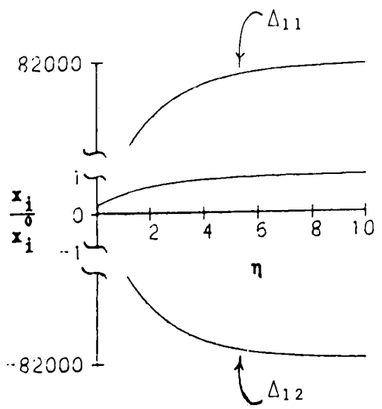

(c)

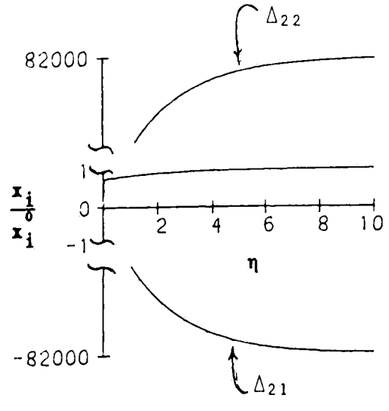

(d)

Fig. 35 Dimensionless Set-Point Responses for L,V in Column's Low and High Purity Separations
a-top loop, low purity b-bottom loop, low purity
c-top loop, high purity d-bottom loop, high purity

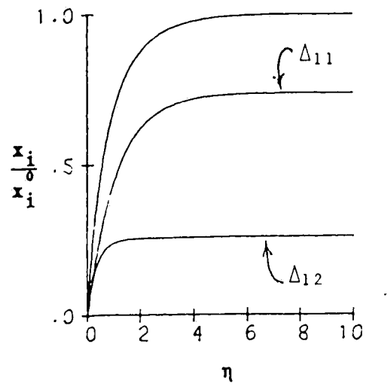

(a)

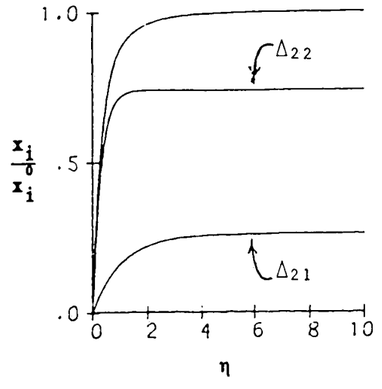

(b)

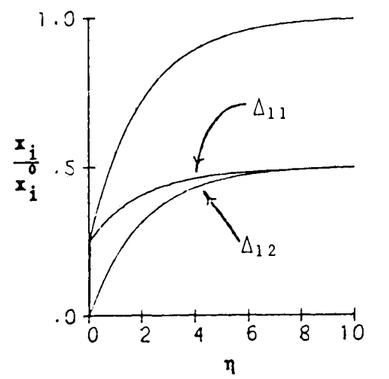

(c)

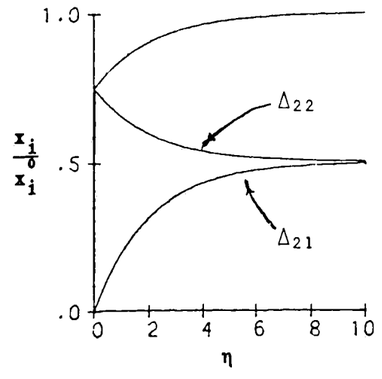

(d)

Fig. 36 Dimensionless Set-Point Responses for D,V in Column's Low and High Purity Separations
a-top loop, low purity b-bottom loop, low purity
c-top loop, high purity d-bottom loop, high purity

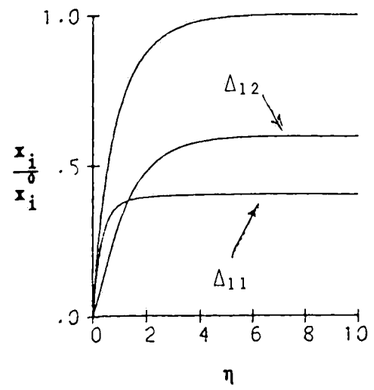

(a)

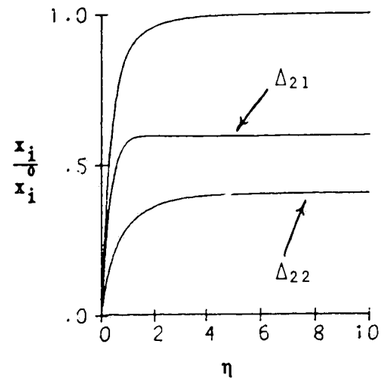

(b)

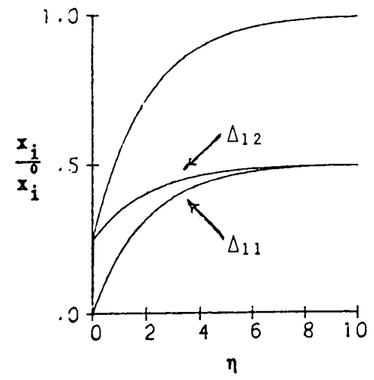

(c)

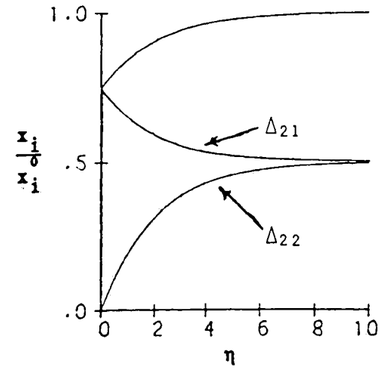

(d)

Fig. 37 Dimensionless Set-Point Responses for L,B in Column's Low and High Purity Separations
a-top loop, low purity b-bottom loop, low purity
b-top loop, high purity d-bottom loop, high purity

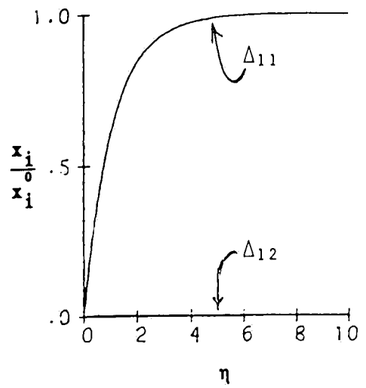

(a)

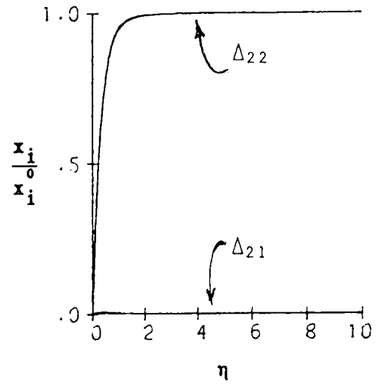

(b)

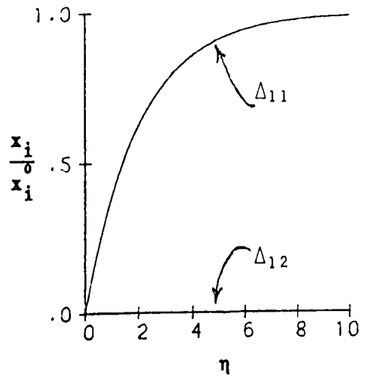

(c)

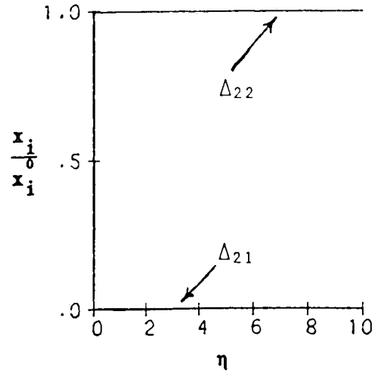

(d)

Fig. 38 Dimensionless Set-Point Responses for EVaCS I in Column's Low and High Purity Separations
a-slow loop, low purity b-fast loop, low purity
c-slow loop, high purity d-fast loop, high purity

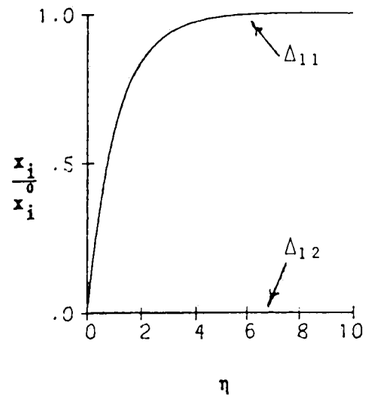

(a)

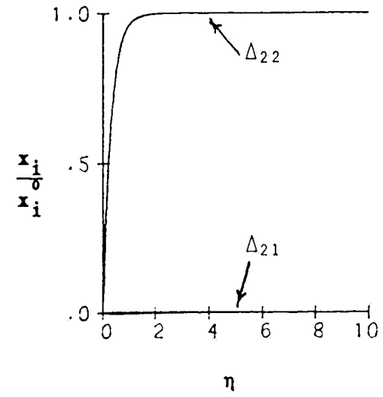

(b)

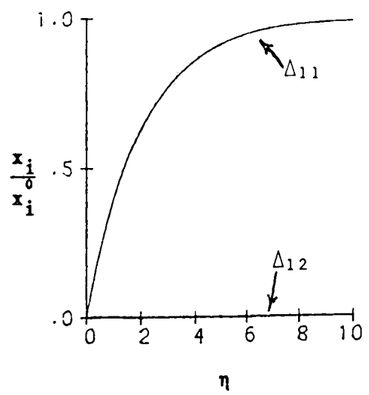

(c)

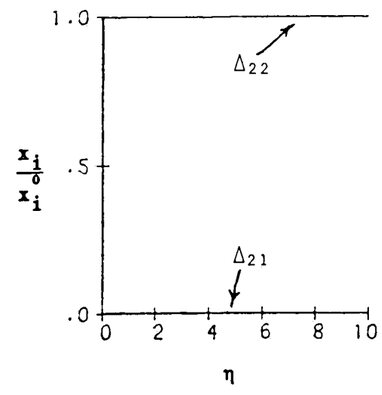

(d)

Fig. 39 Dimensionless Set-Point Responses for EVaCS II in Column's Low and High Purity Separations
a-slow loop, low purity b-fast loop, low purity
c-slow loop, high purity d-fast loop, high purity

clockwise from the positive real axis, would be decreased due to the interaction. These two effects would tend to stabalize the slow loop.

Bode plots of $\Delta(\lambda)$ for the case where the loops are identical and $|\lambda| > 1$ are shown in Figures 40c-d for the two design cases. These plots show that our responses would be highly oscillatory due to the increased loop gains. The speed of response of the loops would not be affected very much. Thus, we would expect to have to decrease our controller gains from their SISO settings when both loops are closed in this situation.

The $\lambda(i\omega)$ from the D,V structure are shown in Figures 41a-b for the respective design cases. These plots show that when the loops have widely separated natural frequencies, the slow loop in the system will exhibit oscillatory behavior. In the low purity separation, the slow loop's speed of response will not be affected. In the high purity separation, the speed of response could be increased or decreased by the interaction depending upon the slow loop's tuning. This seems to imply than an optimum reset time could exist.

Figures 41c-d show Bode plots of $\Delta(\lambda)$ for the situation where

both loops are identical in the D,V structure and $|\lambda| < 1$. These plots show that both loops would exhibit oscillatory responses due to the interaction. The loop speed of responses would not be affected since the interaction phase contribution is negligible. Thus, we would expect to have to decrease our controller gains in the interacting enviroment.

Figures 42a-b show Bode plots of $\lambda(i\omega)$ from the L,B structure for the respective design cases. These plots show that even in this best case analysis where the loop speeds are widely separated, the slow loop's response would be highly oscillatory. In the low purity separation, the slow loop's speed of response would be decreased. In the high purity separation, the slow loop's speed of response could be decreased or increased depending upon the controller tuning. Preferably, the slow loop would have a low reset time so that its natural frequency would be low enough to fall in that region where the interaction's contribution to the phase angle would be favorable, i.e. in that region where the interactive phase angle is negative. In saying this, we assume that the sluggish response that the loop would exhibit in its SISO enviroment would be improved enough due to the interaction in the MIMO enviroment so as to warrant tuning it as such.

Bode plots of $\Delta(\lambda)$ for the L,B structure where both loops are identical and $|\lambda| < 1$ are shown in Figures 42c-d for the respective design cases. The analysis doesn't change much from the analysis given for this system in the situation where the loop speeds are widely separated. Thus, we conclude that this control structure is poor all the way around.

Bode plots of $\lambda(i\omega)$ are shown in Figures 43a-b for EVaCS I and 44a-b for EVaCS II for respective design cases. These plots show conclusively that when the loops speeds are widely separated, one may tune the loops in these structures independently as the interaction is negligible. This is a very desirable thing to be able to do when dealing with multivariable control structures.

Figures 43c-d show the plots of $\Delta(\lambda)$ for EVaCS I in the situation where both loops are identical and $|\lambda| < 1$. This situation would arise when the fast loop was tuned such that it had a large amount of integral action relative to the slow loop. As mentioned earlier, one definitely would not want to tune the system in this manner. Assuming one did anyway, we would expect the loops to exhibit oscillatory responses with the same speed of response as in their SISO enviroments.

Figures 44c-d show the plots of $\Delta(\lambda)$ for EVaCS II in the situation where both loops are identical and $|\lambda| > 1$. This would occur when the fast loop had a smaller reset time than the slow loop. These plots show that we would essentially have no interaction within this structure in either of the two design cases. Considering the fact that this is our worst case analysis, the EVaCS technique becomes more and more appealing.

The next method used to analyze the interaction in these systems was the inverse Nyquist array, which has been described previously. This forthcoming analysis plots the diagonal elements of the inverse of our open-loop transfer function matrix and uses the system's Gershgorin discs to gain insight into the magnitude of the loop interaction.

INA plots with column Gershgorin discs are shown in Figures 45a-d for the L,V structure in the two design cases. In the low purity separation, this system is column dominant, but there still is a fair amount of interaction. This structure is not column dominant, nor was it row dominant, in the high purity separation. Notice the reciprocal of the effective steady-state gain in the high purity separation. As this number is quite large, the effective loop process gains are quite small. Thus, we would

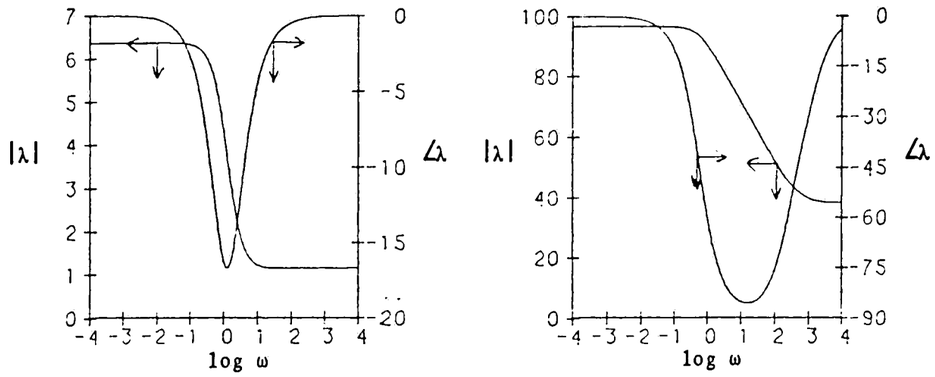

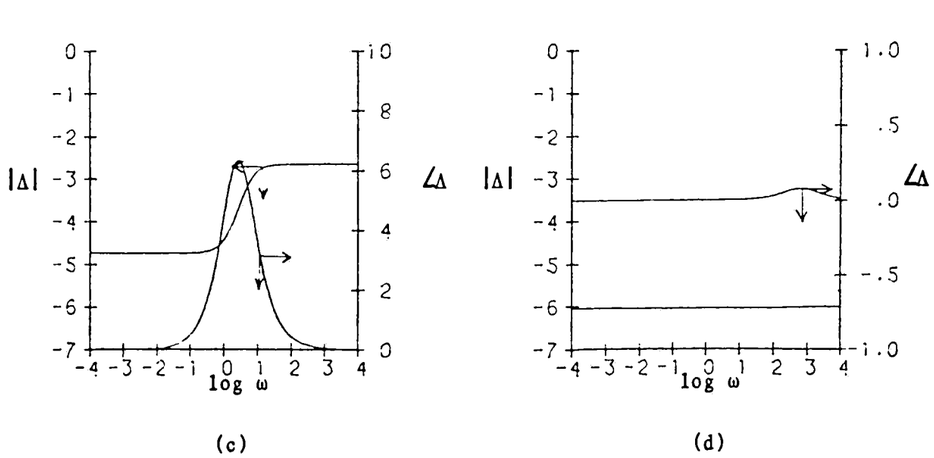

Fig. 40 Dynamic Relative Gain Array Analyses Plots for
L,V in Column's Low and High Purity Separations
a-Bode plot of λ, low purity b-Bode plot of λ, high purity
c-Bode plot of Δ, low purity d-Bode plot of Δ, high purity

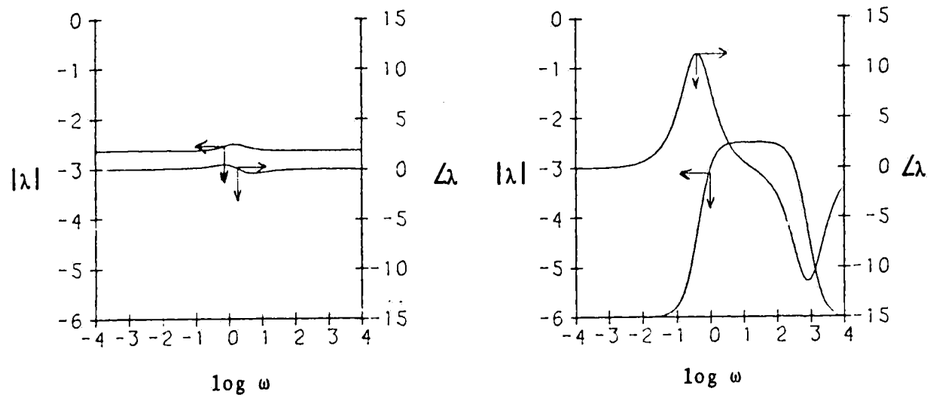

(a)

(b)

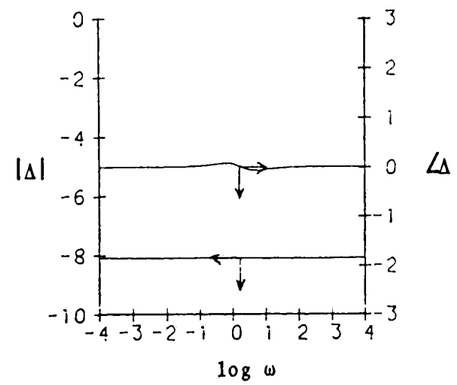

(c)

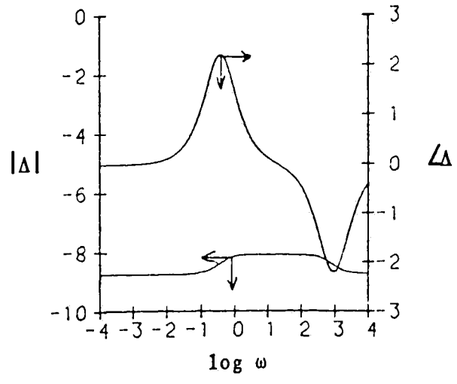

(d)

Fig. 41 Dynamic Relative Gain Array Analyses Plots for
D,V in Column's Low and High Purity Separations
a-Bode plot of λ, low purity b-Bode plot of λ, high purity
c-Bode plot of Δ, low purity d-Bode plot of Δ, high purity

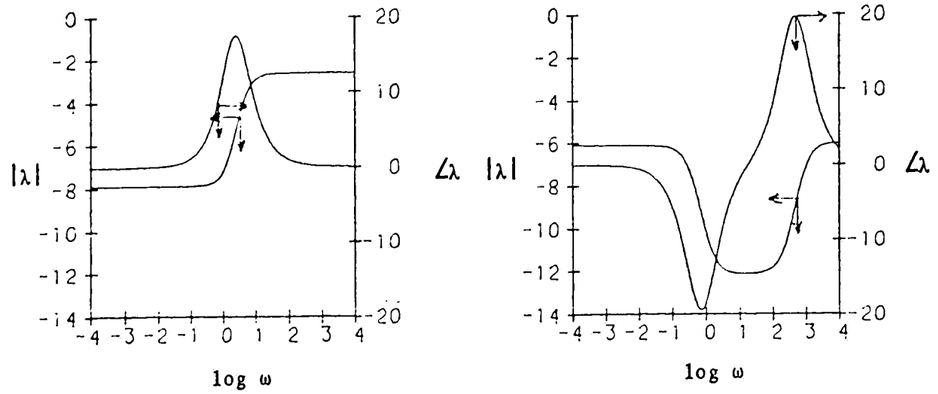

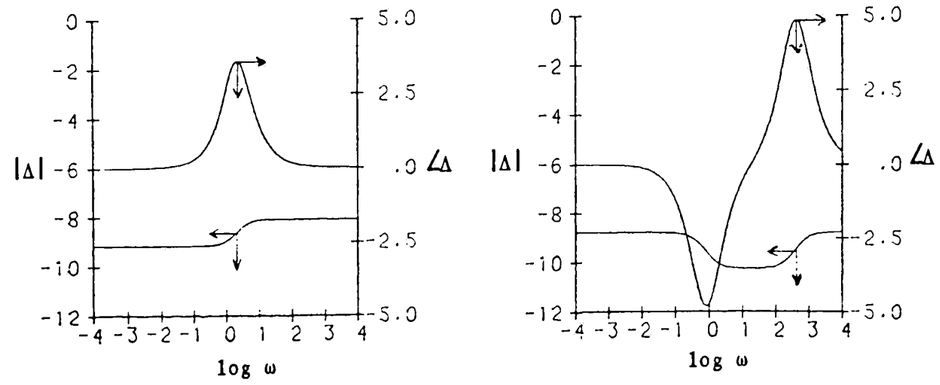

Fig. 42 Dynamic Relative Gain Array Analyses Plots for L,B in Column's Low and High Purity Separations

a-Bode plot of λ, low purity b-Bode plot of λ, high purity

c-Bode plot of Δ, low purity d-Bode plot of Δ, high purity

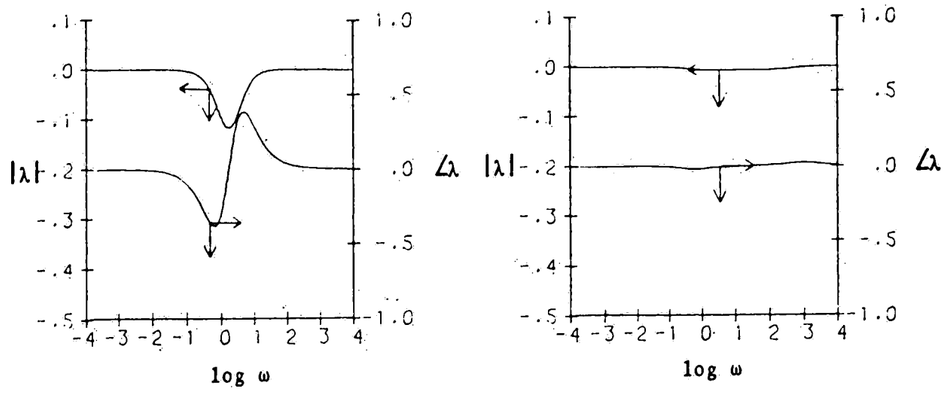

(a)

(b)

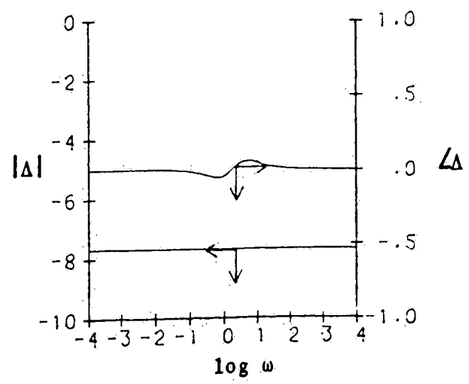

(c)

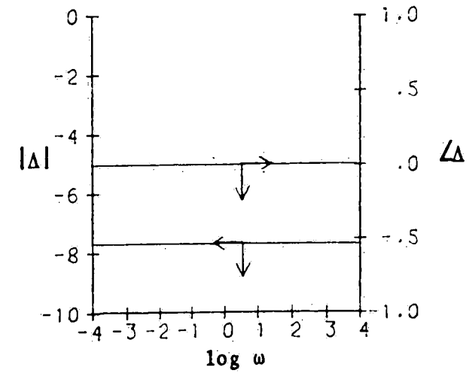

(d)

Fig. 43 Dynamic Relative Gain Array Analyses Plots for EVaCS I in Column's Low and High Purity Separations
a-Bode plot of λ, low purity b-Bode plot of λ, high purity
c-Bode plot of Δ, low purity d-Bode plot of Δ, high purity

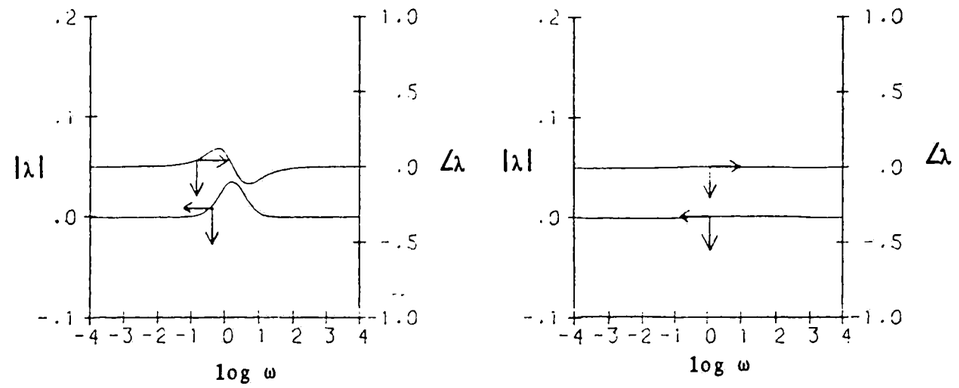

(a)

(b)

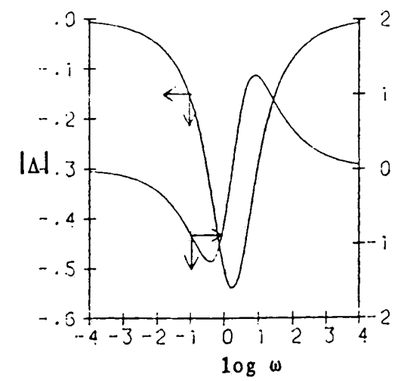

(c)

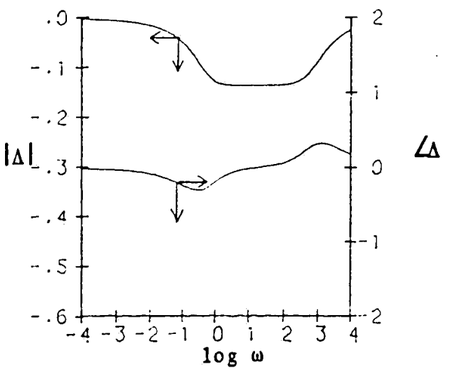

(d)

Fig. 44 Dynamic Relative Gain Array Analyses Plots for EVaCS II in Column's Low and High Purity Separations
a-Bode plot of λ, low purity b-Bode plot of λ, high purity
c-Bode plot of Δ, low purity d-Bode plot of Δ, high purity

expect control difficulties in this situation.

INA plots with column Gershgorin discs are shown in Figures 46a-d for the D,V structure in the two design cases. This system is not column dominant in either separation case due to the excessive interaction of the bottom loop with the top loop. The system was not row dominant for the same reason. Thus, this system would pose control difficulties, especially in the high purity separation, since the bottom loop's process gain is small. Also, when one considers that perfect level control in the accumulator was assumed in deriving the model, this structure becomes even less desirable as the top loop's performance would be degraded in reality.

INA plots with column Gershgorin discs are shown in Figures 47a-d for the L,B structure in the two design cases. This system is not column dominant due to the excessive interaction of the top loop with the bottom loop. Neither was the system row dominant. We would expect control difficulties in the high purity separation, especially, due to the loop interaction and the small process gain in the top loop. Also, when one considers that perfect level control in the sump was assumed in deriving the model, this structure becomes even less desirable as the bottom loop's

performance would be degraded in reality.

Figures 48a-d show INA plots with column Gershgorin discs for the EVaCS I structure in the two design cases. This system is very column dominant. Although there seems to be some rather significant high frequency interference in the slow loop from the fast loop in the high purity separation, technically speaking this is not termed interaction as it is only one-way. Note the effective process gains in the loops. These are not small in either of the design cases. Thus, we would expect better control from this structure than found in the energy balance scheme or either of the material balance schemes.

Figures 49a-d show INA plots with column Gershgorin discs for the EVaCS II structure in the two design cases. This EVaCS structure is very column dominant, also. There is even less interaction in this structure than was present in the EVaCS I structure. Notice how the sensitivity of the slow loop's controlled variable to its manipulated variable actually <u>increases</u> as we go from the low purity separation to the high purity separation, as was the case in the EVaCS I structure. All in all, we would expect good control from this structure when compared to the energy balance scheme and the material balance schemes.

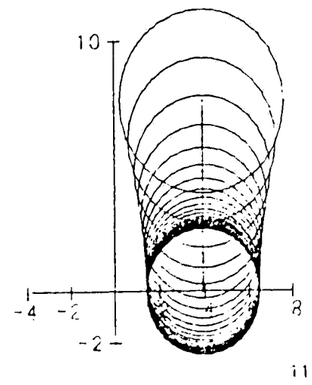

with column discs

(a)

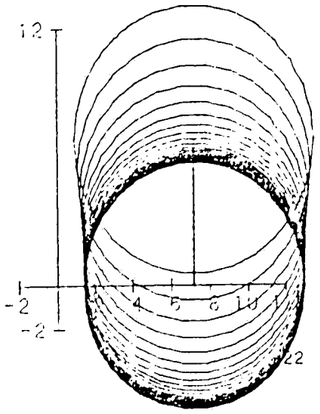

with column discs

(b)

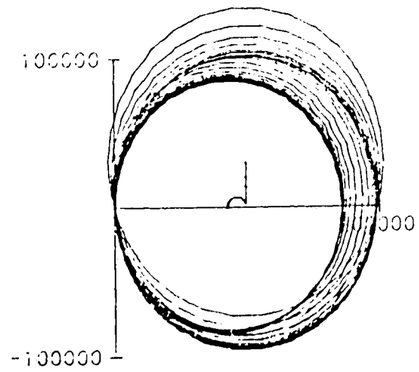

with column discs

(c)

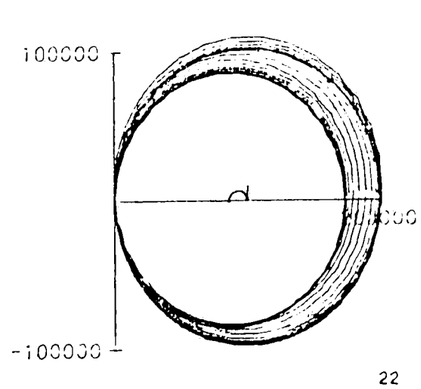

with column discs

(d)

Fig. 45 Inverse Nyquist Array Plots of Diagonal Elements in L,V Structure in Column's Low and High Purity Separations
a-top loop, low purity b-bottom loop, low purity
c-top loop, high purity d-bottom loop, high purity

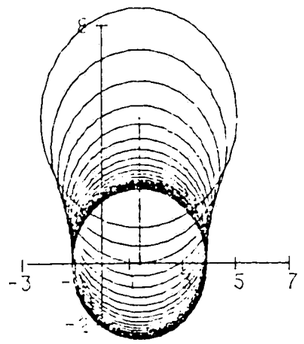

with column discs

(a)

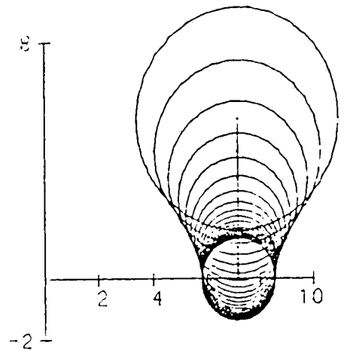

with column discs

(b)

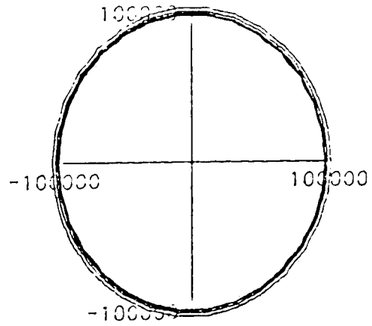

with column discs

(c)

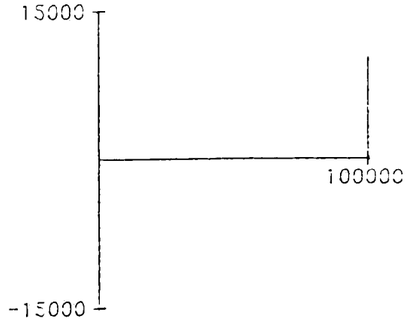

with column discs

(d)

Fig. 46 Inverse Nyquist Array Plots of Diagonal Elements in D,V Structure in Column's Low and High Purity Separations
a-top loop, low purity b-bottom loop, low purity
c-top loop, high purity d-bottom loop, high purity

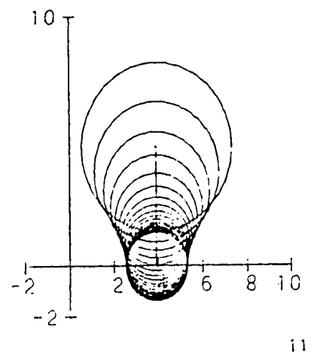

with column discs

(a)

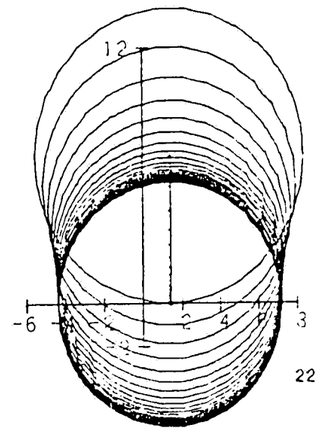

with column discs

(b)

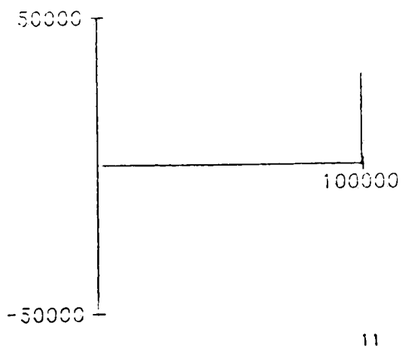

with column discs

(c)

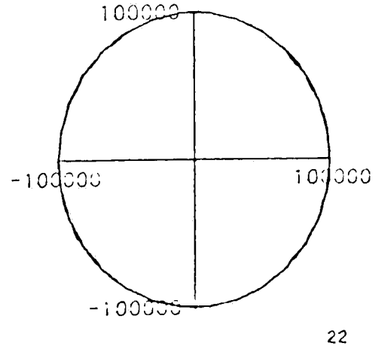

with column discs

(d)

Fig. 47 Inverse Nyquist Array Plots of Diagonal Elements in L,B Structure in Column's Low and High Purity Separations
a-top loop, low purity b-bottom loop, low purity
c-top loop, high purity d-bottom loop, high purity

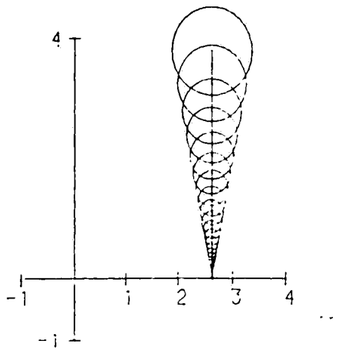

with column discs

(a)

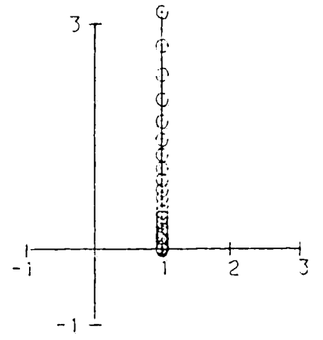

with column discs

(b)

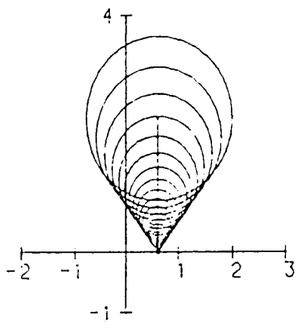

with column discs

(c)

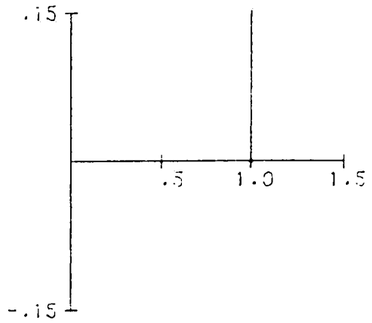

with column discs

(d)

Fig. 48 Inverse Nyquist Array Plots of Diagonal Elements
in EVaCS I Structure in Column's Low and High Purity Separations
a-slow loop, low purity b-fast loop, low purity
b-slow loop, high purity d-fast loop, high purity

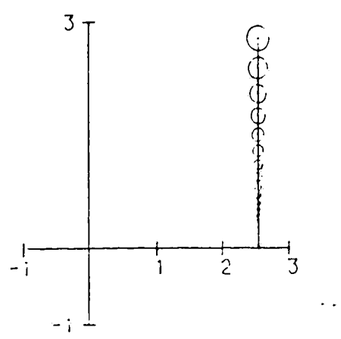

with column discs

(a)

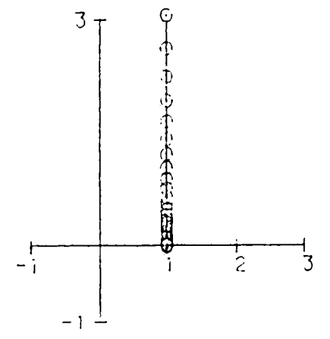

with column discs

(b)

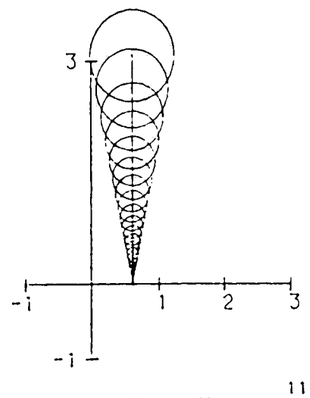

with column discs

(c)

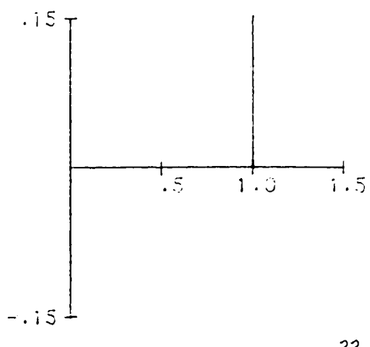

with column discs

(d)

Fig. 49 Inverse Nyquist Array Plots of Diagonal Elements in EVaCS II Structure in Column's Low and High Purity Separations
a-slow loop, low purity b-fast loop, low purity
c-slow loop, high purity d-fast loop, high purity

The final method used to analyze the interaction within these structures was MacFarlane's [15] characteristic loci. This method has been described in detail previously. By looking at the angles between the standard basis vectors and the eigenvectors of the open-loop transfer function matrix, we gain insight into the magnitude of the interactions. A diagonal non-interacting system would have eigenvectors that were perfectly aligned with the basis vectors.

Plots of the interaction angles for the L,V structure in the two design cases are shown in Figures 50a-b. These plots show that the interaction is significant in the low purity separation case, especially at high frequencies. Likewise, it is significant for all frequencies in the high purity separation. Figures 51a-b show the interaction angles for the D,V structure in the two design cases. These plots show that the interaction is significant and becomes more so at high frequencies. The reason one of these angles is zero in the high purity separation is due to the fact that the bottom loop is essentially not functioning because of its small process gain. When one considers the fact that perfect level control has been assumed in these calculations and that in reality the top loop would be less functional than shown, this structure becomes even less desirable. The interaction angles for the L,B

structure in the two design cases are shown in Figures 52a-b. Here also, the interaction is significant in both designs. The reason why one of these angles is zero in the high purity separation is again due to the fact that one of the loops is essentially not functioning. In this structure, i.e. the L,B structure, the top loop is the non-functioning loop.

Figures 53a-b and 54a-b show the interaction angles for the EVaCS I and EVaCS II structures in the different separation cases. In all of these plots, one angle starts at zero and goes to some non-zero value at high frequencies, while the other angle starts at some non-zero value and goes to zero at high frequencies. Only for a limited frequency range are both angles significantly different from zero. Even in this frequency range, the angles are reasonably small which indicates that the interaction is small. Recall from a previous discussion that small angles do not necessarily mean minimal interaction. The reason that we can say that in this case is that all of our previous analyses have confirmed that the interaction is minimal. At the low and high frequencies where one angle is zero, we only have one-way interference, not interaction.

In order to allow the structures to exhibit unstable behavior, it was decided to incorporate analyzer dead times into the various

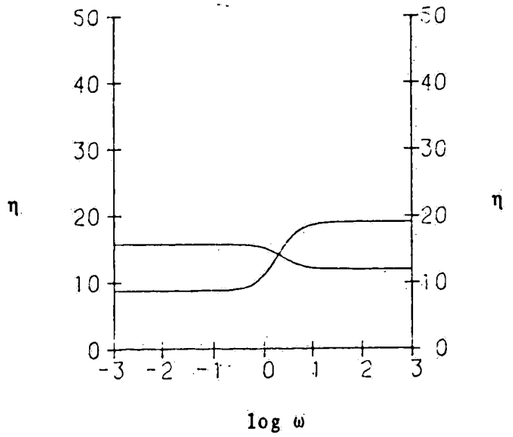

(a)

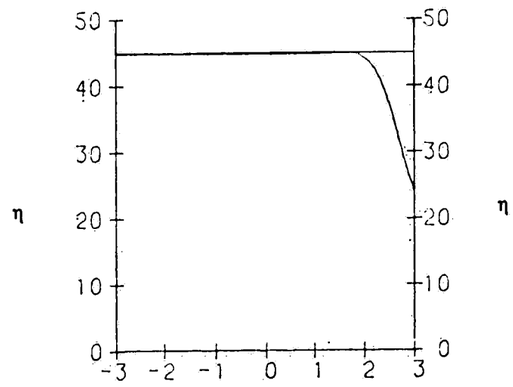

(b)

Fig. 50 Characteristic Loci Interaction Angles in Degrees for L,V in Column's Low and High Purity Separations
a-low purity b-high purity

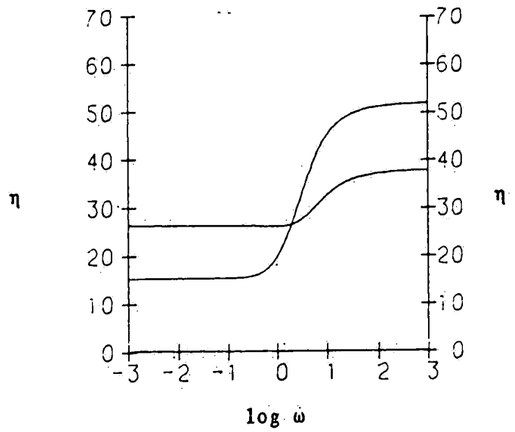

(a)

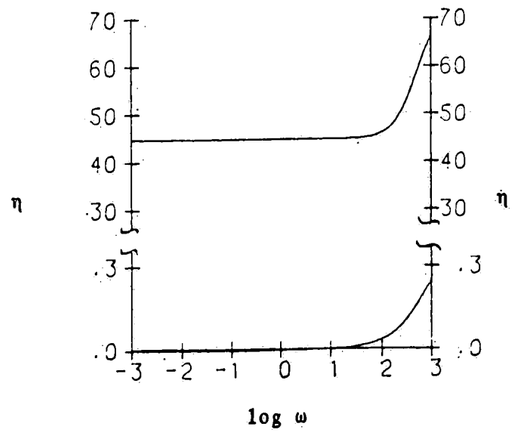

(b)

Fig. 51 Characteristic Loci Interaction Angles in Degrees for D,V in Column's Low and High Purity Separations
a-low purity b-high purity

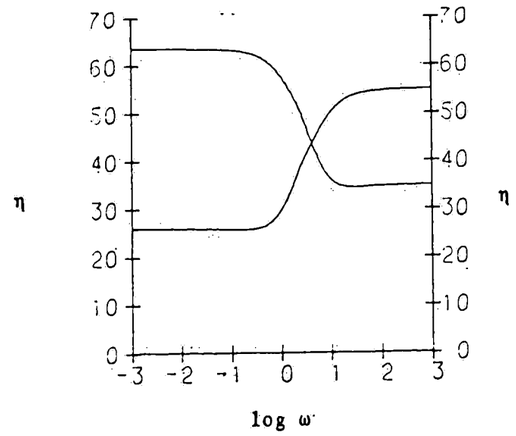

(a)

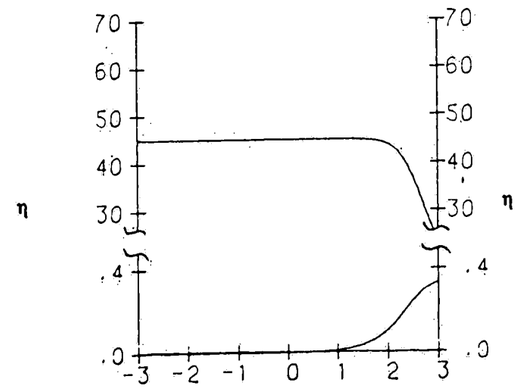

(b)

Fig. 52 Characteristic Loci Interaction Angles in Degrees for L,B in Column's Low and High Purity Separation
a-low purity b-high purity

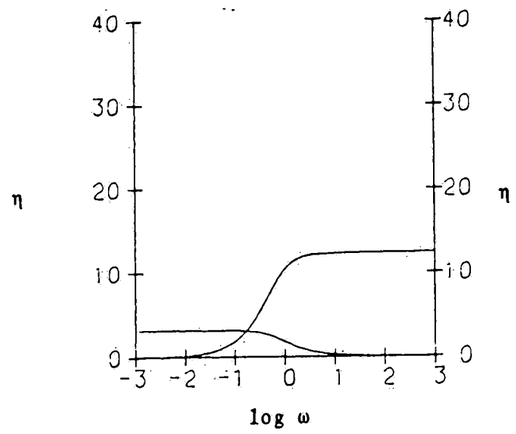

(a)

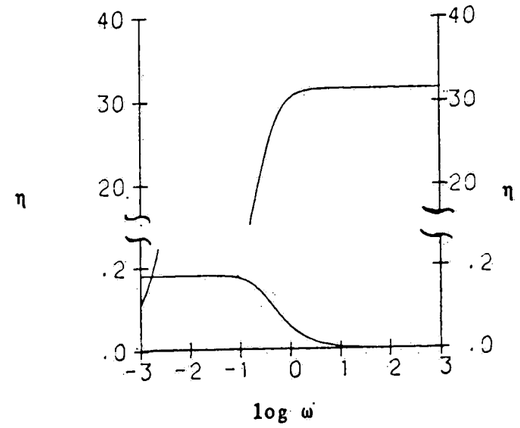

(b)

Fig. 53 Characteristic Loci Interaction Angles in Degrees for EVaCS I in Column's Low and High Purity Separation
a-low purity b-high purity

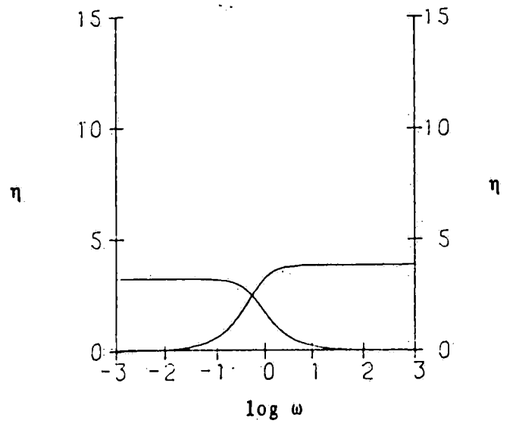

(a)

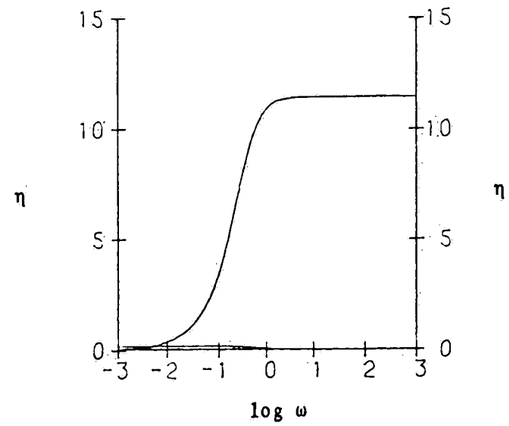

(b)

Fig. 54 Characteristic Loci Interaction Angles in Degrees for EVaCS II in Column's Low and High Purity Separation
a-low purity b-high purity

control systems. A dead time of 0.05 dimensionless time units was used to represent the analyzer dynamics. This corresponded to approximately 5% of the slowest time constant in the low purity separation case, and 2.5% of the same in the high purity separation case. These analyzer times were analogous to five minutes for a two hour column time constant in the low purity separation, and 3 minutes for the same column time constant in the high purity separation. The analyzer dynamics were incorporated into the systems simply by multiplying the various plant transfer function matrices by a matrix of diag[$e^{-0.05s}$]. Using these matrices, gain spaces were calculated for the various structures, as described previously.

The gain spaces for the L,V structure are shown in Figures 55a-b for the respective design cases, while the INA plots used for the gain space approximations are shown in Figures 56a-d. Column Gershgorin discs are used in these plots. This system is dominant only in the low purity separation. The shape of the gain spaces confirm that the interaction in the structure is significant, especially in the high purity separation. The gain spaces for the D,V structure are shown in Figures 57a-b, while the INA plots used to approximate the gain spaces are shown in Figures 58a-d. Column discs were used in these plots in the low purity separation, while

row discs were used in the high purity separation. This system is not column dominant, nor was it row dominant. Note the shape of the gain space in the high purity separation. This confirms the previous assertion that the bottom loop in this system is essentially non-functional. The gain spaces for the L,B structure are shown in Figures 59a-b for the respective design cases. INA plots used to approximate the gain spaces are shown in Figures 60a-d. Column discs are used in the low purity separation, while row discs are used in the high purity separation. This system was neither row nor column dominant, either. Again, note the shape of the gain space in the high purity separation. This confirms that the top loop in this structure is essentially not functioning.

Gain space plots for the EVaCS I structure are shown in Figures 61a-b. The INA plots with column discs that were used to approximate the gain spaces are shown in Figures 62a-d. This structure is strongly column dominant, thus the area of uncertainty in the gain space is sharply reduced. Gain space plots for the EVaCS II structure are shown in Figures 63a-b, while the INA plots used to approximate the gain spaces are shown in Figures 64a-d. These INA plots were made using column discs, too. This structure is even more strongly column dominant than the EVaCS I structure. The gain spaces of both structures show once again that the

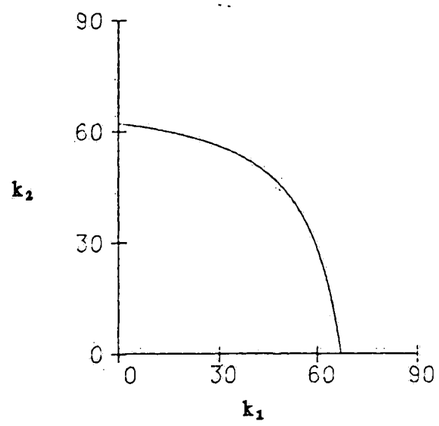

(a)

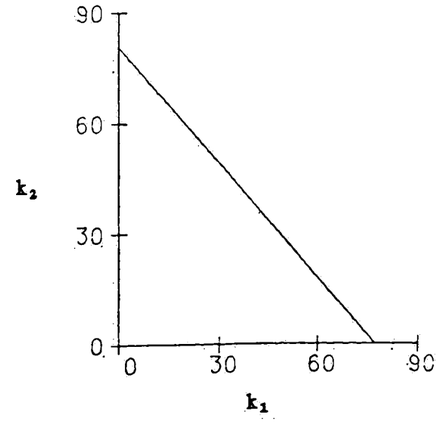

(b)

Fig. 55 Gain Space Plots for L,V
in Column's Low and High Purity Separations
a-low purity b-high purity
k_1 is top loop's proportional gain,
k_2 is bottom loop's proportional gain

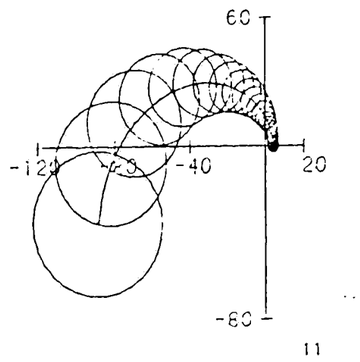

with column discs

(a)

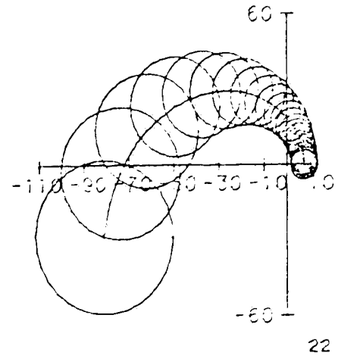

with column discs

(b)

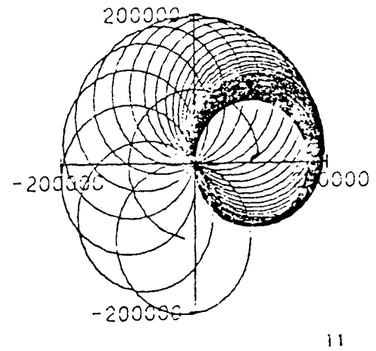

with column discs

(c)

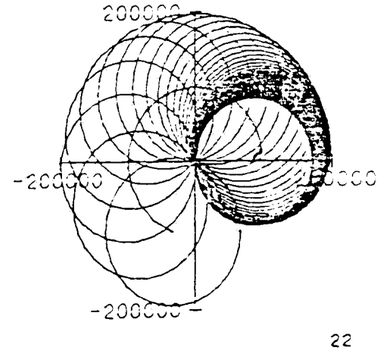

with column discs

(d)

Fig. 56 Inverse Nyquist Array Plots for L,V Gain Space Approximations in Column's Low and High Purity Separations
a-top loop, low purity b-bottom loop, low purity
c-top loop, high purity d-bottom loop, high purity

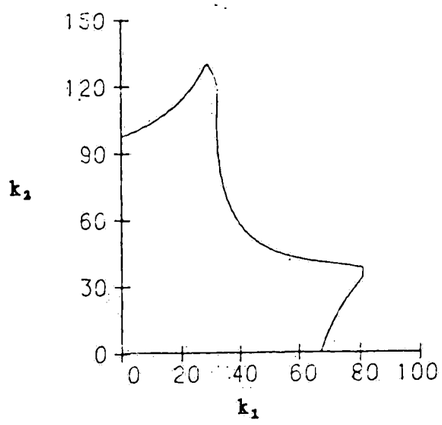

(a)

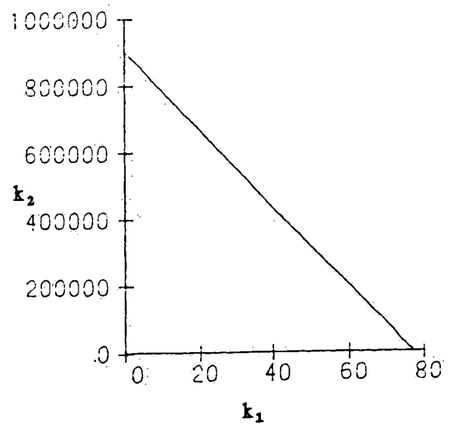

(b)

Fig. 57 Gain Space Plots for D,V
in Column's Low and High Purity Separations
a-low purity b-high purity
k_1 is top loop's proportional gain,
k_2 is bottom loop's proportional gain

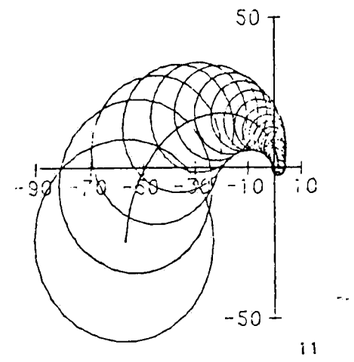

with column discs

(a)

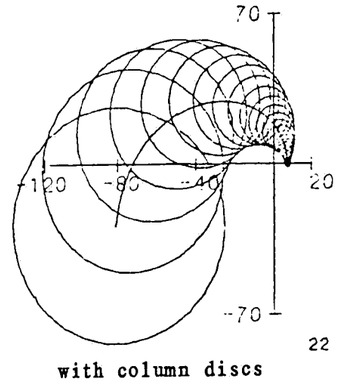

with column discs

(b)

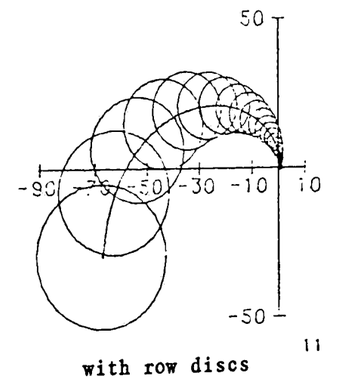

with row discs

(c)

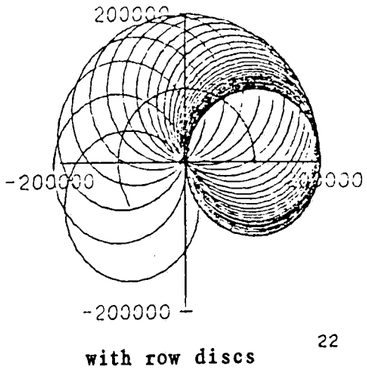

with row discs

(d)

Fig. 58 Inverse Nyquist Array Plots for D,V Gain Space Approximations in Column's Low and High Purity Separations
a-top loop, low purity b-bottom loop, low purity
c-top loop, high purity d-bottom loop, high purity

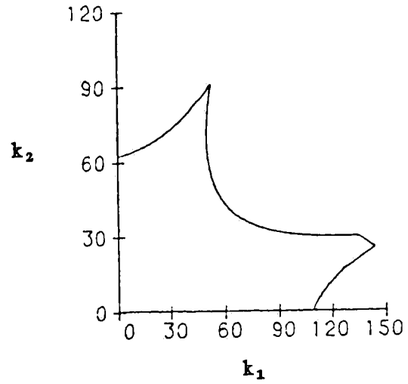

(a)

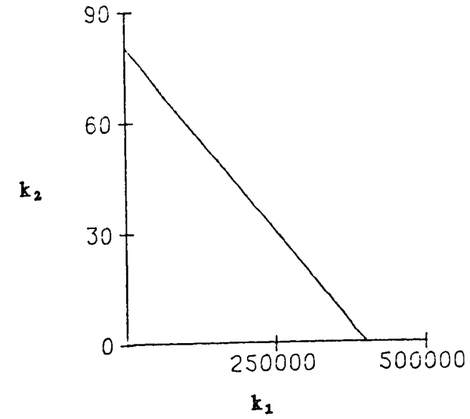

(b)

Fig. 59 Gain Space Plots for L,B
in Column's Low and High Purity Separations
a-low purity b-high purity
k_1 is top loop's proportional gain,
k_2 is bottom loop's proportional gain

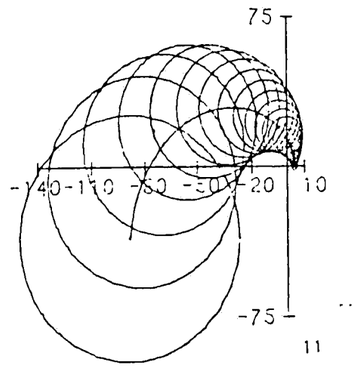

with column discs

(a)

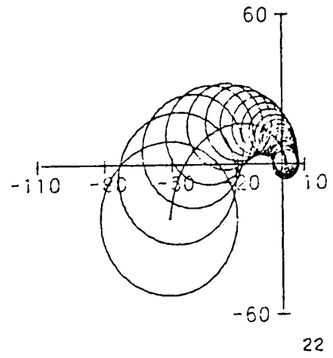

with column discs

(b)

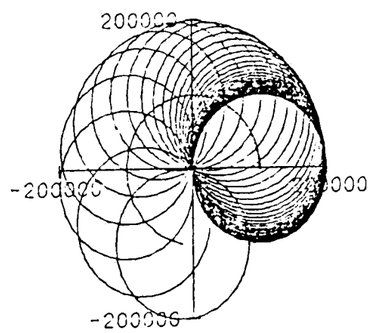

with row discs

(c)

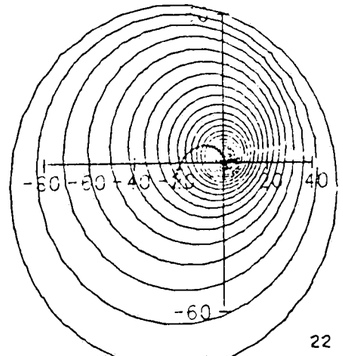

with row discs

(d)

Fig. 60 Inverse Nyquist Array Plots for L,B Gain Space Approximations in Column's Low and High Purity Separations
a-top loop, low purity b-bottom loop, low purity
c-top loop, high purity d-bottom loop, high purity

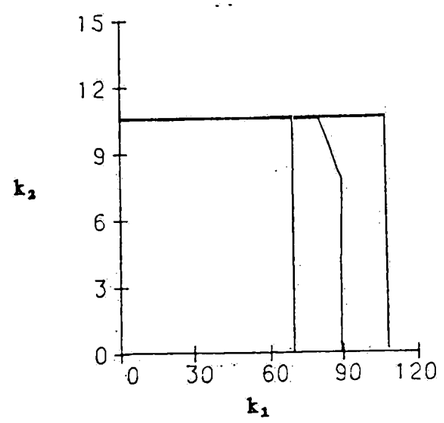

(a)

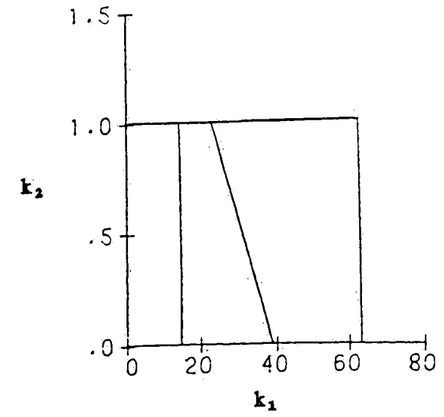

(b)

Fig. 61 Gain Space Plots for EVaCS I
in Column's Low and High Purity Separations
a-low purity b-high purity
k_1 is slow loop's proportional gain,
k_2 is fast loop's proportional gain

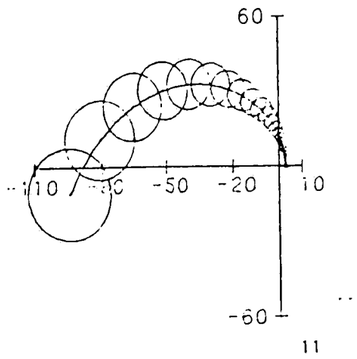

with column discs

(a)

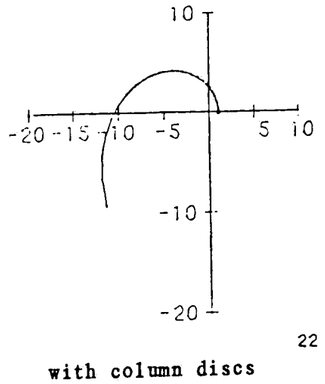

with column discs

(b)

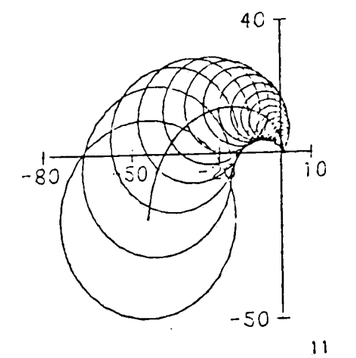

with column discs

(c)

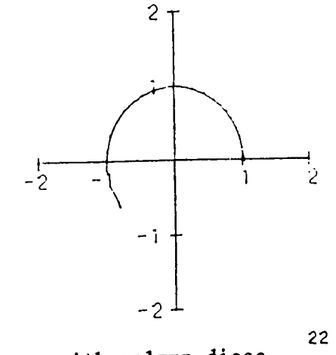

with column discs

(d)

Fig. 62 Inverse Nyquist Array Plots for EVaCS I Gain Space Approximations in Column's Low and High Purity Separations
a-slow loop, low purity b-fast loop, low purity
c-slow loop, high purity d-fast loop, high purity

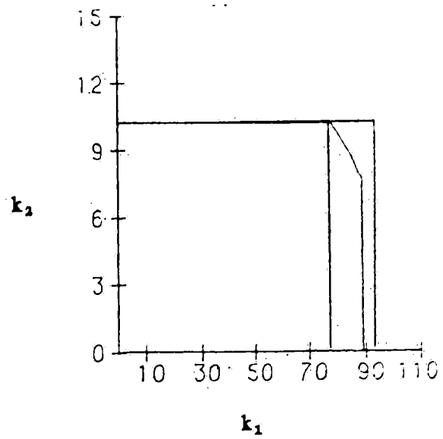

(a)

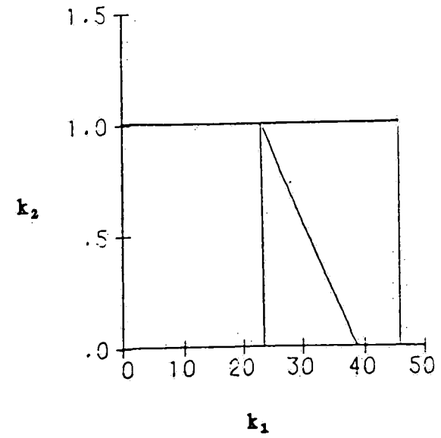

(b)

Fig. 63 Gain Space Plots for EVaCS II
in Column's Low and High Purity Separations
a-low purity b-high purity
k_1 is slow loop's proportional gain,
k_2 is fast loop's proportional gain

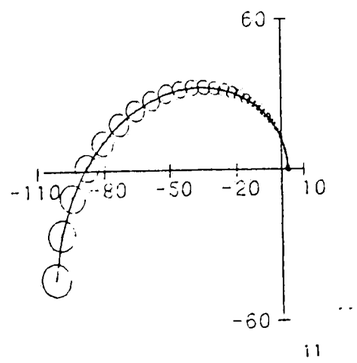

with column discs

(a)

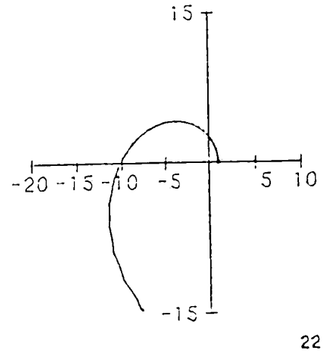

with column discs

(b)

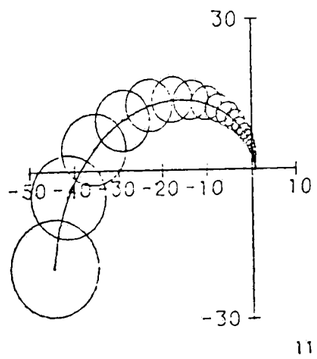

with column discs

(c)

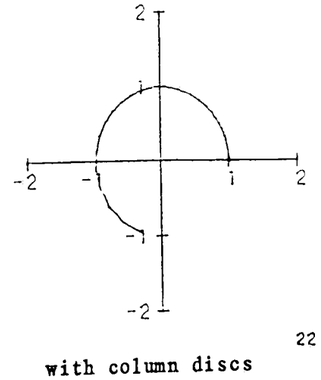

with column discs

(d)

Fig. 64 Inverse Nyquist Array Plots for EVaCS II Gain Space Approximations in Column's Low and High Purity Separations
a-slow loop, low purity b-fast loop, low purity
c-slow loop, high purity d-fast loop, high purity

interaction is minimal.

These analyses have shown that using extensive material concepts one can synthesize two control structures which have zero steady-state interaction and minimal dynamic interaction for this process. The reader should recall the ease with which these structures were synthesized. Both structures clearly have more favorable control characteristics than the conventional schemes. As to which EVaCS structure is best suited for our particular designs, the angle calculations suggest that the EVaCS II structure is favorable over the EVaCS I structure. This seems to be confirmed by the various other analyses presented here.

Chapter 5

Tuning the EVaCS Structures

We have just completed a fairly exhaustive analysis of the interaction in the control structures synthesized by the EVaCS technique. In doing the analysis, we saw that we can tune the principal loops independent of one another as long as we keep the loop speeds separated to some extent. The forthcoming discussion attempts to gain insight into the closed-loop behavior of the indiviual loops. Also, we attempt to determine whether or not we need to include integral action in the controllers, and if so, the extent to which it must be incorporated.

Referring to tables 3-4 and tables 9-10, we see that all of the principal transfer functions of the various EVaCS structures have the following form,

$$G(s) = \frac{K(s + z)}{(s + p_f)(s + p_s)} \tag{5.1}$$

For the purposes of this discussion, we label p_f as the eigenvalue of the fast mode of the system and p_s as the eigenvalue of the slow mode of the system. The fast loop in the structures has a zero approximately equal to the slow eigenvalue, while the slow loop in the structures has a zero approximately equal to the fast eigenvalue. We will label the zero of the fast loop z_f and that of the slow loop z_s.

Using a root locus analysis, we should be able to gain some insight into the performance of the indiviual loops. We will use the form of the transfer function shown in equation (5.1). Notice how in the EVaCS I structures both z_s and z_f are bounded by p_s and p_f, as seen in tables 3-4 and 9-10. The EVaCS II structures' z_s and z_f lie outside the bounds set by p_s and p_f. This is a key point in assessing the differences between the loops in the two structures.

Figure 65 shows root loci plots of the resulting open-loop transfer function for the loops in the EVaCS I structure when proportional-only controllers are used. Immediately, we notice that these controllers will not exhibit oscillatory responses. Looking at the plot for the fast loop, it seems that it might not be as fast as the slow loop when the loops are closed due to its zero blocking the movement of the slow eigenvalue down the negative real axis. This is a bit perplexing at first, but recall that the fast loop's response is due to the fast mode which means we need only look at the position of p_f. Thus, neglecting interaction, we can see that our fast loop gets faster as we increase our gain. Likewise, we see that we can improve the speed of the slow loop as its response is due to the position of the slow eigenvalue. The speed of the slow mode approaches that of the fast mode in its open

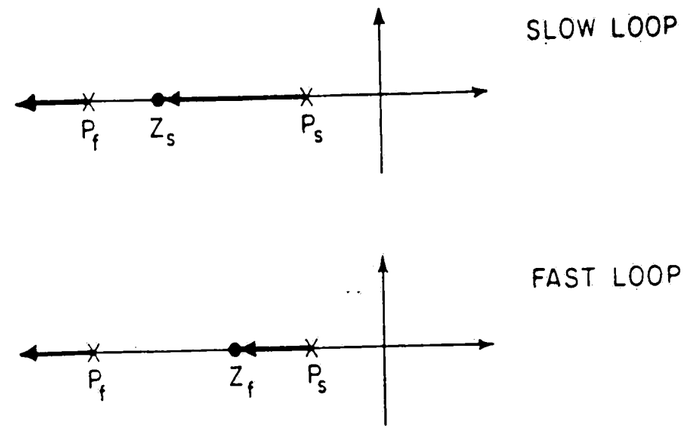

Fig. 65 Root Loci Plots for EVaCS I Loops with P-Only Controllers

loop enviroment as we increase our controller gain. In the difficult control situations, such as a high recycle rate in a reactor system or a difficult separation in a distillation column, the eigenvalues are widely separated. Thus, the improvement in the speed of the slow loop could be significant.

Root loci plots are shown in figure 66 for the EVaCS II principal loops using proportional-only controllers. The slow loop can exhibit oscillatory behavior in this system. If there was any interaction of the slow loop with the fast, it might have a significant affect on the fast loop's response due to the confluency of the eigenvalues. This analysis is really not capable

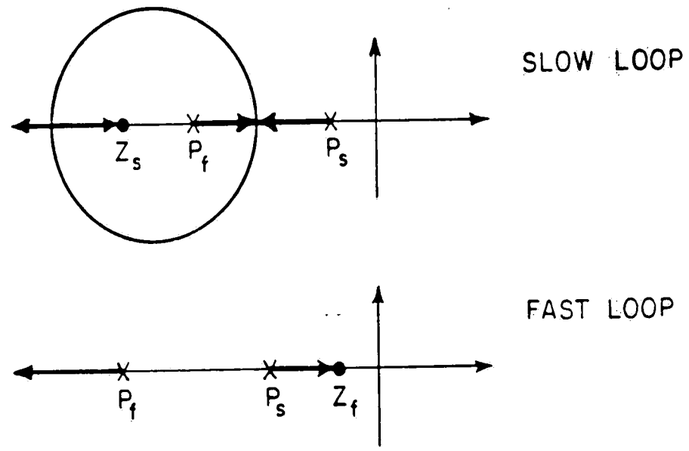

Fig. 66 Root Loci Plots for EVaCS II Loops with P-Only Controllers

of telling us what would happen in this situation. Anyway, we have shown that the interaction of the slow loop with the fast is minimal. The fast loop in this situation just becomes that much faster without exhibiting oscillatory behavior.

We could also employ proportional-integral controllers in these structures. In this case, we have a total of four cases to assess for each of the loops. Figures 67a-d show the various generalized root loci plots in the order of increasing integral action (decreasing reset time) for the loops in the EVaCS I structure. We see that the integral action has added an additional mode to the system. For the slow loop, only plots a,b and d are

worth analyzing as it is doubtful that one would choose a reset time that would cause the integral zero to lie within that segment of the negative real axis bounded by p_f and z_s. Likewise, only plots a,c and d are worth analyzing for the fast loop due to a similar rationale. In these diagrams, we see that we can have a slight amount of integral action in the slow loop and still have a non-oscillatory response. As we increase our integral action, our slow mode becomes confluent with the integral mode and oscillatory behavior results. For the fast loop, we can have a small amount of integral action and still remain non-oscillatory. As we decrease the reset time, our fast eigenvalue remains real, as opposed to complex, so we might not see too much oscillation in the loop since it is the slow mode that becomes confluent with the integral mode. If we ever have a tremendous amount of integral action, as the case shown in plot d, then the speed of the fast loop will be severely affected. Here, we would expect to see very poor performance due to the aforementioned fact and, assuming the slow loop does not have a significant amount of integral action, due to the subsequent increase in the interaction.

Figures 68a-c show the root loci plots in order of increasing integral action that would be applicable to the slow loop in the EVaCS II structure. Here, we see that the slow loop might exhibit

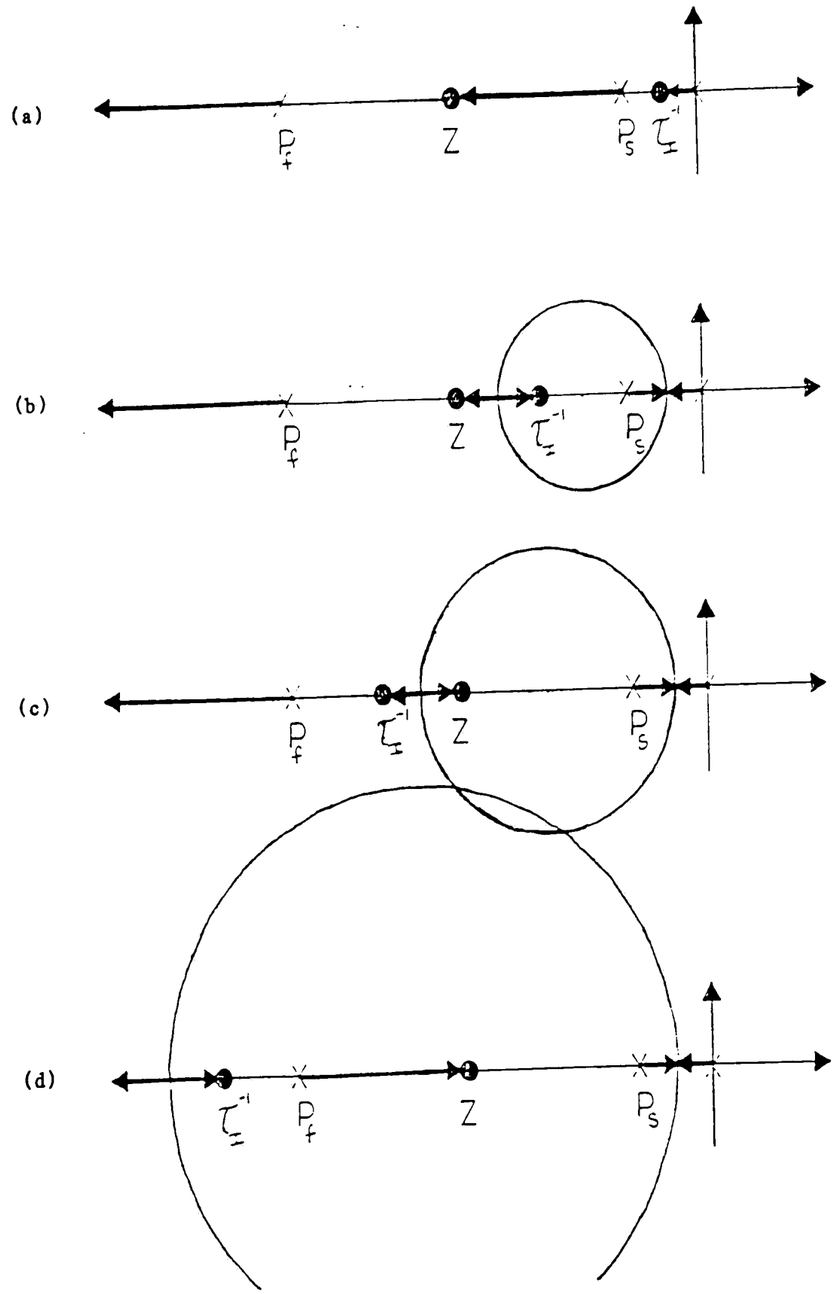

Fig. 67 Root Loci Plots for EVaCS I Loops with PI Controllers

oscillatory responses when a controller with integral action is used regardless of the reset time. For a slight amount of integral action, we might expect to see a bit more interaction of the slow loop with the fast loop as the two system eigenvalues become confluent. In cases b and c, the slow mode becomes confluent with the integral mode. Thus, in order to keep the slow loop in this system from being oscillatory we would have to use a small controller gain. Figures 69a-c show the root loci plots for the fast loop in the EVaCS II structure. Here, we see that this loop would not exhibit oscillatory behavior until a very small reset time was employed in the controller. So, while the slow loop in this structure might have some difficulties depending upon the tuning, the fast loop will have pretty respectable responses.

In determining whether or not to use proportional or proportional-integral controllers, one very big consideration is the elimination of off-set. In general, fast loops tend to have more off-set than slow loops, everything else being the same. On page 54 of his book, Rosenbrock [6] describes a quantitative way of determining the off-set that a loop would have via the inverse Nyquist plot of that loop's open-loop transfer function. Referring to figure 70, the off-set is the ratio of OA to CA, where C is the value of the controller gain.

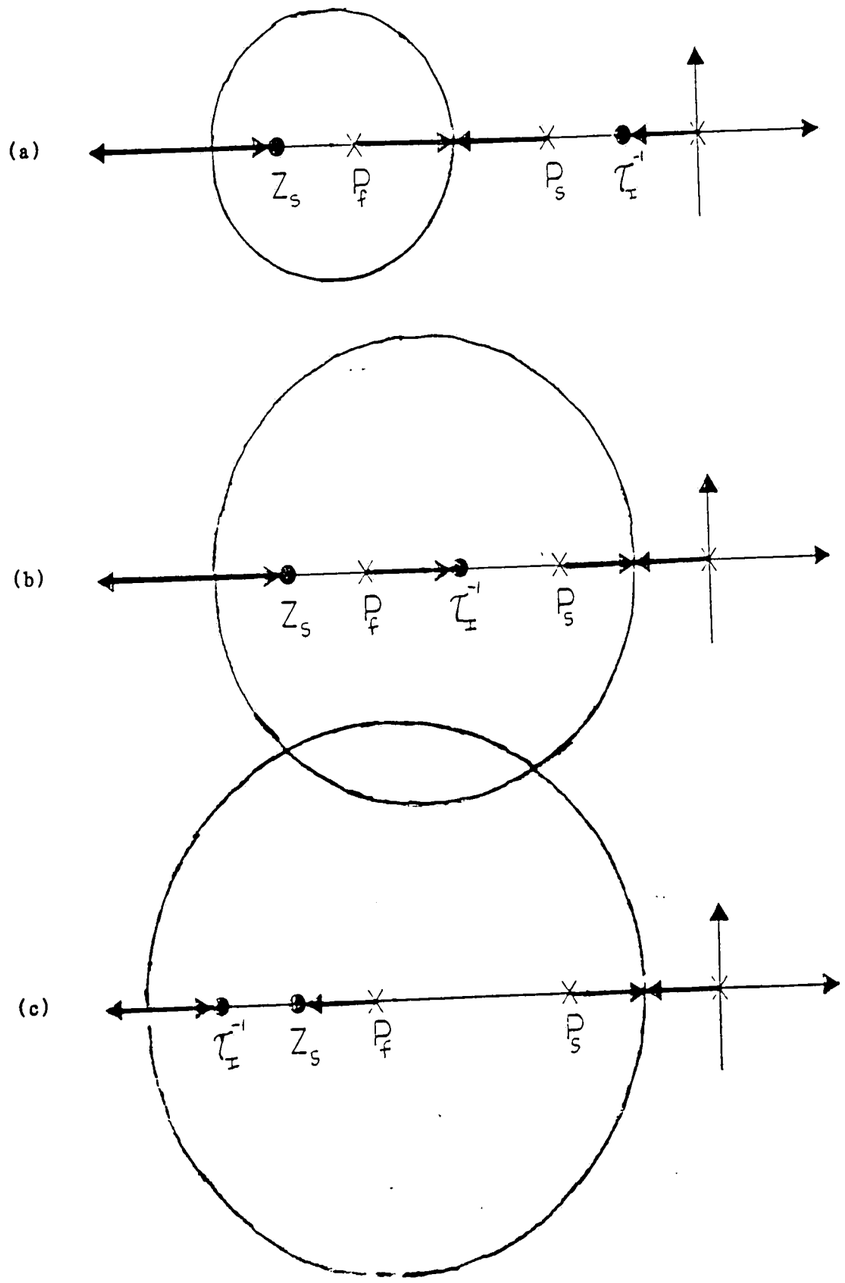

Fig. 68 Root Loci Plots for EVaCS II Slow Loop with PI Controller

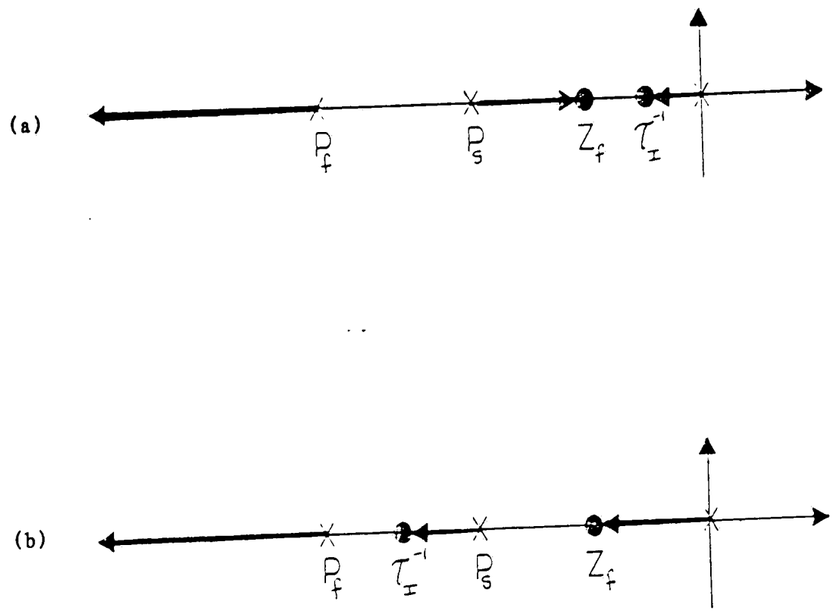

Fig. 69 Root Loci Plots for EVaCS II Fast Loop with PI Controller

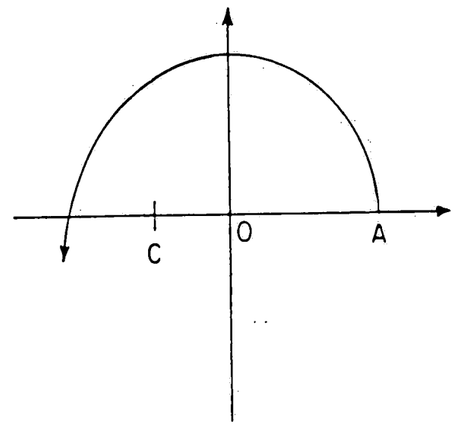

Fig. 70 Determining Off-Set via the Inverse Nyquist Plot

Referring to the INA diagrams for the EVaCS structures in the stirred-tanks in series process, we see that the various loops would exhibit little off-set when using proportional controllers as the plots start very close to the origin. It's interesting to note that whenever a loop has integral action incorporated into it, its inverse Nyquist diagram begins at the origin. Referring to the INA plots for the EVaCS structures in the distillation process, we see that both loops would have little off-set in the low purity separation. In the high purity separation, the slow loop essentially has no off-set while the fast loop has a significant amount of off-set. This is due to the fact that the fast loop is really fast in this case. Recall from a previous discussion that

the faster a loop is, the more off-set it tends to have. Thus, we would want some amount of integral action in the fast loop. In general, we would want some limited amount of integral action in both controllers as this would be necessary in order for the actual intensive variables that are being controlled to reach their set-points after a disturbance had been injected into the system.

In order to see if we could tune the loops in the EVaCS structures independent of one another and still have a stable system, it was decided to calculate Ziegler-Nichols [26] settings for proportional-integral controllers to be used in the various structures we have assessed in the distillation process' high purity design case. The ultimate gains and ultimate frequencies required to calculate the various settings are shown in table 11, while the actual settings employed in the various structures are shown in table 12. Characteristic loci stability plots of the resulting L,V structure's open-loop transfer function matrix's eigenvalues are shown in Figure 71a-b. As seen in the plots, this structure is at the point of instability as the eigenvalue shown in Figure 71a has a magnitude of one when its phase angle is -180 degrees. Characteristic loci stability plots of the resulting D,V and L,B structures are shown in Figure 72a-b and 72c-d, respectively. These plots indicate that both structures are

unstable. The corresponding stability plots for the EVaCS I structure are shown in Figure 73a-b, while the plots for the EVaCS II structure are shown in Figure 73c-d. These structures are clearly stable. Note that by using the Z-N tuning method, the fast loop in the EVaCS structures end up with an exorbitant amount of integral action. This is contrary to the desired tuning procedure for these structures as discussed previously.

In order to confirm these calculations, a time domain simulation was performed. The simulation employed an Euler integration technique and was carried out to ten column time constants using a step size of 1/10,000 dimensionless time units. The state of the system was printed from the program every 1000 iterations giving a total of 101 points to be plotted. A feed composition change from $x_f = 0.5$ to $x_f = 0.6$ was injected into the system as a disturbance.

The time domain simulation for the L,V structure is shown in Figure 74. This figure shows the dynamic responses of both terminal compositions and both manipulated variables. As seen in the plots, this structure does not reject the disturbance as the system reaches a point where the changes in the reflux rate and boil-up rate begin negating each other. Also, we can see that the

Table 11 Ultimate Gains and Ultimate Frequencies for Strucutures used in High Purity Separation

	k_u	ω_u	loop
L,V	77.08	31.42	distillate
	80.43	32.73	bottoms
D,V	77.08	31.42	distillate
	900,072	0.55	bottoms
L,B	402,437	67.18	distillate
	80.43	32.73	bottoms
EVaCS I	38.85	31.73	slow
	1.00	60.99	fast
EVaCS II	38.81	31.73	slow
	1.00	60.99	fast

Table 12 Ziegler-Nichols settings for Structures used in High Purity Separation

	k_c	τ_I	loop
L,V	35.04	0.17	distillate
	36.56	0.16	bottoms
D,V	35.04	0.17	distillate
	409,124	9.52	bottoms
L,B	182,926	0.08	distillate
	36.56	0.16	bottoms
EVaCS I	17.66	0.17	slow
	0.45	0.09	fast
EVaCS II	17.64	0.16	slow
	0.45	0.09	fast

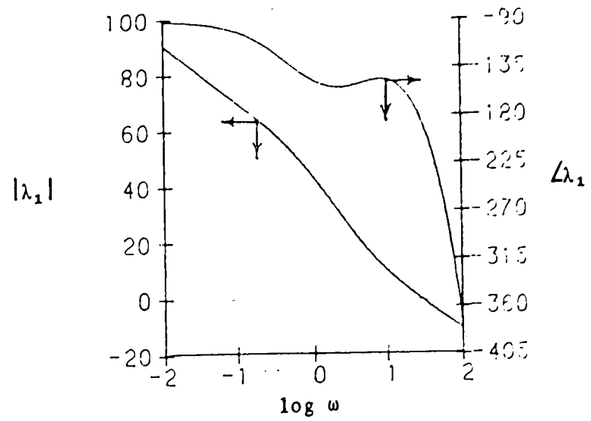

(a)

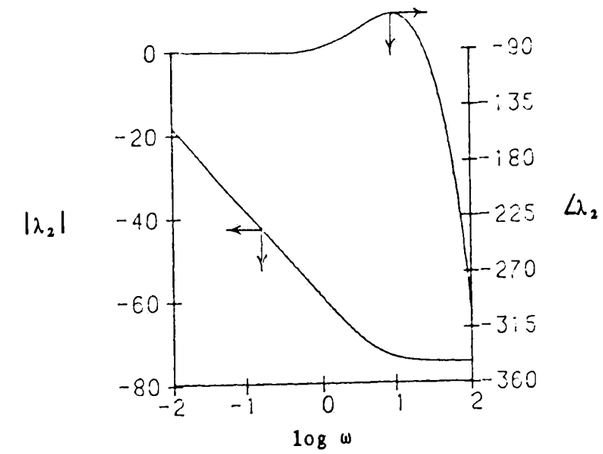

(b)

Fig. 71 Characterisitc Loci Stability Bode Plots for Energy Balance Scheme with Proportional-Integral Controllers in Column's High Purity Separation

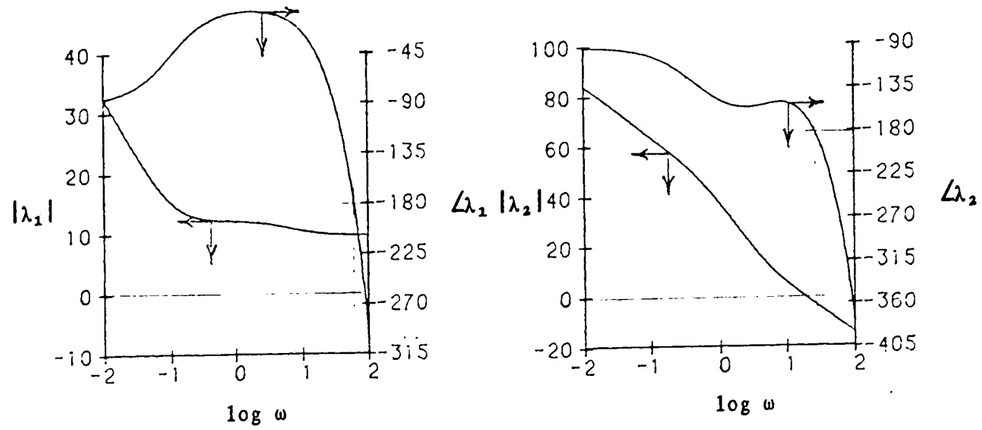

(a) (b)

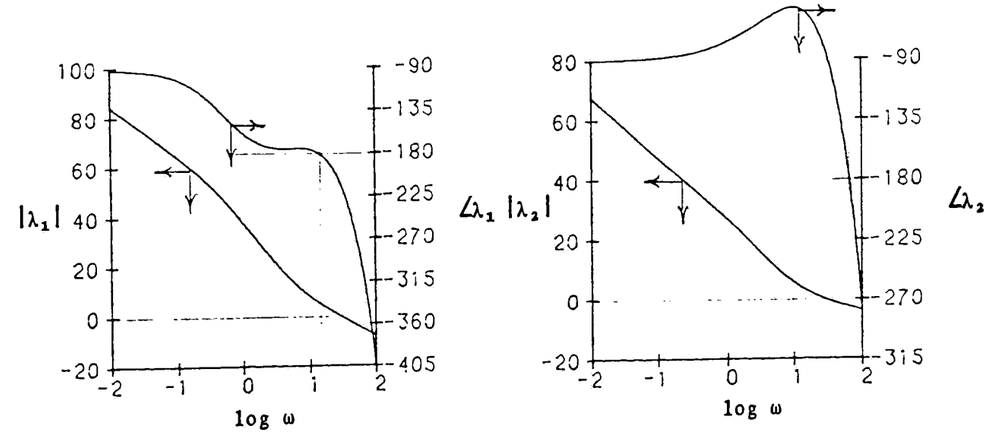

(c) (d)

Fig. 72 Characteristic Loci Stability Bode Plots for
Material Balance Schemes with Proportional-Integral Controllers
in Column's High Purity Separation
a,b-D,V c,d-L,B

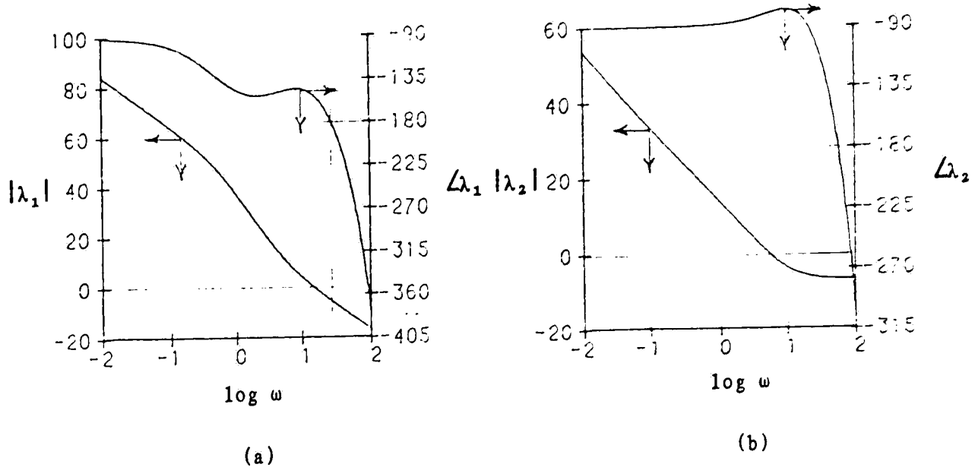

(a) (b)

(c) (d)

Fig. 73 Characteristic Loci Stability Bode Plots for EVaCS Structures with Proportional-Integral Controllers in Column's High Purity Separation
a,b-EVaCS I c,d-EVaCS II

controllers in this structure are not very sensitive to the errors in the loops as tuned since the manipulated variables are changing slowly. Figure 75 shows the time response for the D,V structure. Notice that it gives a stable response, contrary to what was predicted by the characteristic loci stability plots. As this system is highly non-linear, one plausible explanation of this is that the non-linearities within the process have a stabalizing effect on the system. Now, in saying that a stable response was given, attention must be drawn to the magnitude of the changes in the boil-up rate. It is expected that this system would be limited here since it is doubtful that the required boil-up could be given in a realistic situation. The time responses for the L,B structure are shown in Figure 76. Notice that it too gives a stable response while the characteristic loci predicted that the system is unstable. It is expected that this structure would encounter the same limitations as the D,V structure in a realistic situation as it is doubtful that the decrease in the column flows seen in the simulation could be attained.

The time response for the EVaCS I system is shown in Figure 77. These plots show the dynamic responses of the terminal compositions and the column flows. Notice how quickly the terminal compositions return to their set-points. Also, notice that the

dynamics of the column flows are much less here than seen in the material balance schemes. Figure 78 shows plots of the actual controlled and manipulated variables used in this structure. Notice how the response of the total material content of the column, the slow loop, is faster than the response of the rectifying balance, the fast loop. This is due to the exorbitant amount of integral action given to the fast loop by the Z-N tuning method. Figure 79 shows the time responses of the terminal compositions and column flows for the EVaCS II system, while the responses of its total material content (slow loop) and stripping balance (fast loop) are shown in Figure 80. This system rejects the feed composition disturbance well by quickly bringing the terminal compositions back to their set-points with minimal dynamic variation in the column flows. As was the case with the EVaCS I structure, this structure's slow loop's response is faster than the fast loop's response. Again, this is due to the exorbitant amount of integral action in the fast loop.

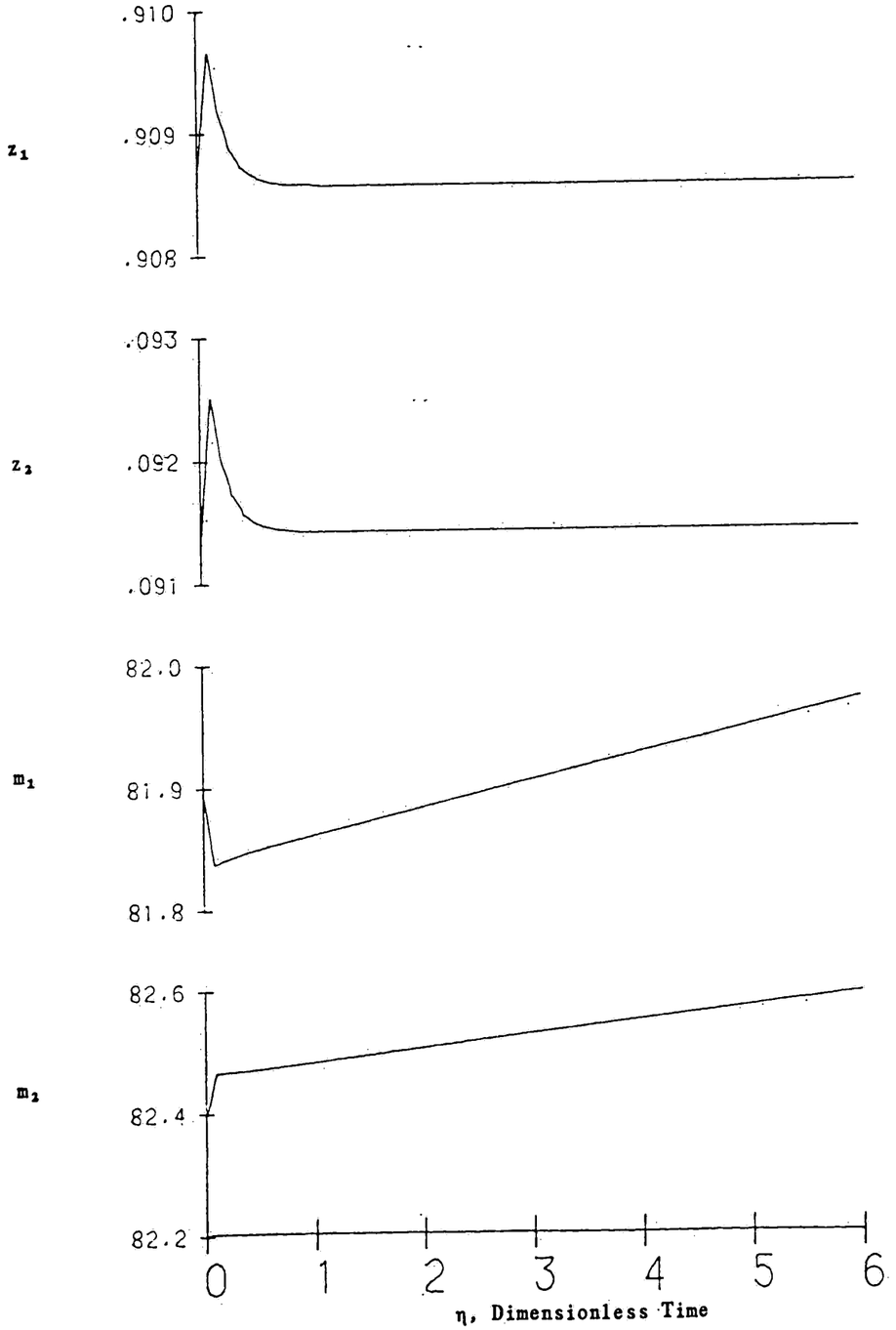

Fig. 74 Transient Response in Column's High Purity Separation for L,V Structure's Controlled and Manipulated Variables

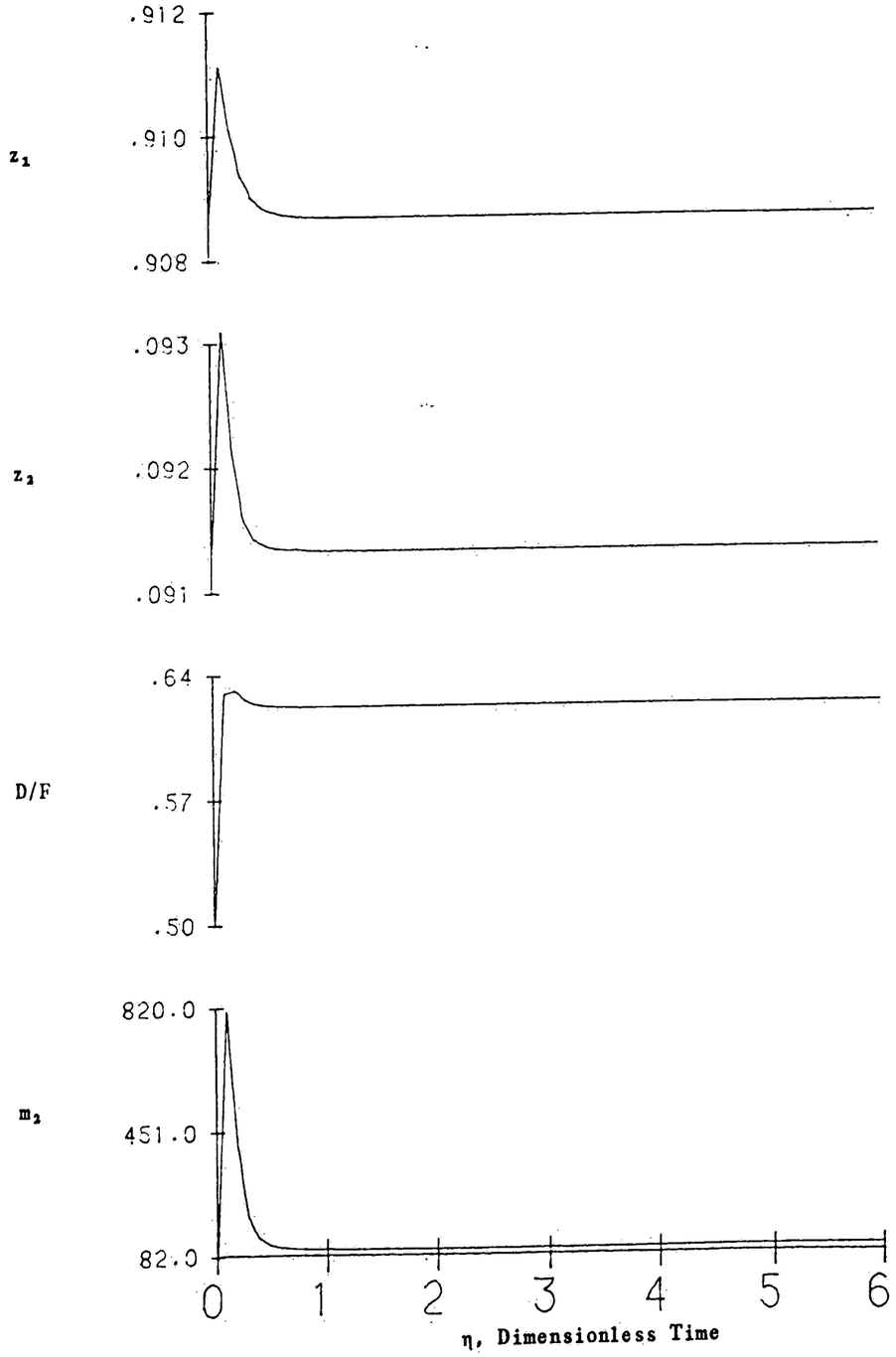

Fig. 75 Transient Response in Column's High Purity Separation for D,V Structure's Controlled and Manipulated Variables

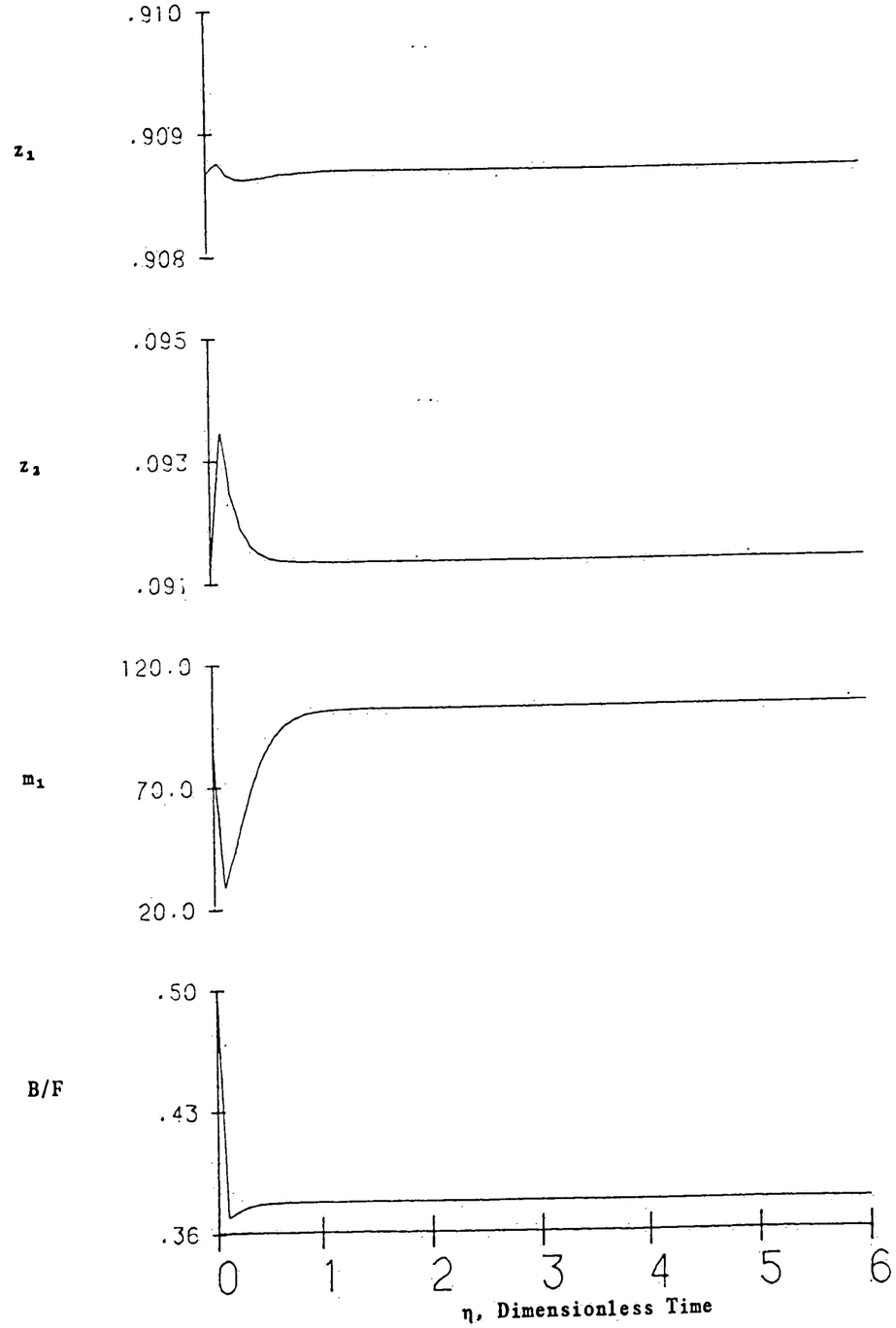

Fig. 76 Transient Response in Column's High Purity Separation for L,B Structure's Controlled and Manipulated Variables

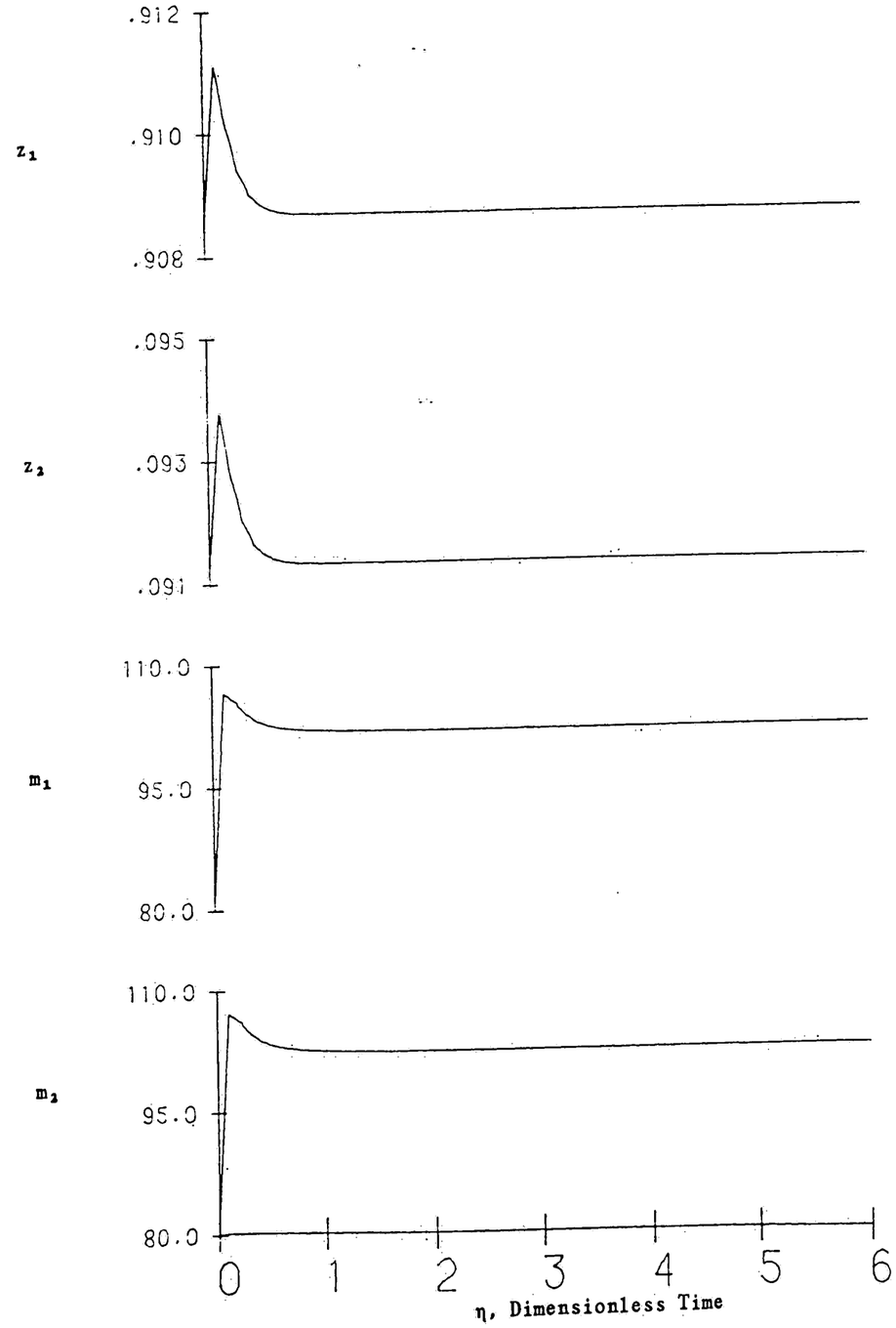

Fig. 77 Transient Response in Column's High Purity Separation for EVaCS I Structure's Terminal Compositions and Column Flows

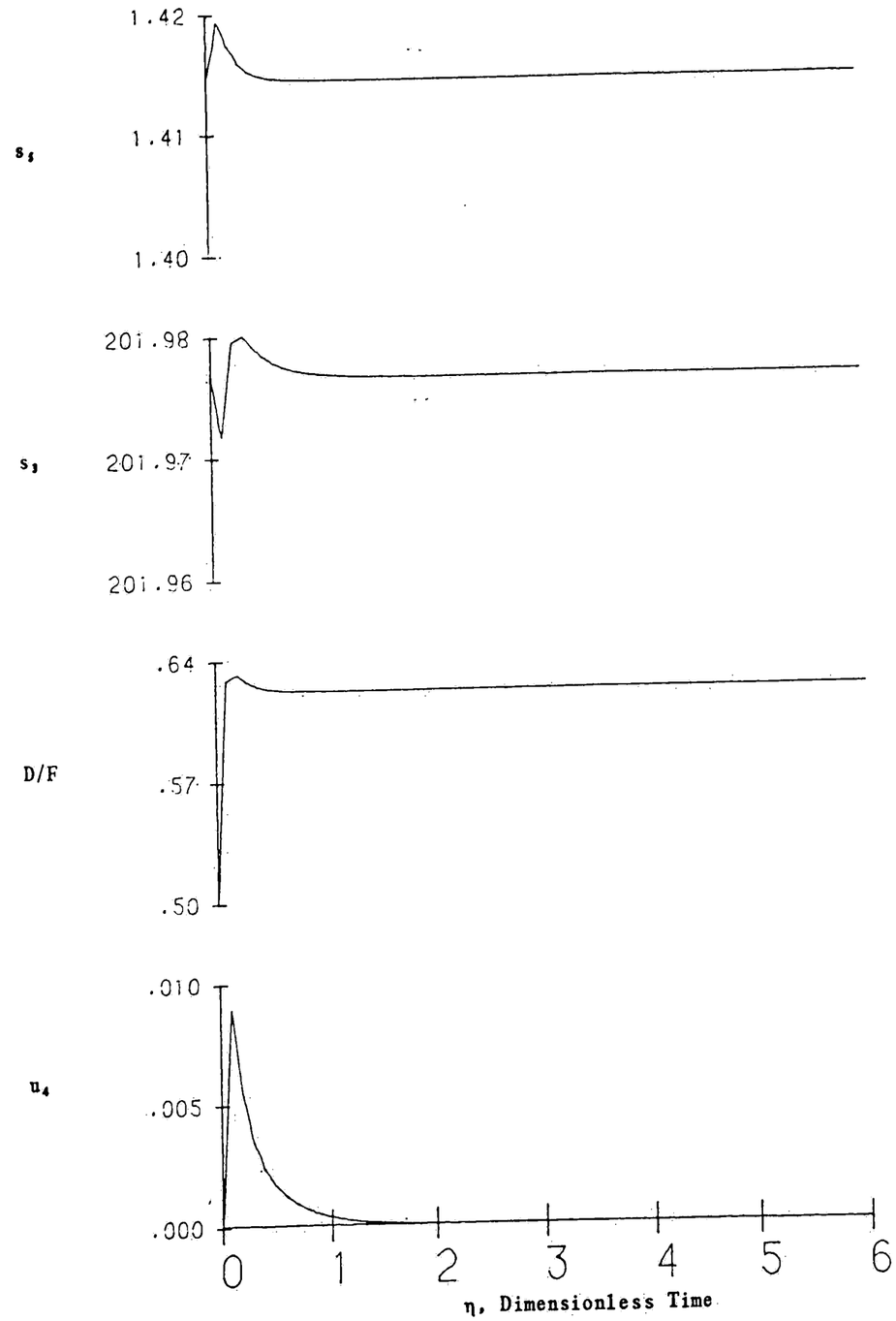

Fig. 78 Transient Response in Column's High Purity Separation for EVaCS I Structure's Controlled and Manipulated Variables

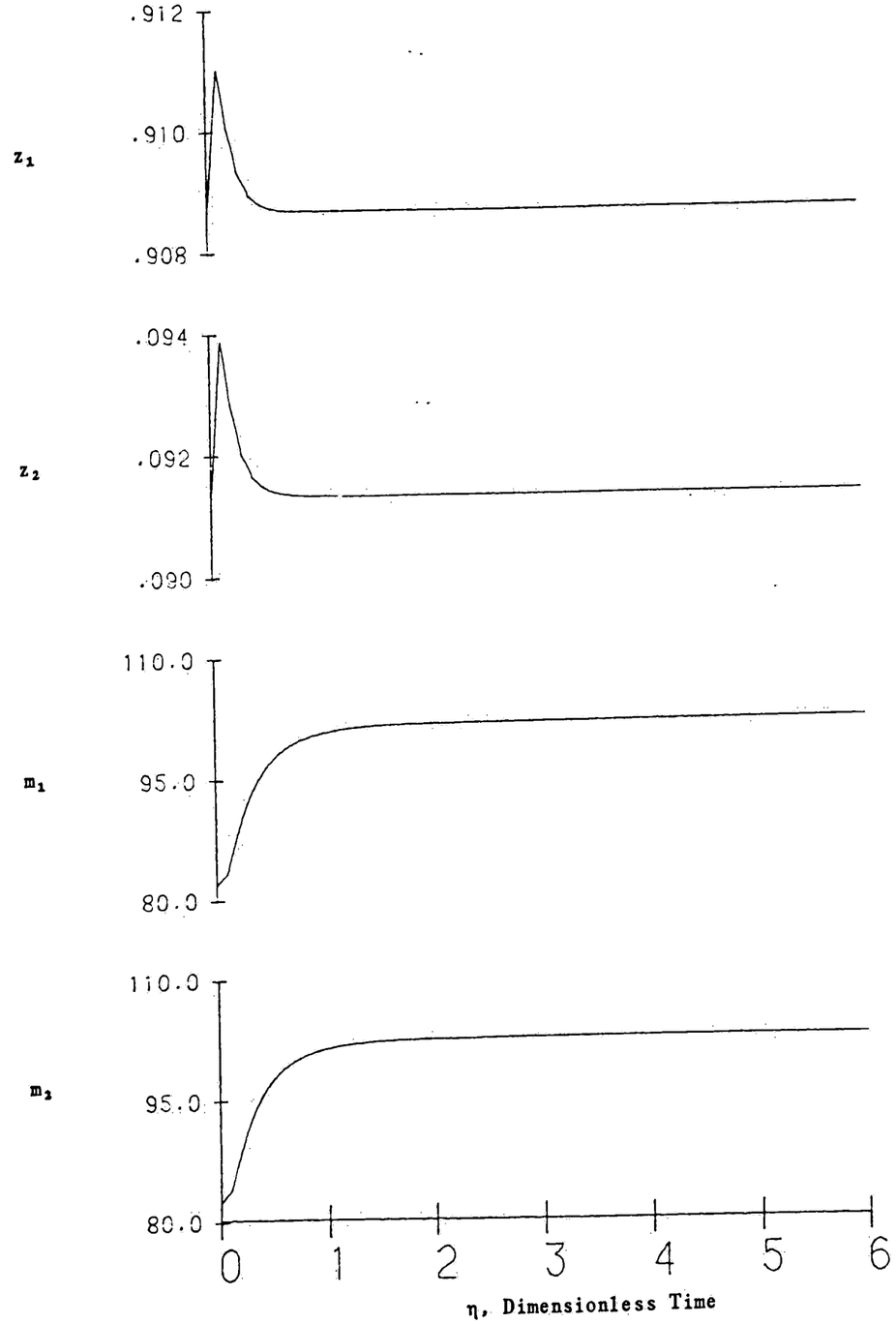

Fig. 79 Transient Response in Column's High Purity Separation for EVaCS II Structure's Terminal Compositions and Column Flows

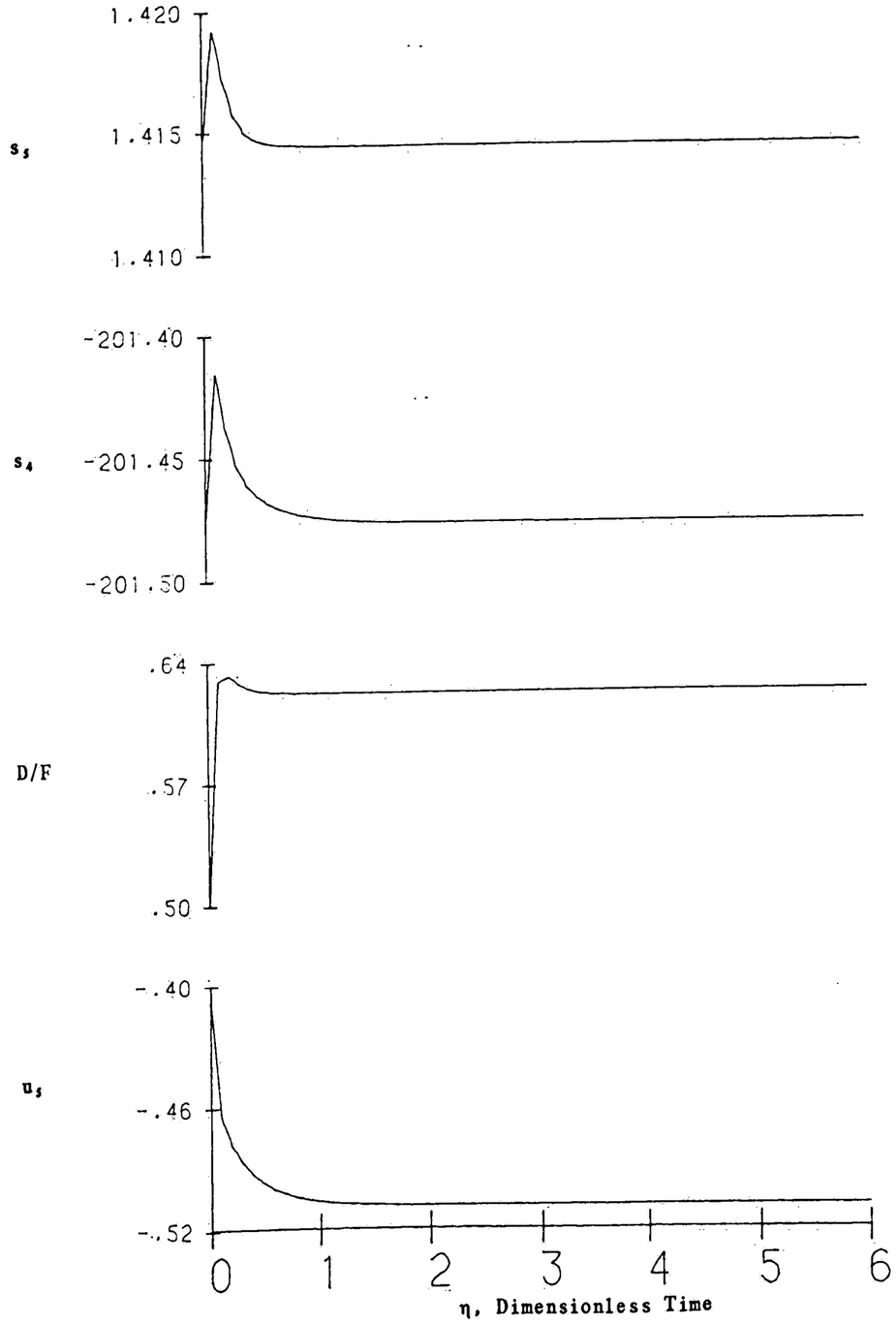

Fig. 80 Transient Response in Column's High Purity Separation for EVaCS II Structure's Controlled and Manipulated Variables

Chapter 6

Conclusions

A fairly large number of analyses have been completed here. We examined two different processes and employed two designs in each process. The first process was two stirred-tank heaters in series connected by a recycle stream. This system approximates a reactor system, the recycle stream being used to increase the overall conversion. The first process design employed here had a low recycle rate while the second design had a high recycle rate. In both designs, the tanks were of equal volume. The second process examined was a two stage distillation column. Equimolal overflow and a saturated feed were assumed in modeling the system. The two design cases employed here consisted of a low purity separation and a high purity separation. In both designs, the rectifying and stripping sections of the column had equal holdups. For each of these four process designs, the dynamic properties of conventional multivariable control structures that might be typically employed in controlling the given process were compared to those properties of the structures synthesized by the Extensive Variable Controller Synthesis technique. The comparisons made in this thesis were based upon five interaction assessment techniques. These techniques consisted of angle calculations between the output coordinating vectors and the state-space plant matrix's eigenrows

(conjugate eigenvectors) and eigenvectors, a modal analysis, the dynamic relative gain array analysis, the inverse Nyquist array analysis, and the characteristic loci analysis.

The conventional control structure used in the stirred-tanks in series process controlled the indiviual tank temperatures with their respective heat inputs. One of the EVaCS structures had one loop that controlled the energy balance of the first tank in the series while the other loop controlled the total energy content of both tanks. The other EVaCS structure had the same loop that controlled the total energy content while its other loop controlled the energy balance of the second tank in the series. In both designs and in all of the analyses, the two EVaCS structures proved themselves superior to the conventional structure. The angle calculations showed that the EVaCS structures approximate the process' modal control structure and do a good job of decoupling the process' internal dynamics. The fact that the total energy content loop was aligned with the slow mathematical mode of the process while the respective energy balance loops were aligned with the fast mathematical mode was seen in the modal analysis. The dynamic relative gain array analysis showed us that the indiviual loops in the EVaCS structures could be tuned independent of one another as long as the natural frequencies of the loops were kept

separated to some extent. The principal conclusion reached in both the inverse Nyquist array and characteristic loci analyses was that the interaction within these structures is minimal.

Three conventional control structures were assessed in the distillation process. The first structure was the energy balance scheme and the remaining two were material balance schemes. The first material balance scheme used the distillate flow rate to control the distillate's composition, while the second material balance scheme used the bottoms flow rate to control the bottoms' composition. One of the EVaCS structures controlled both the material balance of the rectifying section and the total material content of the column. The other EVaCS structure that was synthesized for this process controlled the total content of the column, also, along with the material balance of the stripping section. In both designs and in all of the analyses, the two EVaCS structures proved themselves superior to all three of the conventional structures. In the low purity separation, the EVaCS structures gave very respectable approximations to the column's modal control structure and greatly decoupled its internal dynamics. In the high purity separation, the structures were equivalent to the modal structure and both of them totally decoupled the column's internal dynamics. In both designs, it was

seen in the modal analysis that the response of the total material content loop in the structures was strictly associated with the slow mathematical mode of the system while both of the respective material balance loops had responses that were strictly associated with the fast mathematical mode of the system. The dynamic relative gain array analysis showed that both of the EVaCS structures in each of the design cases had virtually no interaction, thus allowing the two loops in these structures to be tuned in their single-input, single-output enviroments. A dynamic simulation for these structures in the high purity separation design confirmed that we could tune the loops independent of one another and still obtain stable closed-loop responses that were satisfactory. Both the inverse Nyquist array analysis and the characteristic loci analysis confirmed that the interaction within the EVaCS structures was minimal.

The EVACS structures have proven themselves superior in terms of the interaction within the structure to the various conventional structures in all of the various process design cases that we have assessed here. Not only do they minimize the interaction, but they also have an inherent adaptive nature to them as they are designed to the specifications of a given process at a given steady-state. This point is a plus in terms of the robustness of the system.

With today's computers becoming ever more important in process control, the EVaCS technique is especially well suited to exploit their power. Whenever the process is being moved to a new steady-state, the control engineer can easily download some precalculated coefficients for the various required linear combinations to adapt the structure to its new enviroment. In most situations, the controllers in the structure can have minimal integral action to perform their job. As far as the indiviual loop responses are concerned, this point is very desirable as integral control tends to degrade the performance of the loop.

We began the thesis with a discussion about the existing gap between control theory and process control applications. The current width of this gap is being sustained by a continued lack of understanding of the theory on the part of current day practitioners. This lack of understanding is due to the complexity of the required mathematics relative to the training of the majority of process control engineers. The mathematics involved in the EVaCS technique are simple and are founded in concepts which the process control engineer can understand.

We conclude that the EVaCS technique seems to offer a hope for establishing a strong foundation for bridging the current

theory/applications gap. It is going to have to be fed and cared for before growing up to be strong and healthy. The technique does warrant enough attention that the proper precautions should be made to make sure it doesn't get thrown out with the wash water.

BIBLEOGRAPHY

1. Mayr, O.,Origins of Feedback Control, MIT Press, Cambridge (1970)

2. MacFarlane, A.G.J.,''A Survey of Some Recent Results in Linear Multivariable Feedback Theory,'' Automatica, vol. 8, 455-492 (1972)

3. Rosenbrock, H.H.,''Distinctive Problems of Process Control,'' Chemical Engineering Progress, vol. 58, no. 9, 43-50 (1962)

4. Ray, W.H.,''Multivariable Process Control - A Survey,'' Proceedings of the International Symposium on Process Systems Engineering, Kyoto, Japan (1982)

5. Georgakis, C.,''On the Use of Extensive Variables in Process Dynamics and Control,'' submitted to Chemical Engineering Science

6. Rosenbrock, H.H.,Computer-Aided Control System Design, Academic Press, London (1974)

7. Gould, L.A.,Chemical Process Control: Theory and Applications, Addison-Wesley, London (1969)

8. Stephanopoulos, G.,Chemical Process Control, An Introduction to Theory and Practice, Prentice-Hall, Englewood Cliffs, NJ (1984)

9. Ellis, J.K. and White, G.W.T.,''An Introduction to Modal Analysis and Control,'' Control, 9(82),(83),(84), 193-197,252-266,317-321 (1974)

10. Porter, B. and Crossley, R.,Modal Control: Theory and Applications, Taylor and Francis Ltd, London (1972)

11. Rijnsdorp, J.E.,''Interaction in Two-Variable Control Systems for Distillation Columns,'' Automatica, vol. 1, 15-28 (1965)

12. Bristol, E.H.,''On a New Measure of Interaction for

Multivariable Process Control,'' IEEE Trans. Autom. Control, AC-11, 133 (1966)

13. Tung, L.S. and Edgar, T.F.,''Analysis of Control-Output Interactions in Dynamic Systems,'' AIChE Journal, vol. 27, no. 4, 690-693

14. Rosenbrock, H.H.,''Design of Multivariable Control Systems using the inverse Nyquist array,'' Proc. IEEE, vol. 116, 1929-1936 (1969)

15. MacFarlane, A.G.J. and Belletrutti, J.J.,''The Characteristic Locus Design Method,'' Automatica, vol. 9, 575-588 (1973)

16. Gagnepain, J. and Seborg, D.,''An Analysis of Interactions with Applications to Multiloop Control System Design,'' Ind. Eng. Chem. Proc. Des. Dev., vol. 21, 5-11 (1982)

17. McAvoy, T.J. and Witcher, M.F.,''Interacting Control Systems: Steady-state and Dynamic Measurement of Interaction,'' ISA Transactions, vol. 16, no. 3, 35-41 (1977)

18. Gantmacher, F.R.,Matrix Theory, vol. 1, Chelsea, New York (1959)

19. McAvoy, T.J.,''Connection between Relative Gain and Control Loop Stability and Design,'' AIChE Journal, vol. 27, no. 4, 613-619 (1981)

20. McAvoy, T.J.,''Some Results on Dynamic Interaction Analysis of Complex Control Systems,'' Ind. Eng. Chem. Proc. Des. Dev. , vol. 22, 42-49 (1983)

21. Churchill, R.V.,Introduction to Complex Variables and Applications, McGraw-Hill, New York (1948)

22. Tyreus, B.D.,''Industrial Applications of Multivariable Control,'' Distillation Dynamics and Control short course, Lehigh University (1982)

23. MacFarlane, A.G.J.,''The Use of Characteristic Functions and Characteristic Values in Feedback Systems Analysis,'' Int. J. Math. Educ. Sci. Technol., vol. 1, 359-366 (1970)

24. Schwanke, C.O., Edgar, T.F. and Hougen, J.O.,''Development of Multivariable Control Strategies for Distillation Columns,''

ISA Transactions, vol. 16, no. 4, 69-81 (1977)

25. Luyben, W.L., Process Modeling, Simulation, and Control for Chemical Engineers, McGraw-Hill, New York (1973)

26. Ziegler, J.G. and Nichols, N.B., "Optimum Settings for Auotmatic Controllers," Trans. ASME, vol. 64, 759-768 (1942)

I. Plant Matrices and Input Matrices for Stirred-Tank Heaters in Series

This appendix contains the plant matrices, A, and input matrices, B, for the various state-space representations of the control structures of interest in the stirred-tank heaters in series process of Chapter 3. These matrices are given for both design cases assessed in the chapter, those being the low recycle design and the high recycle design.

Low Recycle Design

IVaCS

$$A = \begin{bmatrix} -3.00000 & 1.00000 \\ 3.00000 & -3.00000 \end{bmatrix}$$

$$B = \begin{bmatrix} 2.00000 & 0.00000 \\ 0.00000 & 2.00000 \end{bmatrix}$$

EVaCS I

$$A = \begin{bmatrix} -1.50000 & 0.50000 \\ 1.50000 & -4.50000 \end{bmatrix}$$

$$B = \begin{bmatrix} 1.00000 & 0.00000 \\ -1.00000 & 4.00000 \end{bmatrix}$$

EVaCS II

$$A = \begin{bmatrix} -1.00000 & 0.50000 \\ -2.00000 & -5.00000 \end{bmatrix}$$

$$B = \begin{bmatrix} 1.00000 & 0.00000 \\ 2.00000 & -4.00000 \end{bmatrix}$$

High Recycle Design

IVaCS

$$A = \begin{bmatrix} -6.00000 & 4.00000 \\ 6.00000 & -6.00000 \end{bmatrix}$$

$$B = \begin{bmatrix} 2.00000 & 0.00000 \\ 0.00000 & 2.00000 \end{bmatrix}$$

EVaCS I

$$A = \begin{bmatrix} -1.20000 & 0.20000 \\ 4.80000 & -10.80000 \end{bmatrix}$$

$$B = \begin{bmatrix} 1.00000 & 0.00000 \\ -4.00000 & 10.00000 \end{bmatrix}$$

EVaCS II

$$A = \begin{bmatrix} -1.00000 & 0.50000 \\ -2.00000 & -11.00000 \end{bmatrix}$$

$$B = \begin{bmatrix} 1.00000 & 0.00000 \\ 2.00000 & -4.00000 \end{bmatrix}$$

II. Plant Matrices and Input Matrices for Two Stage Distillation Column

This appendix contains the plant matrices, A, and input matrices, B, for the various state-space representations of the control structures of interest in the two stage distillation process of Chapter 4. These matrices are given for both design cases assessed in the chapter, those being the low purity separation and the high purity separation.

Low Purity Separation

L,V

$$A = \begin{bmatrix} -1.44428 & 1.54692 \\ 0.60948 & -2.72386 \end{bmatrix}$$

$$B = \begin{bmatrix} 0.47633 & -0.16841 \\ 0.18767 & -0.53082 \end{bmatrix}$$

D,V

$$A = \begin{bmatrix} -1.44428 & 1.54692 \\ 0.60948 & -2.72386 \end{bmatrix}$$

$$B = \begin{bmatrix} -0.47633 & 0.30792 \\ -0.18767 & -0.34315 \end{bmatrix}$$

L,B

$$A = \begin{bmatrix} -1.44428 & 1.54692 \\ 0.60948 & -2.72386 \end{bmatrix}$$

$$B = \begin{bmatrix} 0.30792 & 0.16841 \\ -0.34315 & 0.53082 \end{bmatrix}$$

EVaCS I

$$A = \begin{bmatrix} -0.94415 & 0.03240 \\ 1.62758 & -3.22398 \end{bmatrix}$$

$$B = \begin{bmatrix} -0.35925 & 0.00000 \\ 0.61929 & 3.16813 \end{bmatrix}$$

EVaCS II

$$A = \begin{bmatrix} -0.91452 & -0.03138 \\ 0.50017 & -3.25361 \end{bmatrix}$$

$$B = \begin{bmatrix} -0.35925 & 0.00000 \\ 0.19648 & 3.27078 \end{bmatrix}$$

High Purity Separation

L,V

$$A = \begin{bmatrix} -164.13636 & 164.80443 \\ 493.49365 & -497.50635 \end{bmatrix}$$

$$B = \begin{bmatrix} 0.27213 & -0.27048 \\ 0.81487 & -0.81985 \end{bmatrix}$$

D,V

$$A = \begin{bmatrix} -164.13636 & 164.80443 \\ 493.49365 & -497.50635 \end{bmatrix}$$

$$B = \begin{bmatrix} -0.27213 & 0.00165 \\ -0.81487 & -0.00497 \end{bmatrix}$$

L,B

$$A = \begin{bmatrix} -164.13636 & 164.80443 \\ 493.49365 & -497.50635 \end{bmatrix}$$

$$B = \begin{bmatrix} 0.00165 & 0.27048 \\ -0.00497 & 0.81985 \end{bmatrix}$$

EVaCS I

$$A = \begin{bmatrix} -0.49791 & 0.00101 \\ 247.21561 & -661.14480 \end{bmatrix}$$

$$B = \begin{bmatrix} -0.81736 & 0.00000 \\ 405.82338 & 660.64271 \end{bmatrix}$$

EVaCS II

$$A = \begin{bmatrix} -0.49741 & -0.00101 \\ 81.47751 & -661.14530 \end{bmatrix}$$

$$B = \begin{bmatrix} -0.81736 & 0.00000 \\ 133.88684 & 661.31078 \end{bmatrix}$$

ERRATA

Due to an overlooked programming error, the inverse Nyquist analyses shown in Chapters 3 and 4 have Gershgorin discs that are not of the type stated. The two terms have been interchanged and one should be the other.

As the reader may have noticed, the time domain plots of the dynamic responses of the structures in the two stage column's high purity separation are shown out to six dimensionless column time constants, as opposed to ten column time constants (as stated in the text). These simulations were actually carried out to ten time constants, but no significant changes occurred after six time constants.